SEDIMENT DYNAMICS AND RESILIENCE ON TIDAL FLATS

A.C.S. (Sophia) Bats

Utrecht University, Faculty of Geosciences

A.C.S. (Sophia) Bats

4275373

A study on the short-term sediment resilience of tidal flats as indicator for long-term dynamics at the adjacent saltmarshes.

In partial fulfilment of the requirements for the degree of Master of Science in Marine Sciences
At Utrecht University, Faculty of Geosciences

Supervisors:

MSc. Tim Grandjean (NIOZ)
MSc. Jim van Belzen (NIOZ)
Prof. dr. Tjeerd Bouma (NIOZ & UU)

Date: 31 July 2020

Credits: 45 ECTS

Front page image by A.C.S. (Sophia) Bats, Rattekaai (17-01-2020)

Contact: a.c.s.bats@students.uu.nl

Abstract

Background and Aims: Intertidal environments worldwide are of prime importance to biodiversity and coastal defence, acting as a natural buffer to global climate change and sea level rise. However, anthropogenic induced activities and rapid climate change place these environments under stress and risk of drowning, increasing the flood risk in the inhabited areas behind them. Sediment characteristics, biotics, tidal flat morphology and hydrodynamics are often interrelated and prime shaping factors of estuaries and tidal basins. Due to the plethora of processes combined with the expectation of enhanced sea level rise, quick measurable indicators predicting the systems' future development are desired. This provides the option of restoring the system before reaching a critical tipping point. Theoretical approaches have shown that for systems where a decreased ecological resilience is observed, more time is needed to recover back to the state of equilibrium. This can theoretically serve as an early warning signal. This research therefore aims to determine whether this approach can also be applied to tidal basins, and if long-term behaviour can be explained by short-term recovery of the system.

Methods: To account for a wide range of tidal flat characteristics, this research has been executed in two tidal basins in the Netherlands: The Eastern- and the Western Scheldt. The long-term dynamics are determined using satellite imagery over the last 30 years. The short-term tidal flat properties and dynamics are examined during multiple field campaigns. For determining the resilience of the system, the systems are disturbed, and their recovery regularly measured over time.

Key Results: This research shows the significant importance of hydrodynamics from the impact of grainsize and inundation time. The tidal bed-level recovery was found to be in line with the phenomena of 'critical slowing down'. Results also indicate the relations between the systems' exposure to wind energy and long- and short-term behaviour. The state of sediment equilibrium of the system is also important for its response to disturbances. Sediment deficits account for quicker erosion, implying a closer proximity to reaching a critical tipping point in the future.

Conclusions: This research provided insight in the improvement of predictions related to resilience of sediment dynamics in tidal systems. The complexity of the system in terms of their interrelatedness, is emphasised again. It is therefore recommended to build on this research, with measuring the recovery rate of the tidal flats, to monitor the change in resilience providing the possibility to intervene when the recovery rate shows indications of reaching a critical threshold.

Keywords: *tidal flats, saltmarshes, hydrodynamics of tidal basins, resilience, critical slowing down, early warning signals*

Preface

In this report I will present to you about my findings on sediment dynamics and resilience on tidal flats. I started this research for my master thesis project within the Marine Sciences programme at Utrecht University, department of Geosciences and the Royal Netherlands Institute for Sea Research (NIOZ).

I am very interested in the influence of climate change on highly dynamic systems and wanted to gain further insight in key properties influencing them. Moreover, I was eager to expand my experiences in fieldwork and modelling, which has been fulfilled by conducting multiple extensive field campaigns in the tidal flats of the Netherlands.

I would like to thank all my supervisors for showing me the wide field of doing research. In particular, I want to thank Tjeerd Bouma for facilitating my involvement in this project, Tim Grandjean for the good teamwork during fieldwork, but also for providing me with the hypsometric data and the workable data as derived from the ASED-sensors. I would also like to thank Jim van Belzen for his view and input on the disturbance and recovery experiment. Moreover, I want to thank the field and laboratory technicians at NIOZ for explaining the equipment. Furthermore, I want to thank everyone who endured in the fieldwork campaigns.

To finalize I want to thank my friends and family for their support and interest in this subject and everyone providing me with substantial feedback.

I hope you enjoy your reading.

Sophia Bats

Utrecht, July 2020

Table of Contents

List of Figures

List of Tables

List of Abbreviations and Acronyms

ASED	Acoustic Surface Elevation Dynamics
DBD	Dry Bulk Density
DEM	Digital Elevation Model
EI	Exposure Index
NDVI	Normalised Digital Vegetation Index
NDWI	Normalised Digital Water Index
P	Probability value
QQ-plot	Quantile Quantile-plot
r	Correlation coefficient
SEB	Sedimentation Erosion Bars
SLR	Sea Level Rise
SSC	Suspended Sediment Concentration
WBD	Wet Bulk Density

Tidal flats as referred to in this research

BA	Baarland
DM	Slikken van Dortsman
GBS	Groot Buitenschoor
HE	Hellegatpolder
PP	Paulinapolder
RK	Rattekaai
RL	Rilland
RL-BA	Rilland-Bath
VI	Slikken van Viane
WA	Waarde
ZG	Zuidgors

1. Introduction

Worldwide, intertidal environments provide ecosystem services such as creating habitats for unique plant- and benthic species (Allen, 2000), hosting migratory birds (Blew et al., 2005; Van Eerden et al., 2005) and being involved in coastal defence through bed stabilisation and wave attenuation (e.g. Temmerman et al., 2013; Vuik et al., 2016). Their ecosystem services act as a natural buffer to global climate change and sea level rise (SLR) (e.g. Duarte et al., 2013). Anthropogenic induced activities like dredging and shipping however, have shown to impact sediment dynamics in estuaries. With rapid SLR, tidal wetlands and their ecosystem services are increasingly valued while also expected to become more vulnerable (Kirwan et al., 2010; Kirwan & Megonigal, 2013). Hence the urge to understand and protect these areas (Hu et al., 2017).

Estuaries and tidal basins are shaped by intertidal processes regarding sediment characteristics, vegetation and benthic life, and hydrodynamics, which are often interrelated. At the interface between saltmarshes and tidal flats, bed-level dynamics are an important factor in the connection between the long-term biogeomorphological development of the marsh and large-scale physical forcing (Willemsen et al., 2018). One of the aspects responsible for tidal flat evolution is their cyclic behaviour in accretion and erosion, both on the long- and short-term.

Due to the complexity of the system and the interrelations between the shaping processes, it is desired to enable well-measurable short-term indicators in the tidal flat and saltmarsh to help map the vulnerable coastal systems and predict early on how the system will develop on the long-term. Recent theoretical developments might provide the needed framework for developing such indicators, referred to as 'early warning signals'. They show that the recovery rate after (induced) perturbations in a system (resilience) is indicative for the amount of disturbances the system can handle before shifting to an alternative state, referred to as 'ecological resilience'. When decreasing recovery rates are found, this suggest the system needs more time to go back to its original state, implying that increased stress is applied to the system, a phenomena known as 'critical slowing down' (van Nes & Scheffer, 2007; Wissel, 1984). Critical slowing down has been proposed as an early warning signal (small changes a system shows before reaching a lower branch stable state), since it becomes apparent before reaching this threshold. This theory may contribute to predicting the long-term behaviour of tidal wetlands, providing with the possibility to intervene or prepare once the system reaches closer to the threshold of its equilibrium state. However, few measurements on this theoretical approach have been executed in complex (tidal) ecosystems, resulting in the still insufficient comprehension of early warning signals which consequently restricts its implementation in decision-making.

This research aims to better predict long-term vegetation dynamics on saltmarshes and adjacent tidal flats by studying the short-term sediment dynamics after morphological perturbations to those tidal flats. The objective is to understand the influence of exposure to wind over the last 30 years and the suspended sediment concentration (SSC) of the system to the short-term saltmarsh (vegetation change) and adjacent tidal flat dynamics (sediment properties and morphology). It is expected that saltmarsh and tidal flat dynamics are related to wind exposure and SSC, where more exposure relates to higher dynamics and SSC influences the recovery to perturbations. By determining the influences of tidal flat properties, SSC, and exposure to wind on the capacity of tidal flats to recover from disturbances, this research aims to provide insight into early warning signals for shifts to alternative stable states in complex tidal ecosystems.

To answer these research aims, a multi-approach method has been applied after sketching the theoretical framework. Six fieldwork and four additional sites to enhance the scope of the long-term research were chosen in the Eastern- and Western Scheldt. These tidal basins were chosen due to their contrasting SSC values, for which the Eastern Scheldt shows a deficit caused by the construction of the Storm Surge Barrier in 1986. To minimize the biotic effects of chlorophyll-a, seedling establishment and benthos on for example enhancing the erosion threshold, as much as possible (Menge et al., 2019; Willemsen et al., 2018), this research has been executed during the winter season of 2019/ 2020. During rising water temperatures in spring, the biological activity increases while it decreases during the colder winter (Andersen et al., 2005), allowing for the focus to be primarily on the morphological and hydrological influences to the system, since the presence of certain types of seasonally effected biota have shown to generally overshadow the dependence on physical parameters at tidal flats (Jesus et al., 2009; Widdows et al., 2000).

The long-term dynamics of the tidal flats have been researched by first determining the long-term exposure gradient to wind for all the locations, followed by focussing on the saltmarsh trajectories by use of satellite imagery. For understanding the short-term dynamics and the factors explanatory for the recovery, first the tidal flat properties and daily tidal flat sediment dynamics have been determined, to understand the differences for each tidal flat. Next, a field campaign has been set up, applying small perturbations to the system, and intensively tracing the process of recovery with time. The results from the long- and short-term analyses are compared and used to discuss the results.

2. Scientific Background

To better understand the research approach following the scientific knowledge gaps as explained in chapter 1, the necessary background information will be provided. This section explains the functioning of tidal systems, with their sediment- and hydrodynamics as shaping forces. The theory on complex systems is used to explain the coherence of the shaping factors in the system, by elaborating on the equilibrium profile- and resilience theory.

2.1 Estuaries

In this report, the definition of an estuary as proposed by Perillo (1995) is used, which is defined as follows:

> *"A semi-enclosed coastal body of water that extends to the effective limit of tidal influence, within which sea water entering from one or more free connections with the open sea, or any other saline coastal body of water, is significantly diluted with fresh water derived from land drainage, and can sustain euryhaline biological species from either part or the whole of their life cycle."*

The intertidal area of a tidal basin is visualised in figure 1 and ranges from the lower elevated tidal flat region (closest to the tidal channel) to the higher vegetated zone, with a pioneer zone and saltmarsh. The transition from tidal flat to saltmarsh is generally found at the mean high water level mark (Cleveringa, 2014). Within saltmarshes, tidal creeks are present and tidal channels often appear on the bare tidal flats for water drainage.

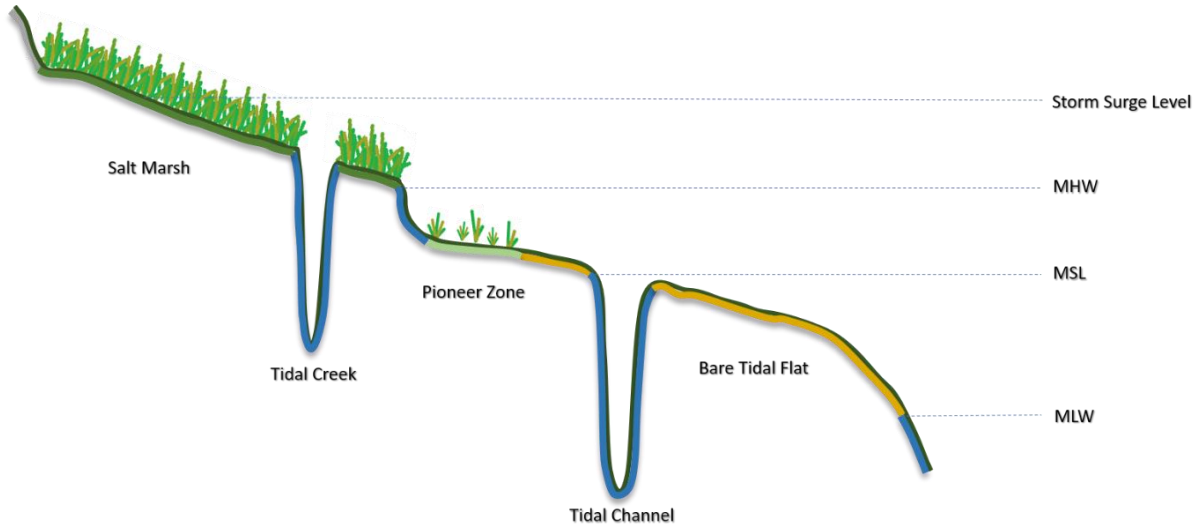

Figure 1 - Cross section of the intertidal area. From the higher saltmarsh towards the pioneer zone and bare tidal flat, ending with the main tidal channel. Modified after Cleveringa (2014) and Dijkema et al. (2001). *The approximate area, the water from the tidal channel will reach Mean High Water (MHW), Mean Sea Level (MSL) and Mean Low Water (MLW) are indicated by the blue dotted lines.*

2.1.1 The Tidal Flat Area

The bare tidal flat is the low relief, unvegetated, unlithified area, generally comprised of sand and mud, between the highest and the lowest tide mark (Dyer et al., 2000; Friedrichs, 2011). Hydrodynamic forcing within this environment causes distinctive sediment processes by advection, dispersion, and bottom shear stress. In coastal areas, the tide, wind-induced circulation, waves, density-driven circulation and drainage processes are the most common forcing's (Le Hir et al., 2000). Strong fluctuations in water elevation on both a temporal and spatial scale, resulting from the tide,

wind-induced circulation, waves, density-driven circulation and drainage processes are the most common forcing's (Le Hir et al., 2000) causing different inundation times.
The existence of an intertidal flat is determined by tidal force, consisting of a cross-shore and longshore component (figure 2). Cross-shore currents are uniform in the lower part of the flat and show a decreasing pattern towards the shore. This current induces the filling and emptying of the flat, while long-shore currents cause large-scale circulation around the flat (Le Hir et al., 2000). (Strong) wind events often cause large-scale variations within the water surface elevation and flow patterns that either modulate or counteract the tidal currents. Wave action can be induced by propagating offshore waves and local winds. The wind fetch is an important factor for this, the longer the wind can propagate over the water before reaching the coast, the more energy the waves contain.

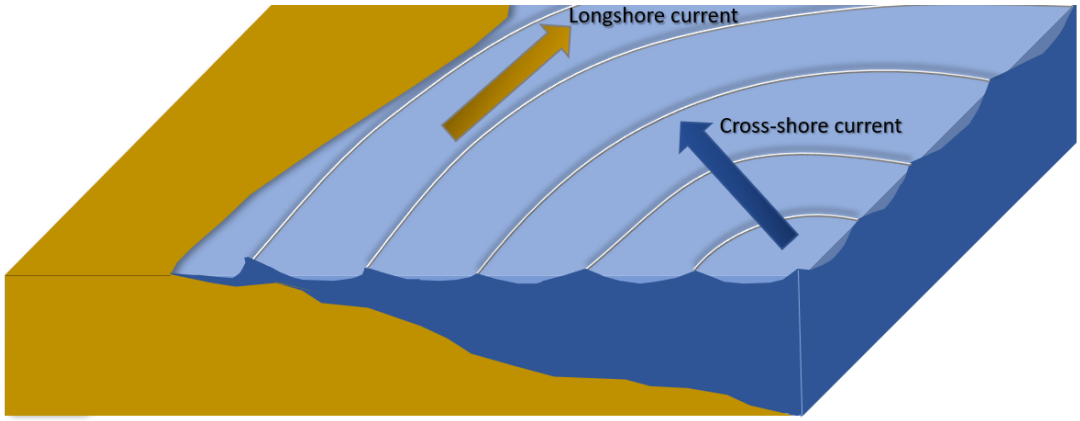

Figure 2 - Longshore and cross-shore currents along the coast

Where saline water comes in from the sea and fresh water from the river, salinity gradients occur. These gradients result in density-driven circulation surrounding the tidal flats. Drainage is also an important shaping factor, accounting for both the flow of surficial freshwater from upstream and the elimination of upper sediment porewater when the water table decreases during the falling tide. The permeability of the surface sediment is essential, as low permeabilities prevent the flow of porewater within the bed (Bassoullet et al., 2000). Furthermore, drainage impacts the flats' long-term stability, as drainage-modulated seaward transport counterbalances for tidally induced accretion.

2.1.2 The Pioneer Zone and Saltmarsh

The pioneer zone is located between the bare tidal flat and the saltmarsh (figure 1). This zone is characterised by the abundance of limited and sprouting vegetation (figure 3). Compared to the tidal flat, waves are smaller due to the attenuating effect of vegetation. Moreover, the current velocity also decreases (Callaghan et al., 2010).

Figure 3 – Pioneer zone vegetation, the formation of patches of Spartina vegetation and a close-up.

As shown by Schwarz et al. (2018), colonisation behaviour of different pioneer vegetation can affect the wetland evolution landscapes. Whilst seedling establishment is a very important process regarding saltmarsh development (Bouma et al., 2014), short-term sediment dynamics can majorly disturb this process (Cao et al., 2018). According to Bouma et al. (2016) and Laegdsgaard (2006), the establishment of seedlings is especially important for the occupation of large bare tidal flats which are disconnected from the existing vegetation. Recruitment events of seedlings can be encouraged by the absence of physical disturbance, like tidal currents, wind, waves, and sediment dynamics, which is referred to as the "window of opportunity". This indicates the critical time interval where lack of disturbances allows for seedlings to establish and gain the strength to withstand disturbances in the future (Balke et al., 2014; Hu et al., 2015).

Landward of the pioneer zone, the saltmarsh is found (figure 1). These densely vegetated areas are located at higher elevations compared to the bare tidal flats and are inundated during spring tide and storm surges. The vegetation dampens the wave energy and attenuates currents, protecting the sediment surface from erosion. Resulting feedbacks driven by vegetation can result in the compensation of saltmarshes for both SLR and land subsidence due to sediment accretion (Kirwan et al., 2016). The width of the saltmarsh is not static, the location of the marsh edge potentially changes up to several meters per year and is determined by lateral dynamics. This movement is a cyclic alteration between erosion and sedimentation which is determined by a combination of two key processes: the initiation of marsh erosion and expansion caused by seedling establishment (Bouma et al., 2016) and the growth of clonal shoots (Silinski et al., 2016). Globally, wetland ecosystems have declined more than 50% within the last century (e.g. Davidson, 2014). An important reason for this is the process of coastal squeeze. This arises when coastal areas have to grow to higher elevations due to sea level rise and consequently move inland, yet are prevented by their landward migration by natural or manmade flood defences (Pontee, 2013).

2.1.3 Wetland Satellite Research

Studies on the dynamics of tidal flats and saltmarshes have often been limited in terms of space and time. By using satellite imagery, this field can be researched over longer time periods. Empirical and modelling studies show contrasting conclusions in whether tidal wetlands can keep up with SLR in the (near) future. Important perspectives regarding the understanding of the multivariate dependence on different variables could be retrieved from large-scale and long-term analyses of these dynamics, using remote sensing techniques (Laengner et al., 2019). Different remote sensing classification techniques can be used for wetland identification, either supervised or unsupervised image classifications.

2.2 Sediment Dynamics

This section addresses the lithology and sediment transportation in tidal basins. For the understanding of the impact of tidal flat properties on the long- and short-term dynamics, the effect of the grainsize to cohesiveness and packing density is also explained. The equilibrium profile theory and the resilience theory are also elaborated on in this section.

2.2.1 Lithology

Sediment from the tidal creeks will be brought into suspension due to wave and, or tidal action influencing the lithology of the intertidal area. The concentration of the sediment is often determined by the energy-driven concentration gradient influenced by the tidal/ wind induced wave force. The

sediment movement across tidal flats, causing the Suspended Sediment Concentration (SSC) to change, is supply driven. This combined effect is visualised in figure 4. From this figure it can be observed that next to the channels (where the velocity is highest) the sediment is coarser, decreasing in diameter further from the channel where the velocity decreases (Friedrichs, 2011). The grainsize close to the saltmarsh are therefore often characterised as mud.

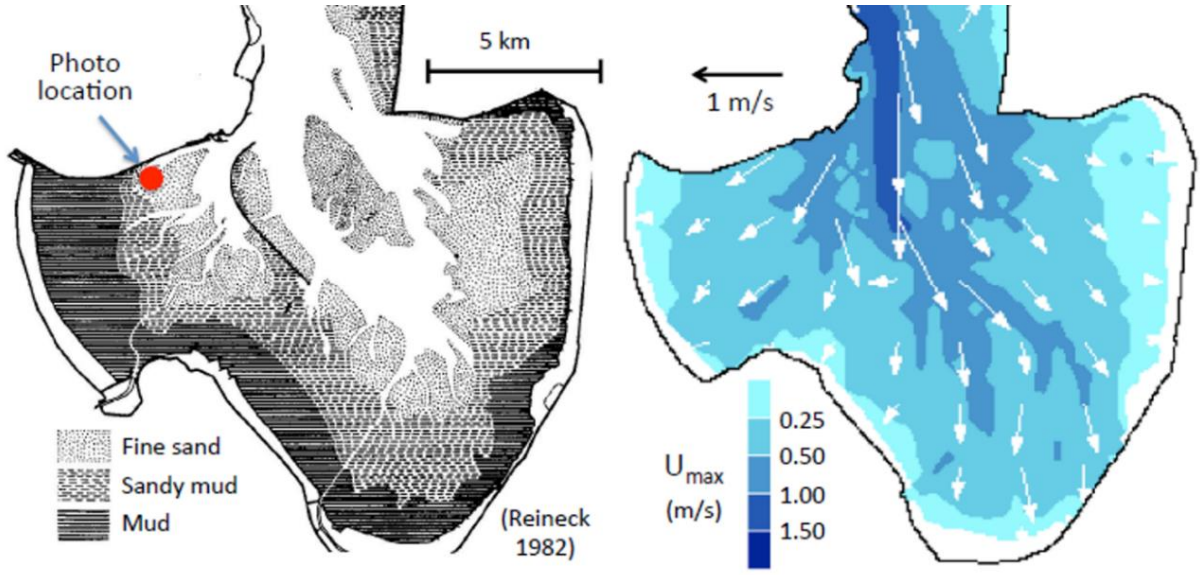

Figure 4 - The combination of sediment content and water velocity. Where the water flow is slowest, mud is deposited, and the grainsize is decreasing towards the channel with the highest flow velocities.(Grabemann et al., 2004)

For mud, the mutual bonding between clay particles, is referred to as the cohesion (Jacobs et al., 2011). For low values of the bed shear stress, individual flocs can already erode from the surface. For higher shear stress values, a clear threshold from which sand and mud particles erode simultaneously and uniformly, has been observed. For increasing packing densities, the erosion threshold seemed to become larger (Jacobs et al., 2011). Thus, moving away from the channel towards the saltmarsh, would result in finding lower grainsizes but also higher cohesiveness when the system contains muddy sediments.

The weight per unit volume of a soil sample is an important soil feature and indicator for soil compaction and is quantified by using the Dry Bulk Density (DBD) (Arshad et al., 1997). A relation between the density of the sediment and erosion rates has been found by Jacobs et al. (2011) and Roberts et al. (1998). The DBD affects the infiltration capacity, rooting depth, available water capacity, porosity, plant nutrient availability and soil microorganism activity of the concerned soil. A high DBD indicates low soil porosity and high soil compaction, impacting its water capacity and root growth (Arshad et al., 1997). The DBD of freshly deposited sediment is dependent on the grainsize distribution, deposition mode and the chemicals regime of the water. The DBD however stays vulnerable to changes after deposition as a result of pressure, grainsize distribution, drying of the sediment, permeability and the time after deposition (Mahmood, 1987).

2.2.2 Sediment Transportation

It has been shown by Friedrichs & Aubrey (1996) that the processes of morphodynamics and hydrodynamics are interrelated. The magnitude of sediment transport on the tidal flat is determined by physical processes and driven by tidal currents and wind generated waves (De Brouwer et al., 2000).

Changes in wind direction, speed and fluctuations in the tidal currents result in a system where transportation quickly switches into deposition and vice versa.
The Hjulström diagram shows the thresholds for erosion and deposition as a function of the particle diameter and flow velocity for a 100 cm water level flow (figure 5). This diagram illustrates how more energy (flow velocity) is required to put sediment into motion than is essential to keep it in transportation. For the sediment to be deposited, a sufficient energy reduction is needed. The diagram thus displays how larger amounts of energy are needed to cross the threshold of erosion, while transportation is already possible at lower energy levels. Deposition of sediments from the water column can also be explained by a reduction in energy (e.g. when facing resistance formed by saltmarsh vegetation).

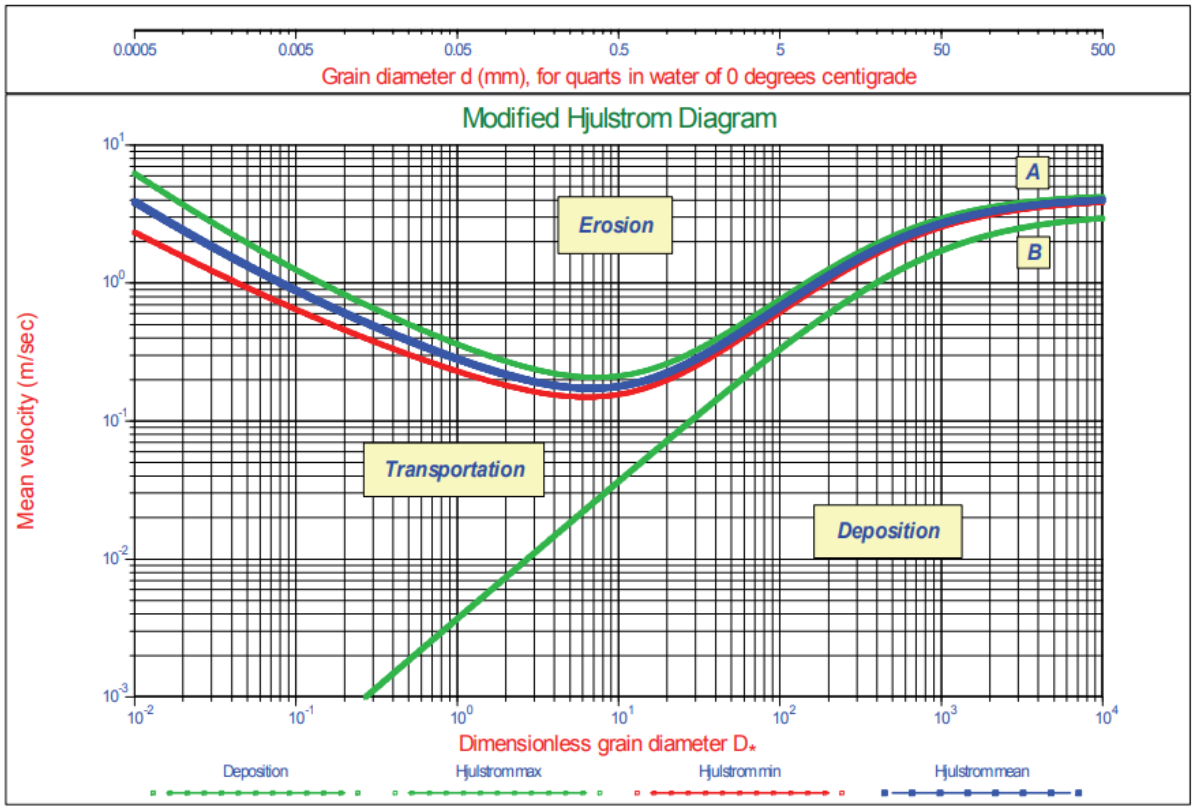

Figure 5 - Shield diagram, modified by Hjulström (Miedema, 2010).

Waves are mainly wind driven, causing wave energy on the tidal flat to increase during storm conditions. However, current velocity does not show differences at tidal flats between stormy and calm weather conditions. Thus, it seems that there is an approximate constant tidal flat current speed between different weather conditions. Due to the nature of 'regular' waves and tidal waves, the erosional and depositional effect during low and high energy events differ. As observed in figure 6, the response of tidal flats to storm waves result in erosion of the flat, but deposition on both the saltmarshes and in the channels. However, the opposite is observed for regular tidal action, for which sediment deposition occurs on the tidal flats and causes erosion of the channels (Yang et al., 2003). The horizontal surface area with respect to elevation is referred to as the hypsometry. The shape of the tidal flat hypsometry can provide insight in the type of equilibrium, which is reached during uniformity of maximum bottom shear stress. This shear stress can be dominated by either tidal currents or is wave induced. When the system is dominated by tidal currents, a convex hypsometry is favoured, while a wave-dominated system accounts for a concave hypsometry. A system where wind

waves are occurring, the systems shear stress is often dominated by waves (Friedrichs & Aubrey, 1996).

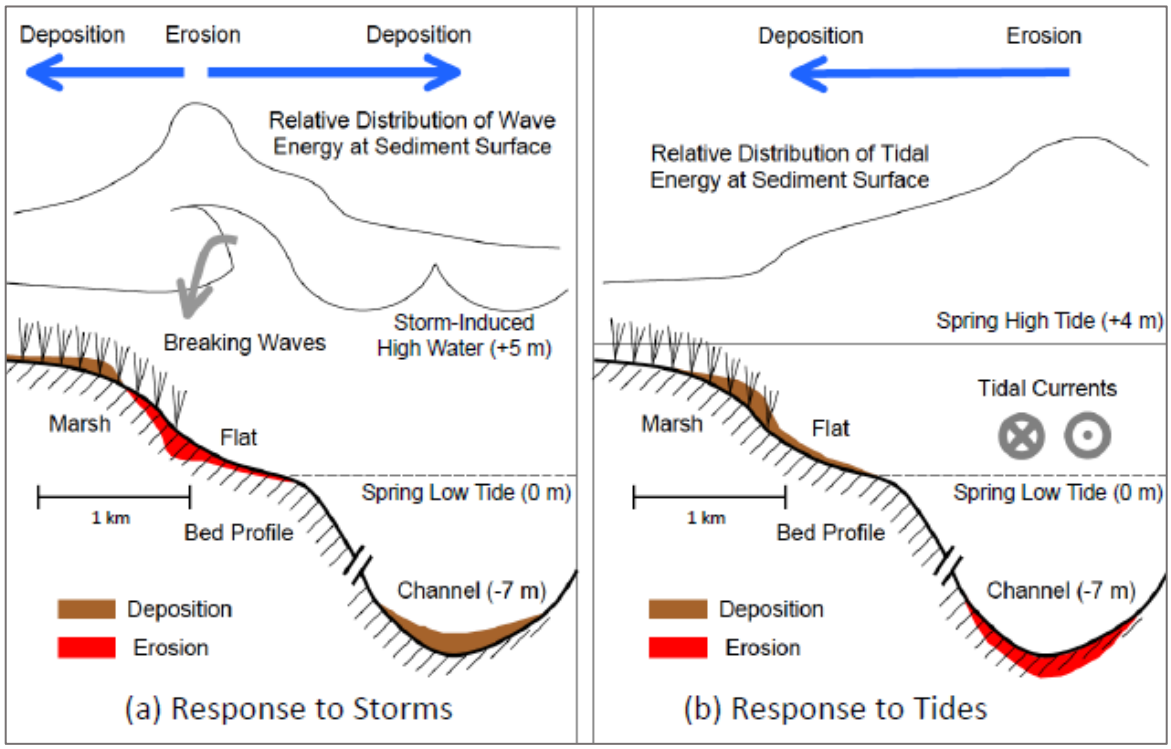

Figure 6 - Conceptual model for the morphodynamic response to both storms (a) and tides (b) of the intertidal coastline (Yang et al., 2003). *The deposition and erosion system behave different to the external factors in both a and b, and consequently makes for a different profile.*

2.2.3 The Resilience Theory

The response of ecosystems to gradual changes in external conditions like climate can differ between smooth and continuous (figure 7.a) and inert until a critical level is approached after which a stronger reaction is observed (7.b). Alternatively, a system can also show multiple alternative stable states, separated by an unstable equilibrium (7.c) (Scheffer et al., 2001).

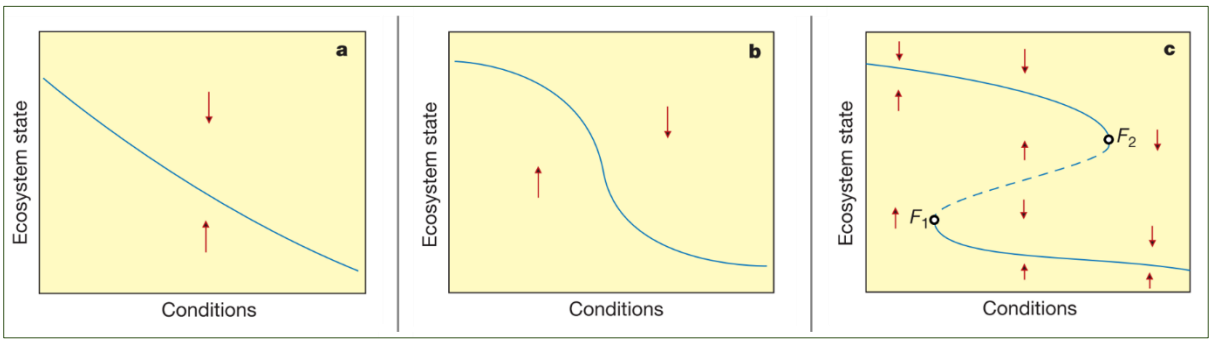

*Figure 7 – Ways in which ecosystem equilibrium states can vary following changes in external ecosystem conditions. In conditions **a** and **b**, each condition has one equilibrium state. Condition **c** shows a folded equilibrium curve indicating three stable states can exist. The arrows indicate the direction of change, implying an unstable state at the dashed line between stable state F_1 and F_2* (Scheffer et al., 2001)

After sufficient change in ecosystem conditions, the presence of multiple stable states potentially results in catastrophic transitions to the lower branches. Before a switch occurs, the system shows small changes, but these 'early-warning signals' are difficult to attain. After passing the threshold (F_2)

and reaching the lower branch stable state, it is not possible to switch to the upper branch stable state by restoring to the external environmental conditions from before the collapse. This can only be achieved by reaching the return threshold F_1. Then the system restores by shifting to the upper branch. Both the size of the attraction basin and the ecosystem perturbation are important in the movement between alternating stable states: smaller perturbations might be enough to cause shifts in stable states for smaller ecosystems, while the same size perturbation will not cause a shift in larger ecosystems (figure 8) (Scheffer et al., 2001). This is referred to as 'ecological resilience', where the size of the attraction basin (figure 8.a,b) corresponds to the maximum perturbation (figure 8.c,d) without resulting in a shift to an alternative stable state (Holling, 1973; Scheffer et al., 2001). The size of the attraction basin reduces with gradually changing conditions, without effecting the ecosystem state. However, the reduced size does results in resilience loss, making the system increasingly fragile (lower ecological resilience) to stochastic events in the future.

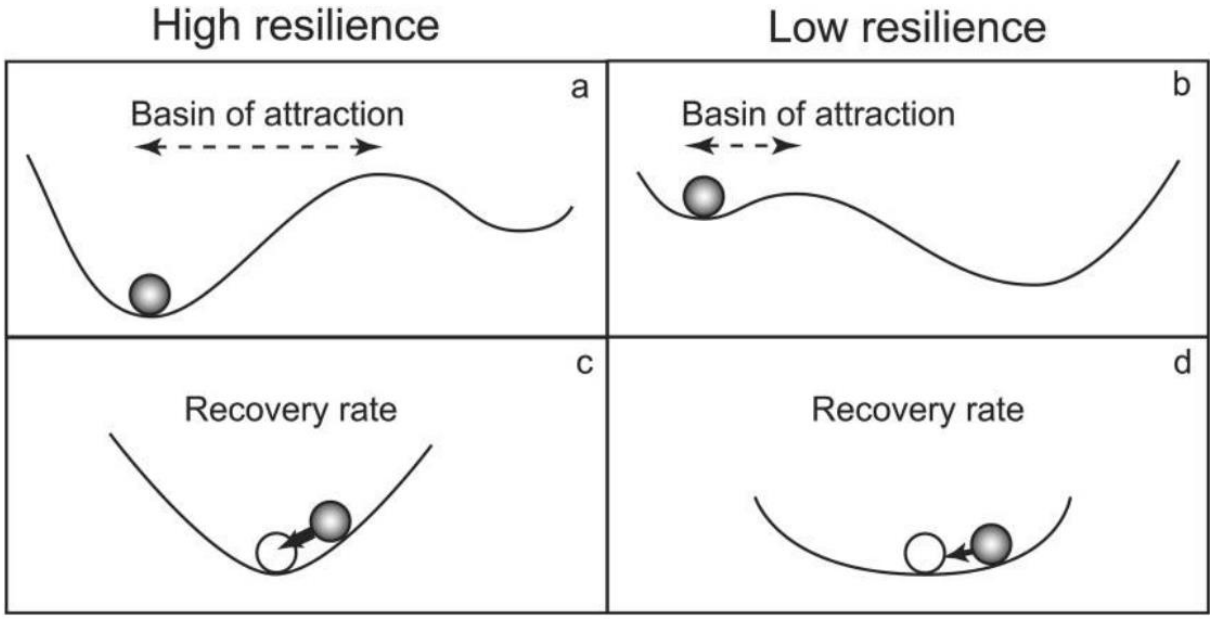

*Figure 8 – The stability properties of an ecosystem. The attraction basins' size (**a**, **b**) indicates the amount of disturbance the system can handle before shifting to an alternative state, referred to as "ecological resilience'. The rate of recovery following a small perturbation (**c**, **d**) indicates the local equilibrium stability.* (Van Nes & Scheffer, 2007)

This fragility can cause ecosystems to shift to an alternative state easier. Due to the possible catastrophic ecological consequences, it is desired to measure the ecological resilience to intervene or prepare. Van Nes & Scheffer (2007) showed how the recovery rate (rate of return to equilibrium, after a disturbance (Pimm, 1984) of a system to small perturbations works as a good indicator for this ecological resilience. This is referred to as the 'resilience' (Holling, 1973). When the time needed to recover from a disturbance lengthens because of increased stress applied to the system this is known as 'critical slowing down' (van Nes & Scheffer, 2007; Wissel, 1984). This phenomenon is implied to be used as an early warning signal since it becomes apparent before reaching the threshold. Ecological resilience and its (in)direct indicators have been determined by theoretical approaches, using models ((Bennett et al., 2005; Carpenter et al., 2001). Because these model results are not accurate enough, the development of measurable generic indicators is desirable. 'Critical slowing down' is such an indicator and can be measured after a small experimental perturbation (van Nes & Scheffer, 2007). This phenomenon has also been observed for the vegetation recovery in tidal marshes (Van Belzen et al., 2017). Besides the recovery rate, fluctuations over time can provide insight in the vulnerability of a system (e.g. Carpenter & Brock, 2006; Scheffer et al., 2009; van Nes & Scheffer, 2007).

3. Site Description

In the Eastern- and Western Scheldt, ten tidal flats were chosen for the long-term analyses, from which six are also used for the short-term measurements (figure 9). The assigned locations are selected on contrasting levels of lithology (sand/ mud), their location relative to the preferred wind direction (affecting their wind exposure) and salinity level (meso- and polyhaline (salt and brackish water)) (table 1). Due to the lack of a significant salinity gradient in the Eastern Scheldt, the six fieldwork sites were unevenly divided between the Eastern- (two) and the Western Scheldt (four). Further, the locations were chosen for their accessibility and minimal disturbance by manmade structures preventing wind (and thus waves) to affect the flat in a natural way. The predominant sediment fraction of all sites has been obtained by visual inspection of the ecotope maps (figure 11 and 12).

Figure 9 - Research Sites in the Western- and Eastern Scheldt with the names of the tidal flats. The blue diamonds indicate the fieldwork locations and the red dots the locations added for satellite analyses. A special case accounts for Rilland and Bath, Rilland is the fieldwork location, while Rilland-Bath is used as a combined tidal flat system during the satellite analyses.

Table 1 - Assigned fieldwork locations in the Eastern Scheldt (ES) and the Western Scheldt (WS) with their abbreviation, salinity values, main lithologic value and their location relative to the preferred wind direction.

Research sites	Abbreviation	Salinity [psu] (S = Salt, B= Brackish)	Lithology fraction	Relative to preferred wind direction
Paulinapolder (WS)	PP	25 (S)	Mud	Perpendicular
Zuidgors (WS)	ZG	28 (S)	Sand	Parallel
Baarland (WS)	BA	28 (S)	Mud	Parallel
Hellegatpolder (WS)	HE	23 (S)	Sand	Perpendicular
Rilland(-Bath) (WS)	RL(-BA)	20 (B)	Sand	Parallel
Groot Buitenschoor (WS)	GBS	5 (B)	Mud	Perpendicular
Waarde (WS)	WA	21 (B)	Sand	Parallel
Slikken van Viane (ES)	VI	29 (S)	Sand	Parallel
Slikken van Dortsman (ES)	DM	29 (S)	Sand	Parallel
Rattekaai (ES)	RK	29 (S)	Sand	Perpendicular

3.1 Eastern Scheldt

The Eastern Scheldt has changed from an estuary to an elongated and tide-dominated, saline tidal basin since the riverine freshwater input has been shut off since 1987 (Smaal & Nienhuis, 1992). It has an approximate length of 50 km and a surface area of 350 km^2 (Eelkema et al., 2013). Before the construction of the Storm Surge Barrier in 1986, fine sand (150 µm – 200 µm), which is the main sediment type on the bottom of the Eastern Scheldt, could easily be transported with flow velocities reaching up to 1 or 2 m/s during average tides. After the 1953 storm, which caused for major destruction of a large part of the southwest of the Netherlands, the Dutch government assigned a special 'delta commission' to prevent similar disasters in the future. Advice as framed in the 'Deltaplan', was to close several tidal channels in Zeeland. Consequently, most of the sea inlets in Zeeland were closed between 1960 and 1986 (Figure 10). After constructing the first dams (figure 10.B), the tidal volume of the Eastern Scheldt increased and consequently also the flow velocities, leading to deeper channels (Huisman & Luijendijk, 2009).

The construction of the Eastern Scheldt Storm Surge Barrier in 1986 (figure 10.C) caused the inlet width of the Eastern Scheldt to decrease, causing for a significant decline of tidal volume. As a result of the direct relationship between the amount of water flowing through a channel and the area of these channels, the decrease of water flowing through the channels caused for a decreasing channel area. As a result, the Eastern Scheldt system now tries to reach a new equilibrium within the channel area and the declined tidal prism causing the channels to decrease in area. However, the unavailability of more sediment causes a disequilibrium in the channel system. This is not expected to be further influenced by SLR (Maldegem & Van Pagee, 2005). Moreover, the construction caused the tidal flow velocities in the basin to decrease and thereby blocked of sediment transport from the North Sea into the basin (Huisman & Luijendijk, 2009).

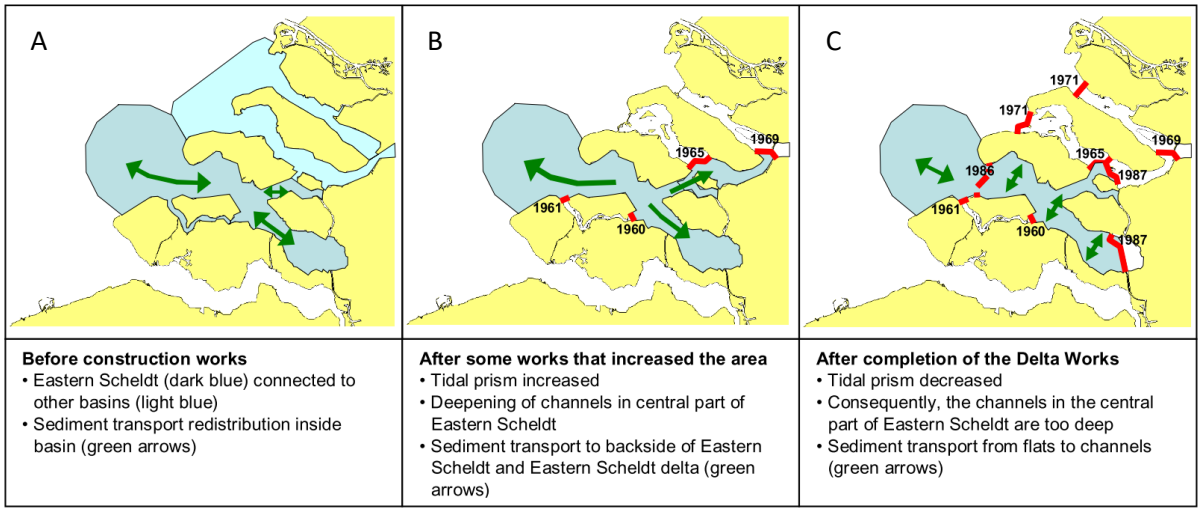

Figure 10 - Eastern Scheldt area before construction works (A) after some works that increased the area (B) and after completion of the Delta Works (C) (Huisman & Luijendijk, 2009).

Due to the sediment deficit in the system, the channels will fill up with material from the tidal flats and the shorelines, causing erosion of the intertidal area, and consequently changing the morphology. Moreover, some of the saltmarshes retreated more than two meters per year. In total, the intertidal area here decreased with almost 10% since the construction of the Storm Surge Barrier. It is extrapolated that in the current evolution of the area, some of the tidal flats will be disappeared within 100 to 300 years, depending on their location. Due to this erosion, the ecological value of the Eastern

Scheldt declined. Besides the re-establishment of the sediment equilibrium, SLR influences the area of tidal flats which might lead to their permanent flooding, or a decreasing dry period and consequently a decrease of a factor 1.5 of the intertidal area. Due to the importance of these flats as foraging area for many bird species increasing inundation time, which changes the environmental conditions for benthic organisms, (the most important food source for these birds) is expected to be a serious threat to foraging bird species (Geurts van Kessel, 2004). In figure 11, the ecotopes present in the Eastern Scheldt are shown. It becomes visible that the area consists of mostly sandy material. Moreover, most of the Eastern Scheldt intertidal area is categorised as low dynamic.

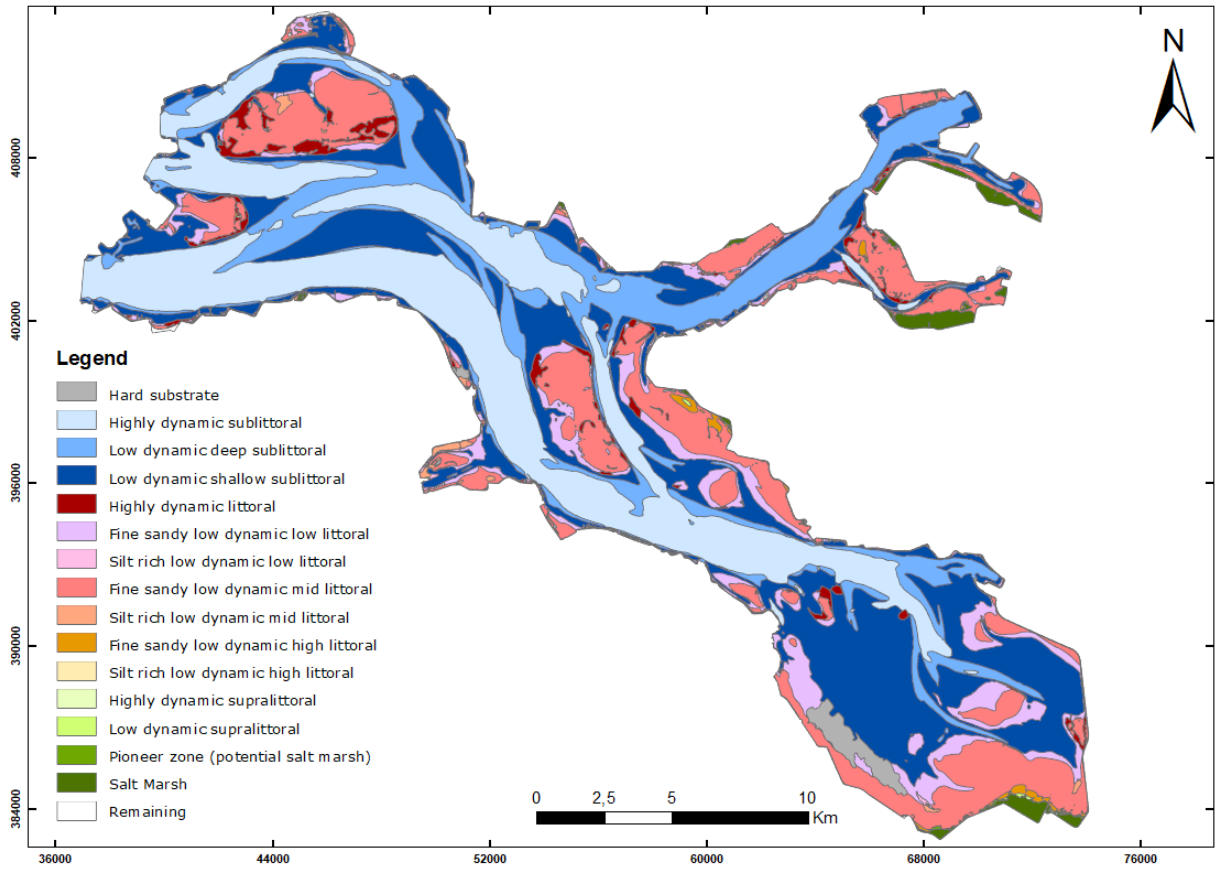

Figure 11 - Ecotopes in the Eastern Scheldt (Rijkswaterstaat, 2016).

3.2 Western Scheldt

The Western Scheldt is located in the southwest of the Netherlands (figure 9) and is classifies as tide-dominated (Baeyens et al., 1998). This estuary experiences a salinity gradient from salt water closest to the inlet to brackish and eventually fresh further inland. It is different from other estuaries in north-western Europe because it is one of the last remaining pristine nature places in this area.

The Western Scheldt is important economy wise as it holds shipping lanes to the harbour of Antwerp. Consequently, dredging operations are needed to maintain the navigation channel. The navigation channels have been deepened in the 1970s to 14.5 m. The already deeper ebb-channels where further deepened by dredging to 16 m in 1997 (De Vriend et al., 2011). This material was dumped in the shallower flood channels. Dumping can influence the stability of the two-channel system, eventually making it unstable after reaching the critical level of dumping. While dredging alone does not influence the stability of the two-channel system, dredging in one channel together with dumping in the other channel does negatively influences the stability of the two-channel system. The two-channel system

can even turn into a one-channel system under the dredging and dumping influence (Wang & Winterwerp, 2001).

The lithology on the tidal flats is different for each location across the tidal flats. Generally, the mud concentrations are highest where tidal velocities are lowest (section 2.2). In figure 12, the ecotopes present in the Western Scheldt are shown. It becomes visible that the area only holds a very little amount of hard substrate. Moreover, the Western Scheldt hold a bigger part of highly dynamic area, compared to the Eastern Scheldt. Besides, the area holds more silt- rich and less sandy sediments.

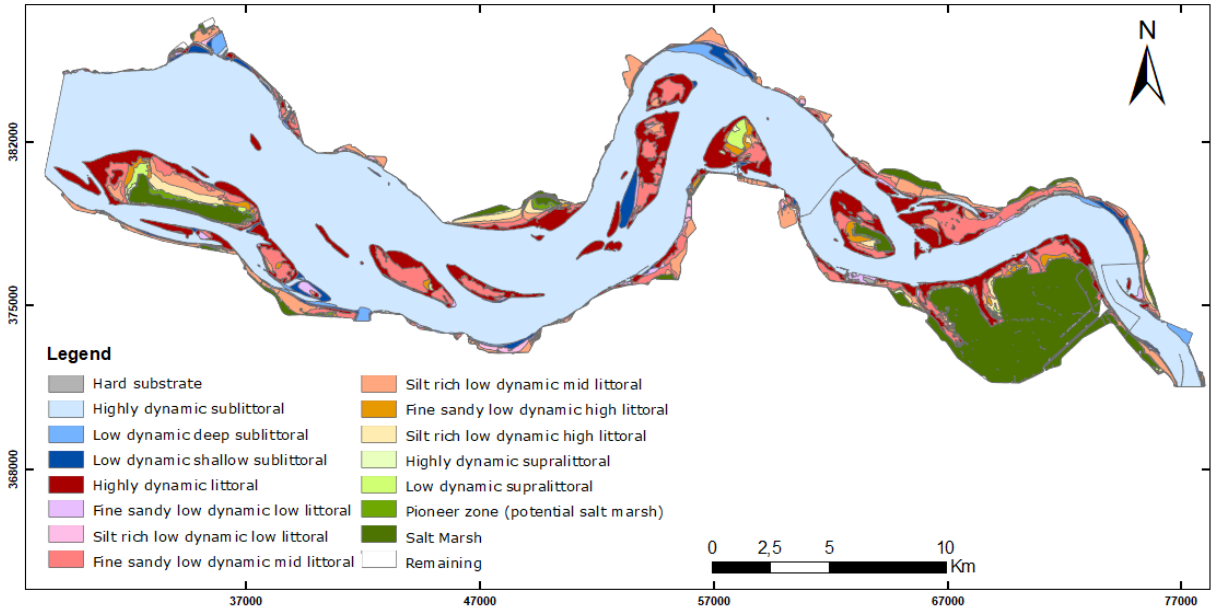

Figure 12 – Ecotopes in the Western Scheldt 2018 (Rijkswaterstaat, 2018).

4. Methods

To better understand how to predict long-term vegetation dynamics on tidal flats and adjacent saltmarshes by short-term sediment dynamics, a multi-approach method has been used for the Eastern- and Western Scheldt (figure 13). First, the long-term observations are analysed by satellite imagery and long-term wind data from KNMI weather stations in the area is studied. This is followed by the short-term dynamics, starting with sampling for the site-specific properties and sediment dynamics during different field campaigns. The last part will explain the approach for measuring the resilience.

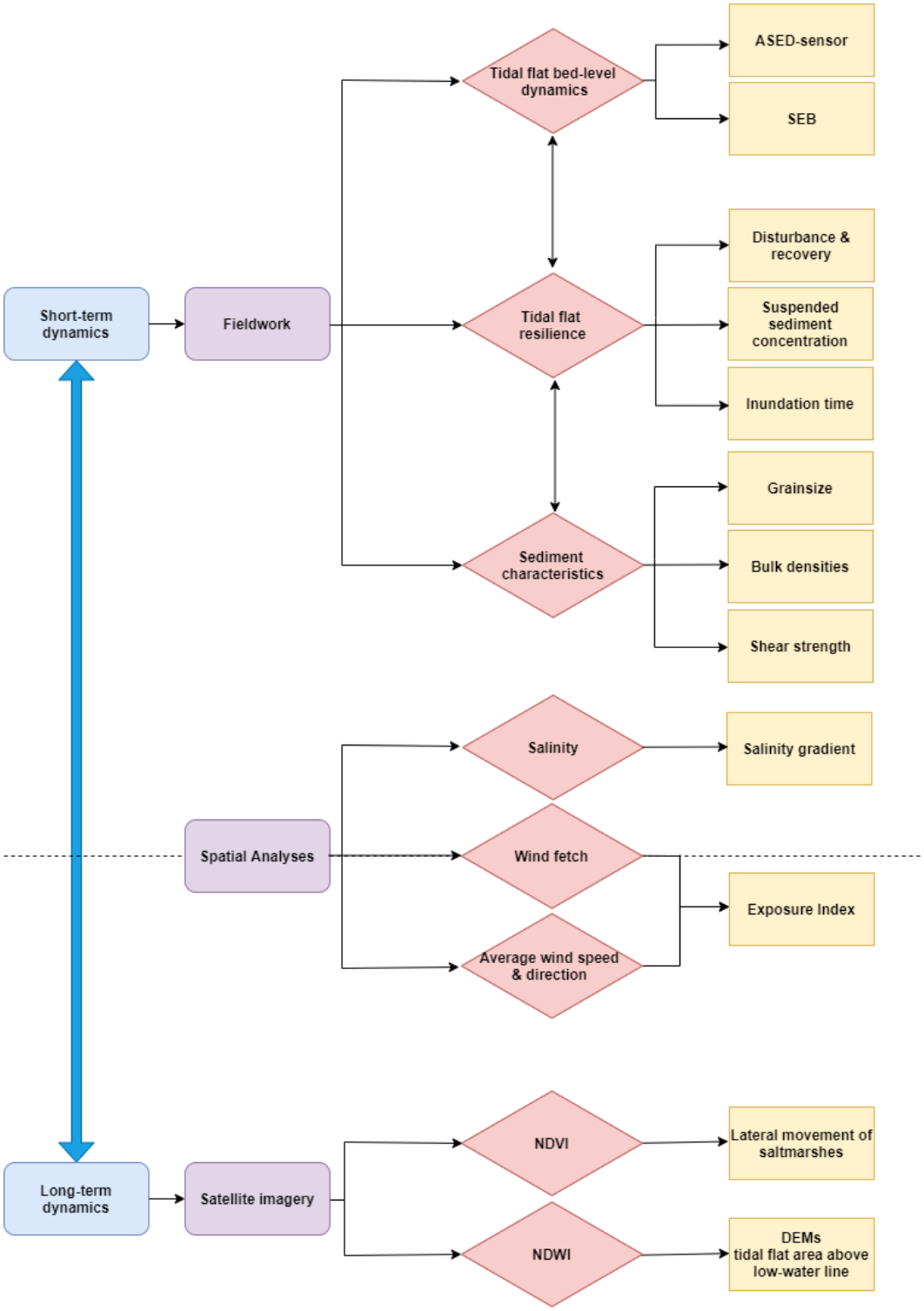

Figure 13 - Flowchart of the research outline. The research is divided over long- and short-term dynamics. During the fieldwork, ASED-sensors and the SEB were used to obtain measures of the tidal flat bed-level, proving information of daily erosion/ deposition in the area. sediment samples were taken to analyse the sediment characteristics. Moreover, the resilience of the tidal flats has been researched and linked to different tidal flat properties. Spatial analyses have been executed to understand the influence of the environmental indicators to the locations. Satellite imagery analyses for seasonal and long-term (~30 year) are used to determine the trajectories of the intertidal area.

4.1 Long-Term analyses

4.1.1 The exposure of the saltmarshes to wind

Waves are for a large extent driven by wind and its impact can significantly affect the morphology of the intertidal area. Consequently, it is important to understand the influence of wind dynamics on the tidal wetland morphology. For this, the degree of exposure to wind for the different locations should be considered. This factor is dependent on the wind fetch, the wind direction and the frequency (Mason et al., 2018). The wind fetch (km) is calculated in RStudio in combination with coordinates gained by use of ArcMap. Along the saltmarshes' edge multiple points were used as input to calculate the length of the wind fetch from those points. Assumed is that the maximum fetch length is reached at the North Sea border. The frequencies of the wind speed and directions have been calculated with RStudio by using 30 years of data (1989 – 2019) as collected by the KNMI at their climate station in Vlissingen for the Western Scheldt and station Oosterschelde for the Eastern Scheldt (KNMI, 2019). Subsequently, the Average Wind Exposure was calculated by use of equation (1) (Keddy, 1982). The average wind velocity is in $km \cdot h^{-1}$, the frequency in Hz and the fetch in km. The exposure has been calculated for a 30-year period (1989 – 2019), for both summer and winter conditions and the yearly total.

$$Average\ Wind\ Exposure = Average\ Wind\ Velocity * Frequency * Fetch \quad (1)$$

To normalize this data, the maximum outcome of the Average Wind Exposure has been set to index value 1, and all the other winter and summer values have been calculated as a relative to this value. The same procedure has been executed for the yearly total values. The calculated values represent the Exposure Index (EI). Based on the outcome of the yearly exposure index, the tidal flats are labelled as being 'Exposed' or 'Sheltered', visually divided.

4.1.2 Saltmarsh and adjacent tidal flat trajectories over 30 years

For the long-term dynamics (~30 years) of tidal flats, analyses of satellite imagery were conducted. Satellite images from Landsat 5 and 7 were deployed to gain a continuous dataset since 1984 to 2017 (Appendix A). Each image is selected on base of their geographic location (Western- and Eastern Scheldt and zoomed in on the specific area of interest; the tidal flat area from dyke to main tidal channel) and its cloud content, which must be ≤ 30 %. Moreover, only Landsat scenes with the highest available data quality (Tier 1) are placed into the collection category and considered suitable for time-series analyses. Images with lower quality could for example cause shifts in projection and were therefore classified as unsuitable for this research. With the images, the Normalised Difference Vegetation Index (NDVI) and Normalised Difference Water Index (NDWI) have been calculated.

The Normalised Difference Vegetation Index (NDVI) analyses

The Normalised Difference Vegetation Index (NDVI) quantifies the health or structure of the vegetation. It is the index of greenness ranging between -1 and +1. The negative values indicate the presence of water and positive values account for vegetation. More positive values account for healthier vegetation, or increasing biomass (Tucker, 1979). The NDVI calculation is based on the physics of light reflection and absorption of the electromagnetic spectrum (equation (2)). Healthy vegetation reflects light strongly in the near infrared band, while it absorbs almost all the visible red

part of the spectrum hitting the vegetation. For unhealthy vegetation, relatively more light is reflected in the visible spectrum, accounting for the difference in the imagery.

$$NDVI = \frac{NIR\ (Near\ Infrared) - RED}{NIR + RED} \quad (2)$$

The NDVI calculations were executed in Python on the Landsat images of the research area since 1984. All the imageries are averaged together over time intervals of three years. The band combination as applied for the vegetation analyses are SWIR1 (band 5), NIR (band 4) and RED (band 3) (Appendix A). Satellite imagery data has been obtained from 1984 to 2018, from imagery of the newest Landsat satellite in operation, between Landsat 5 and 7 (Appendix A). A classification procedure for the saltmarshes was used to make decisions for the pixels which are assigned as being saltmarsh vegetation. This is important to exclude algae blooms that may occur on tidal flats (Van der Wal, Wielemaker-van den Dool, & Herman, 2010), which would otherwise be detected as saltmarsh vegetation (Laengner et al., 2019). Consequently, salt-marsh vegetation is defined as NDVI ≥ 0.3. The other classification is executed for all NDVI < 0, which is assigned as water. These classifications are executed for all the satellite images (figure 14).

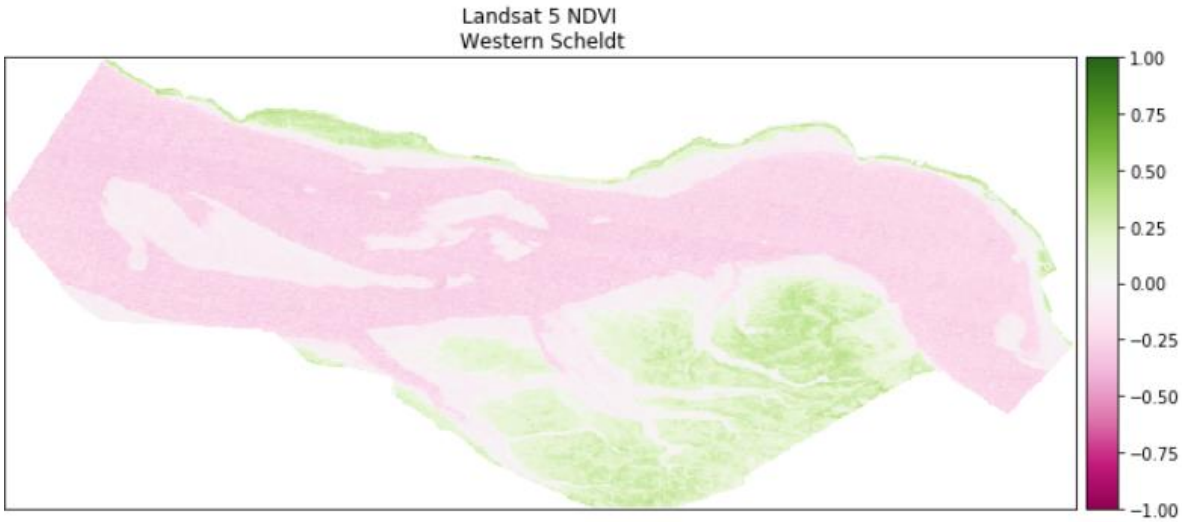

Figure 14 - NDVI from the Western Scheldt, by use of a Landsat 5 image. Pink shows water, light green 0-0.3 shows algae and green > 0.3 vegetation. The greener the vegetation, the healthier the vegetation.

After the NDVI calculations of all satellite images have been executed, the satellite imageries were averaged over periods of three consecutive years. Lateral movement in the intertidal vegetation over 30 years is quantified, by comparing images over a three-year time interval from 1984 to 2017 for the Western Scheldt and 2014 for the Eastern Scheldt due to data availability. Also, to avoid overestimation of the saltmarsh area due to benthic algae blooms, a threshold of > 20% vegetation is set on the pixel over the three-year averaged image (Laengner et al., 2019). The vegetation abundance and location of its boundary differs seasonally, affecting the morphology of the intertidal area. In the final stage of these calculations and with the above-mentioned threshold, only the vegetation values have been selected. To all the pixels with NDVI ≥ 0.3, the value 100 has been assigned, to distinguish them from the other unvegetated pixels. Subsequently, these pixels were converted to area (km^2) and visualised using RStudio.

Hypsometric analyses

In order to gain an idea of the height of the tidal flats, a hypsometric analysis has been performed per steps of three years, corresponding to the NDVI long-term analyses. DEMs were analysed for this, gained by satellite imagery analyses of Landsat 5 and 7 images. The images were downloaded by use of Google Earth Engine. These images where corrected atmospherically (LEDAPS), for their cloud, shadow and snow content (CFMASK) and provided with surface reflectance images, filtered on the best quality (Tier 1). This provided with a GREEN, RED, NIR and SWIR band as a raster file. The areas of interest have been manually drawn in ArcMap as polygons, by the visual observation of the tidal flat extend. The bands are now clipped to the extent of the polygon. Next would be the Normalised Difference Water Index (NDWI) calculation to classify water and land (equation (3)) (Murray et al., 2012).

$$NDWI = \frac{Green - NIR}{Green + NIR} \quad (3)$$

However, when using this normal NDWI calculation, the reflectance between turbid (river) water and wet soil (figure 15) in the GREEN and NIR band is minimal. This could be problematic for tidal flats within estuaries because, even when the area between the low-water line and the high-water line is not submerged, the soil is very wet. Subsequently, the outcome of calculation (3) would not give an unambiguous water/ land classification. Therefore, a new NDWI calculation specifically altered for the use in turbid tidal areas has been proposed (equation (4)) (Grandjean, 2020, internal communication).

$$NDWI = \frac{Green - (NIR + SWIR)}{Green + (NIR + SWIR)} \quad (4)$$

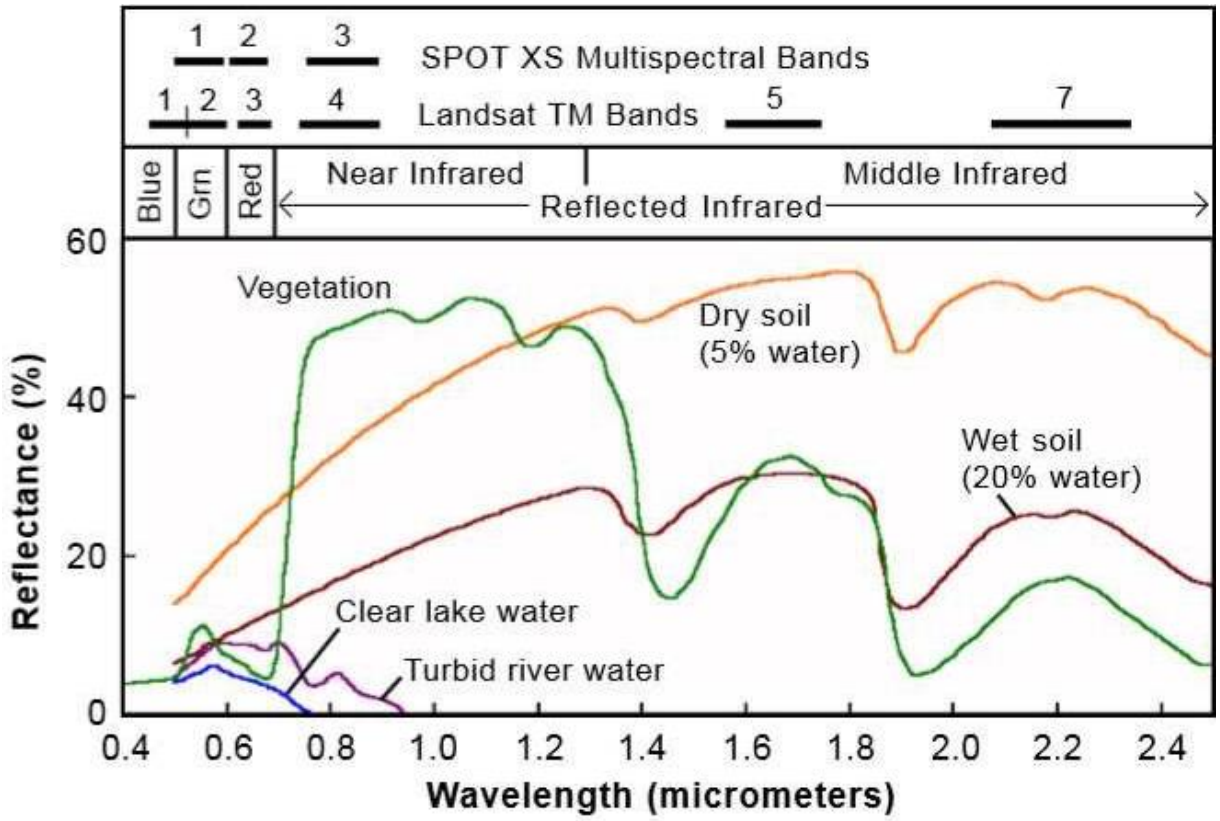

Figure 15 - Reflectance (%) values over different wavelengths, for vegetation, dry soil, wet soil, turbid river water and clear lake water (Jadhav & Patil, 2014).

After applying equation (4) on the images, the NDWI is converted to water masks and errors caused by clouds are removed from the water mask, to get a clean image (figure 16).

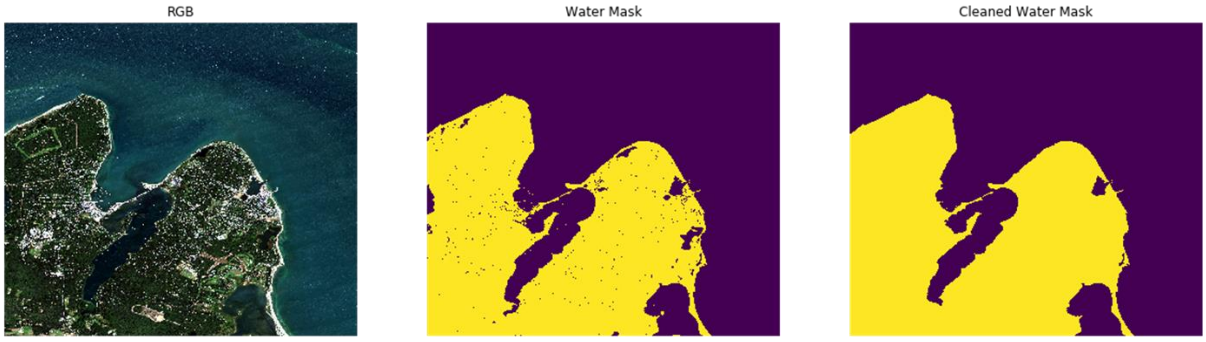

Figure 16 – Conversion from water index to water mask to water mask without errors (Gleason, 2018).

Form *worldtides.info*, modelled water levels for the areas for the same moments as the satellite images where taken have been retrieved. The land area is now classified with these modelled water levels. The images are manually checked for misclassifications and if found, these images are removed from the database. From the water height, the height of a certain location has been determined. The water has the 'tidal height' and the location on the land to where the water comes has that same height. In this way, the land receives an elevation. The masked images are now stacked together, from lowest elevation to highest elevation. With this data, the area for each height can be subtracted, and used for making hypsometric curves.

The percentage of vegetated area per tidal flat has now been calculated for each tidal flat within this research for a 30-year period. This calculation resulted in the relative vegetation change (%) for each area between 1988 and 2014. To analyse the correlation between the observed trends in relative vegetation change and EI, the correlation coefficient has been calculated using RStudio.

4.2 Short-term Analyses

To examine the possible correlation between tidal flat properties, sediment dynamics and resilience and long-term saltmarsh trajectories, measurements were executed at each tidal flat. The tidal flat dynamics have been measured site specifically by using the ASED-senor and a SEB. Per tidal flat, three fixed locations were chosen perpendicular to the saltmarsh edge: at 25, 100 and 200 meters (figure 17, Appendix B). Choosing multiple locations helps to understand the different behaviour of sediment on tidal flats and the influence of inundation time. Fixed distances were chosen over percentages due to the nature of some of the flats in terms of accessibility.

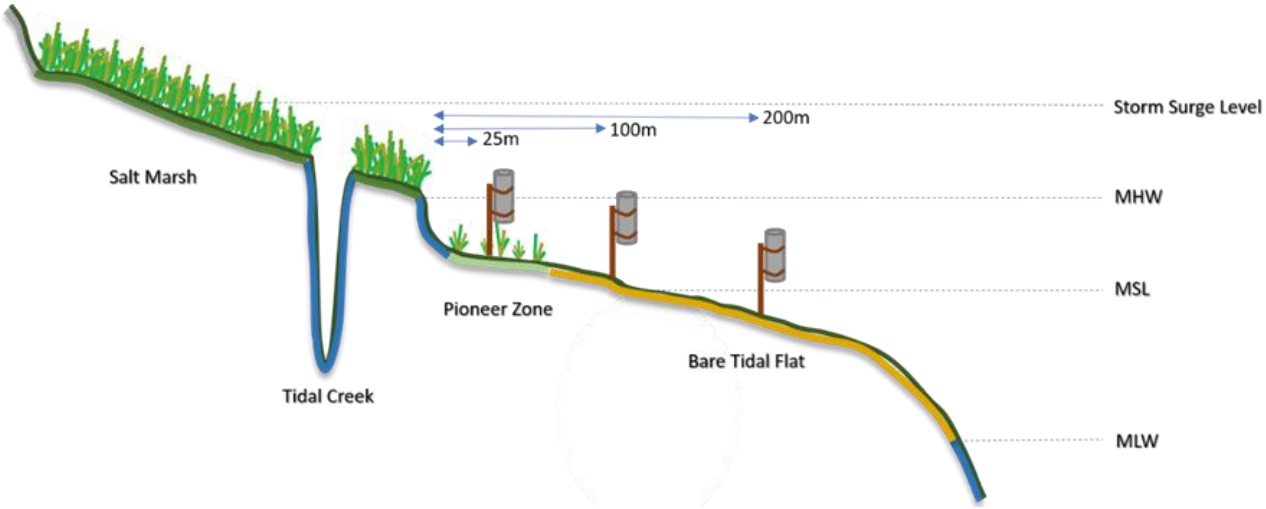

Figure 17 – Field locations for each study site where the measurements will take place. On these locations, the SED sensors have been placed, the (sediment) samples were taken and the flume experiment has been executed. Sketch after (Cleveringa, 2014; Dijkema et al., 2001).

For obtaining the field data, multiple field campaigns were carried out during the winter of 2019/ 2020. The first campaign happened in the second half of December, the rest with an interval between one day to eight weeks later up to and including March 2020, depending on the type of research.

4.2.1 Site Specific Tidal Flat Properties

Sediment Properties

In the area surrounding the ASED-sensors, five bulk density sediment samples have been taken during multiple field campaigns. The first campaign happened during the second half of December, and this was repeated every six to eight weeks up to the end of March. They were randomly taken of the top 3 cm bed layer, besides or behind the ASED-sensors to minimize disturbance to the sensor. The samples were weighed (wet weight) and put in a -18°C freezer for at least 48 hours, where after they were put in a freeze dryer (+ 0 atm), also for at least 48 hours or until all the water was evaporated and weighted again. Proving with the data necessary to calculate the Wet Bulk Density (WBD) (equation (6)) and the Dry Bulk Density (DBD), (equation (7)).

$$WBD\ [g/cm^3] = \frac{Mass\ of\ wet\ sediment}{Volume\ of\ sediment\ sample} \quad (6)$$

$$DBD\ [g/cm^3] = \frac{Mass\ of\ dry\ sediment}{Volume\ of\ sediment\ sample} \quad (7)$$

Following, the samples were and carefully homogenised over a 1 mm sieve and put up for grain size analyses. This analysis has been done by use of a Laser Defraction Analyser*, the Malvern Mastersizer 2000.* This instrument has a detection range of 0.02 – 2000 µm. This analyser works with the principle of light diffraction. A small amount of the homogeneous sediment is put in the stirring water column of the machine during this step, possible clumps of sediment will fall apart. The laser diffractor emits light beams which will be scattered back into space by the sediment particles. Besides the light source, the size and optical properties of the particles are decisive for the angle and intensity of the scatter. The calculation of the particle size is thereafter executed by using physical properties of Rayleigh- and Forward scattering, for which the calculation is based upon the Mie-theory. To account for both bigger (> 63 nm - 2000 µm) and smaller (≤ 20 nm) two light sources are used by the Mastersizer: consecutively a 632.6 nm red Helium Neon laser and a LED blue (NIOZ (2020), Internal communication). The shear strength was also measured during the field campaigns. The method and results can be found in appendix C and N.

All the acquired sediment data have been statistically analysed in RStudio. The data was visually tested by a boxplot analysation. A Tukey Honestly Significant Difference (HSD) test was applied to determine whether the results from the individual samplings were significantly different. Because the Tukey HSD test assumes normality, a visual test has been performed (Quantile-Quantile-plot (QQ-plot)), showing the fit of the data points to the normal distribution line and a statistical test is conducted by performing a Shapiro-Wilk normality test. The significance of the data between the two measurements was tested by a paired t-test. The *Lm* function (equation (8)) has been applied to check how external factors (the location, distance from the saltmarsh edge and the field campaign) were determinative for the outcome of the data.

$$Model = lm(value \sim mudflat + distance + Fieldcampaign, dataframe) \qquad (8)$$

The correlation between different sediment properties was examined by applying a Pearson's product-moment correlation coefficient.

4.2.2 Site Specific Short-term Sediment Dynamics

Short-term bed-level change has been measured with both a vertical and temporal frequency. To understand the behaviour of the sediment on the tidal flats, and possible observed differences in the tidal flat dynamics between different locations with their specific traits, multiple ASED-sensors (figure 18.A & B) have been placed. These sensors measure the daily bed-level dynamics with an accuracy between 2 and 4 mm and uses acoustic pulses of approximately 300kHz (Mus, 2019). When the sensor is submerged, the signal is reflected by the bed and is detected by its sudden increase in amplitude. The travel time of the signal from the sensor to the bed and back to the sensor is converted to a distance, which is used to obtain bed levels relative to the initial height of the sensor relative to the bed level (Mus, 2019). The retrieved datapoints have been processed by their net change in Python.

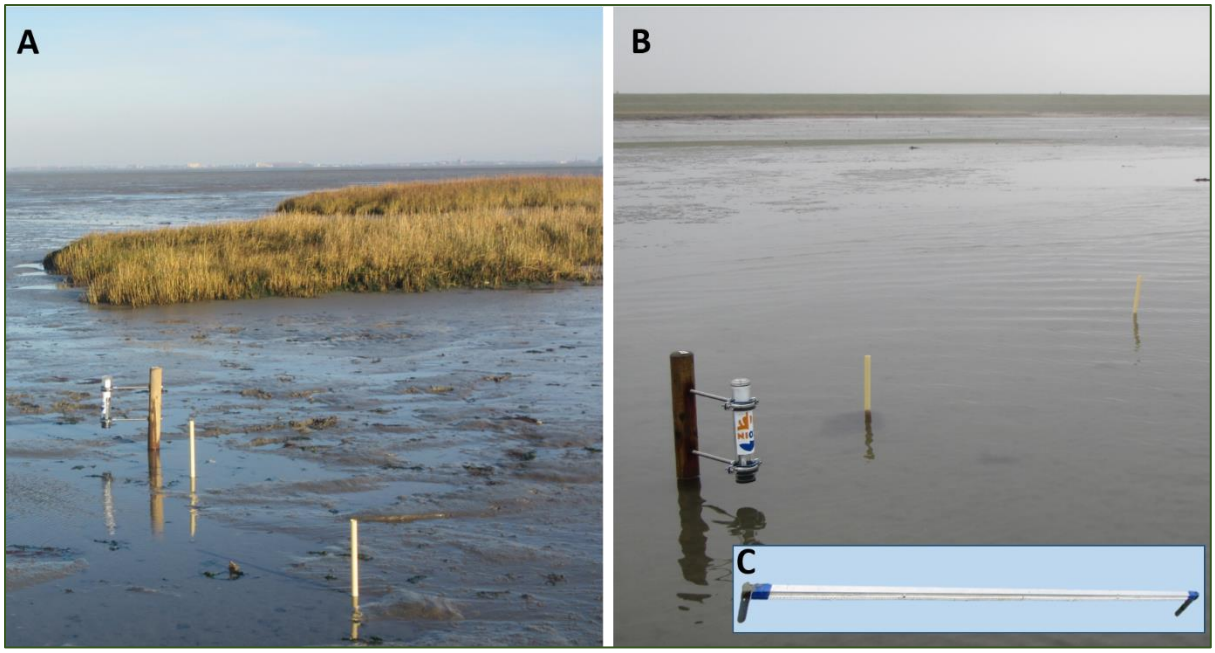

Figure 18 - ASED sensor in the field, during low water (A) and high water (B). The measurements are done in situation (2). Next to the SED sensor, two yellow tubes are located, the SEB (C) is placed over these tubes to measure the relative height.

Despite their high spatial resolution, ASED-sensors are liable to errors. To keep being able to monitor bed level dynamics, SEB's (figure 18.C) have been placed next to the ASED-sensors (Hu, Lenting, et al., 2015). With this devise, short-term surface elevation change can be measured manually (Van Wijnen & Bakker, 2001) with a vertical resolution of 1.5 mm (Nolte et al., 2013). Two poles were placed 1 m deep in the sediment, 2 m apart, horizontally aligned and levelled. During each measurement, a 2 m long (mobile) bar is placed over the poles. With a ruler, the distance between the bed and the bar is measured for every 10 cm. By comparing the values to the initial value, the distances gained during the first field campaign, relative bed level change has been quantified. The measurement at 10 and 190 cm can be an over estimation of erosion, because the pole changes flow velocity and turbulence (Veihe et al., 2011) and may subsequently lead to scouring of sediment. These two measurements were therefore left out of the calculations. The bed-level change has been calculated in RStudio by taking the average value from the 20 to the 180 cm measurement, and calculating the standard deviation, to show how close the individual measurements were related. The change in bed level has been calculated as the subtraction of each measurement by the previous bed level. This way, the data representation shows the erosion or accretion per timestep, for each tidal flat and each distance from the saltmarsh edge. Within this data visualisation, the moments the winter storms hit the Netherlands have been highlighted to observe the influence of extreme events on the systems.

4.2.3 Site Specific Recovery after induced disturbances

The resilience of the different locations is measured by executing a disturbance experiment and analysing the recovery. To determine the design of the experiment in terms of its spatial and temporal scale, a pilot study has been carried out (Appendix D).

The main disturbance/ recovery experiment started on the 28th of February 2020. First, the experiment was carried out at the locations in the Western Scheldt, until the 18th of March. Subsequently, the experiment was repeated for the Eastern Scheldt locations stared the 27th of February, until the 18th of March. For the setup of the experiment, holes where dug until a bucket of

20 L was filled with the sediment. Thereafter, this sediment was carried 5 m further (along the same horizontal 'line' of the ASED-sensor and used to build a pile (figure 19). This was repeated five times. In both the holes and piles a pole was placed. The length of the pole was measured, together with the length of the pile or hole relative to the bed (figure 20). The measures following this initial one, only measured the length of the pole. These measurements could then be linked to the initial reference value. The heights of the piles and holes have been measured during multiple follow ups, until the location was fully recovered (back to the original state) or no further changes where observed for multiple tidal cycles.

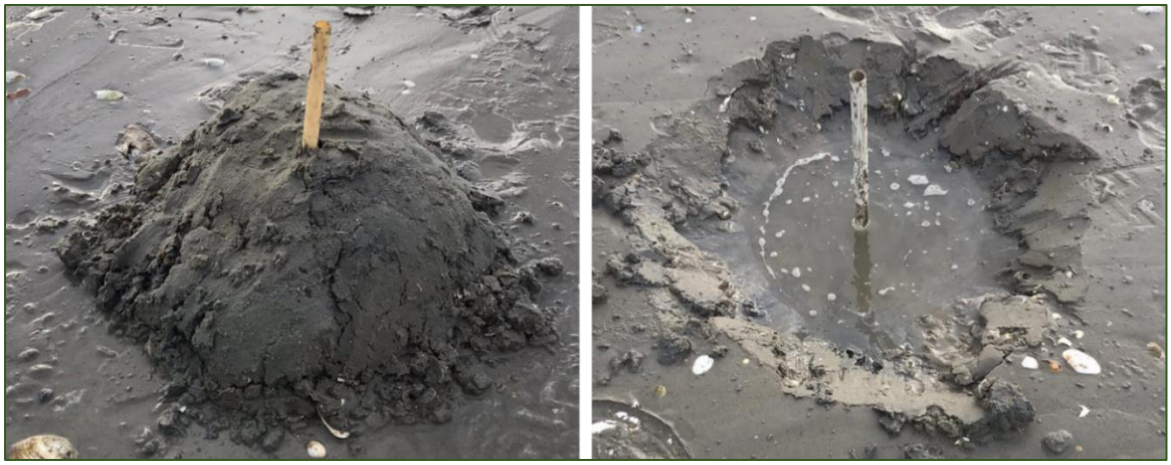

Figure 19 – Disturbance and recovery experiment. Left a pile and on the right a hole.

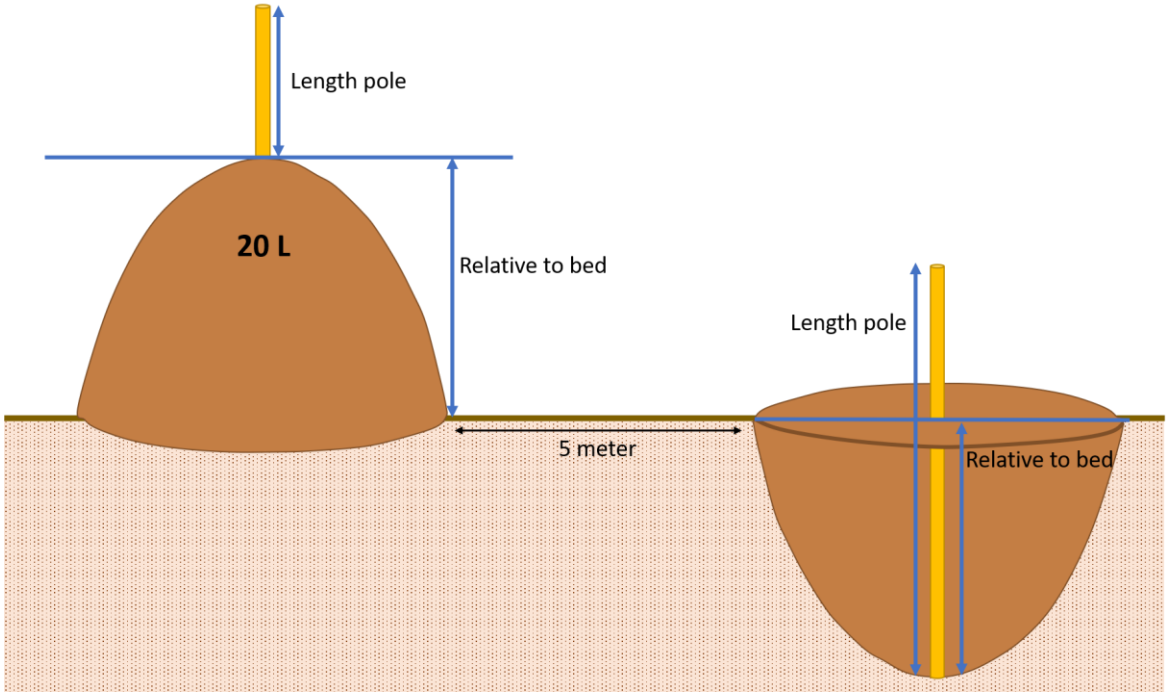

Figure 20 – Schematic of the disturbance and recovery experiment. Left is the visualisation of the pile, and right the hole.

Data Analyses

For analysing the obtained field data, RStudio has been used. The height of the piles and the depth of the holes have been put against time (tides). Analysing the data, replica 4 hole and 5 pile of DM had to be considered lost within the measuring period. From visual observation and mathematics, most of the data seemed to have an exponential relationship, as explained by equation (9), calculating the

base (a) and the exponent (b), x represents the amount of tides passed. Together with the function, the best fit of the model (R^2) has been found by applying the nls-function in RStudio.

$$a * exp(b * x) \quad (9)$$

To calculate the recovery rate (λ) following the disturbances, equation (10) has been applied (Van Belzen et al., 2017). In this equation, Δt is the duration of the experiment (tides) and f is the fraction of recovery.

$$\lambda = \frac{-\log(1-f)}{\Delta t} \quad (10)$$

The method originally used by van Belzen et al. (2017) has been altered for this study, since they applied the method on biomass recovery, instead of sediment recovery. Biomass is unlikely to erode after the initial disturbance event and will only recover, while sediment is prone to both accretion and erosion. Consequently, f is determined relative to the undisturbed bed-level (measured by the ASED-sensor), using the mean values of the five replicas per tidal flat and per distance (figure 21).

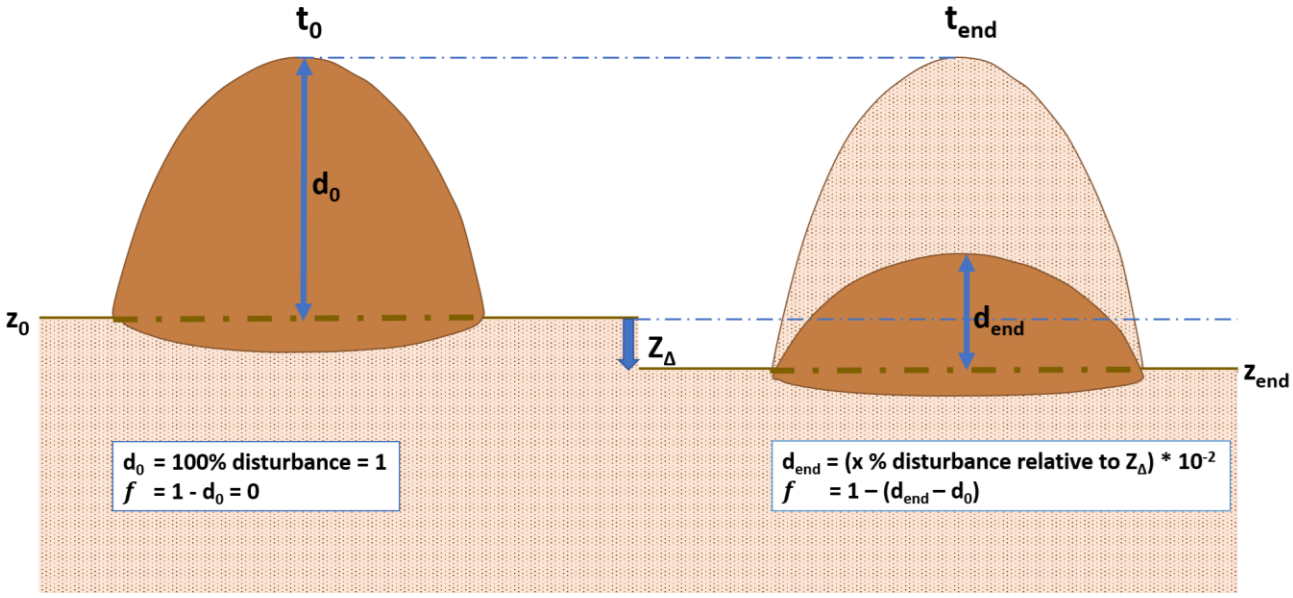

Figure 21 – Schematic of the recovery value f, which is determined by the disturbance at t_{end} relative to the initial disturbance d_0. The value of f is calculated to a fraction.

It is important to work with f values ≤ 0.9, but also as close to 0.9 as possible in equation (10). When the disturbance is fully recovered, it is not certain when this happened exactly. It is therefore important to include the measurement uncertainty in f which is expected to be between 5 and 10 %. To accommodate this, f must be calculated for measurements where the disturbances of the bed-has not yet reached full recovery. To increase the reliability of the data, it was important to find these f-values after ≥ 4 tides (Δt). Because $\Delta t \leq 4$ and/ or $f > 0.9$ for the recovery at RL 25 and 200 m and the technical deficit for the ASED-sensor at RL 100, this tidal flat has been taken from further data analysis. After collected the correct data with the best f- values, it was statistically analysed in RStudio. The recovery rates of both piles and holes were examined for the correlation between them but also with the average tidal flat properties, distance from saltmarsh edge and the EI, by applying a Pearson's product-moment correlation coefficient.

5. Results

The results regarding the long-term vegetation patterns and short-term sediment dynamics are stated and statistical comparisons are shown.

5.1 Long-term Analyses

5.1.1 The exposure of the saltmarshes to wind

The results following from analysing the wind direction and frequency over a 30-year period (1989 – 2019) show that the Eastern Scheldt experiences higher wind speeds more frequent, compared to the Western Scheldt. Moreover, while at both locations the preferred wind direction is to the southwest, the preference at the Western Scheldt is slightly more to the west. During the summer months, the frequency of higher wind speeds decreased for both the Eastern- and Western Scheldt relative to the winter months, with the preferred direction being west-southwest, but an increase in northward frequency (Appendix E). The results from the fetch length and direction for the saltmarshes showed how some locations are never in the preferred wind direction (SW) and the fetch length is limited by land or civil engineering boundaries (figure 22). Consequently, an inland fetch length decrease for the Western Scheldt is observed. Moreover, all fetches except for PP, reach a land boundary before reaching the North Sea.

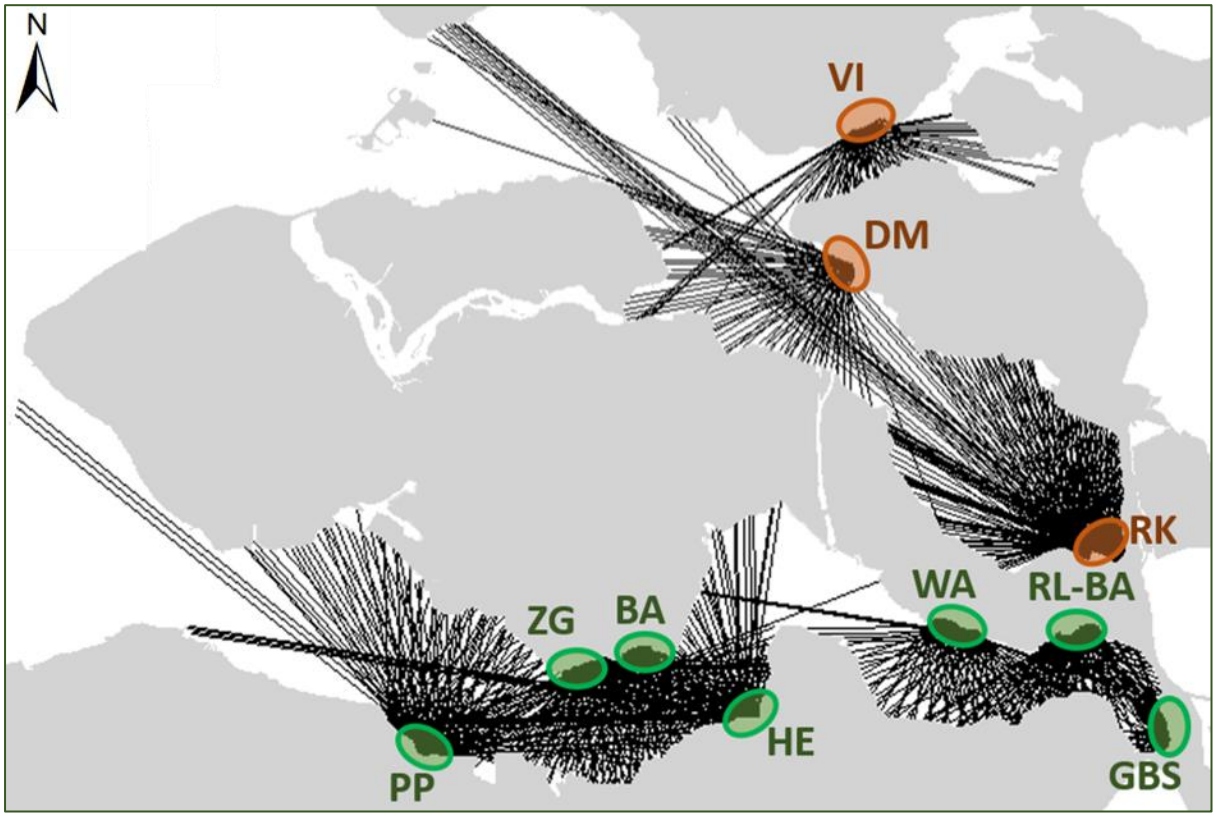

Figure 22 - Wind fetch for the satellite locations in the Western (green)- and Eastern Scheldt (orange).

The Exposure Index (EI) was calculated for 1988 – 2019, combining the wind direction, frequency and fetch length. The results show a decreasing trend further inland and the EI is generally higher for the Eastern Scheldt compared to the Western Scheldt (figure 23). Between the winter values, a clear distinction is observed between high values (ZG, BA, WA, VI and DM) and low values (PP, HE and GBS). The high values show to have a larger difference between the summer and winter EI compared to the low values. RL-BA and RK however lie in between these distinctive values. All locations are visually

divided between being ‘exposed’ or ‘sheltered’ based on their average winter exposure index and the difference between the winter and summer values (≥ 0.2). Due to the last criterium, RL-BA is categorised as an exposed site and RK as a sheltered site during winter (Appendix F).

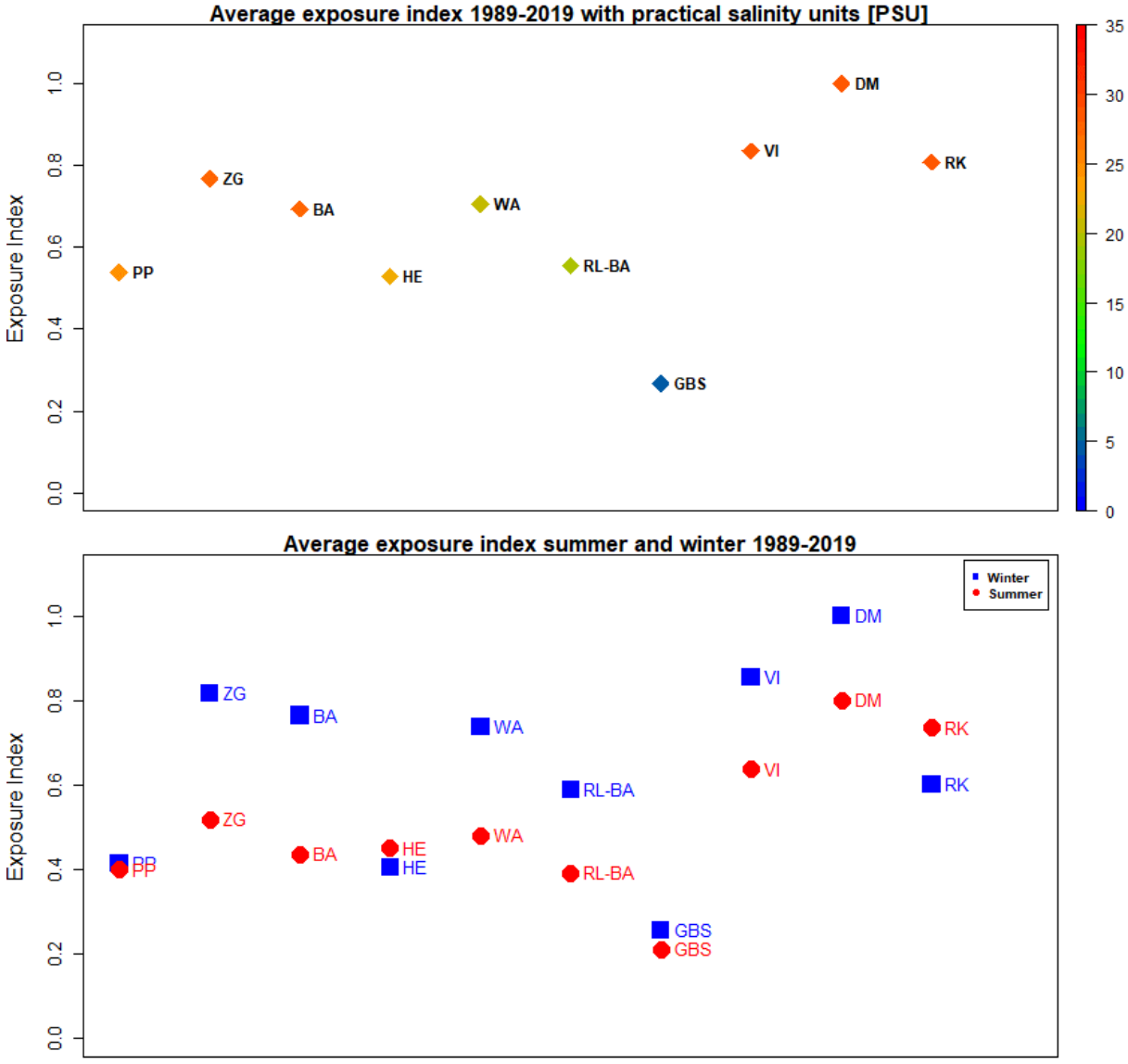

Figure 23 - Wind Exposure Index of tidal flats located within the Western- and Eastern Scheldt. The top graph shows the yearly average over 30 years and the colour of the diamond shapes indicate the salinity [psu] of these areas (Smolders & Ides, 2013). The second graph indicates the exposure for both the summer and winter season. The flats are placed in order from closest to the North Sea to furthest inland.

5.1.2 Saltmarsh and adjacent tidal flat trajectories over 30 years

The results regarding the vegetation trajectories of the past 30 years show how the saltmarsh area responds different for the exposed sites compared to the sheltered sites. The exposed sites show a negative change and the sheltered sites a positive change. This does not account for VI, showing no net change, as observed in figure 24. Besides the net change, cyclic behaviour is observed where the vegetated areas slightly increase and decrease almost alternatingly between each time step (Appendix G). Between the Eastern- and Western Scheldt, the vegetated area changed more in the Western Scheldt sites. Among the two systems, the site with the largest vegetated area is found in the Eastern

Scheldt (RK). This observation deviates from the general trend between both Scheldts where the generally larger vegetated areas are found in the Western Scheldt.
The long-term relative vegetation change and the EI are not significantly, yet negatively correlated (r=-0.501, P>0.05) (figure 24). When removing vegetation change outlier ZG from the data file, still no significant correlation is observed (r = -0.560, P>0.05). Within the Western- and the Eastern Scheldt, the influence of the exposure on the relative long- term vegetation index remains negative, as for the combined correlation. However, it shows a higher correlation coefficient, and a lower probability. The Western Scheldt shows a correlation of -0.729 (P=0.06) and the Eastern Scheldt -0.985 (P>0.05) (Appendix H).

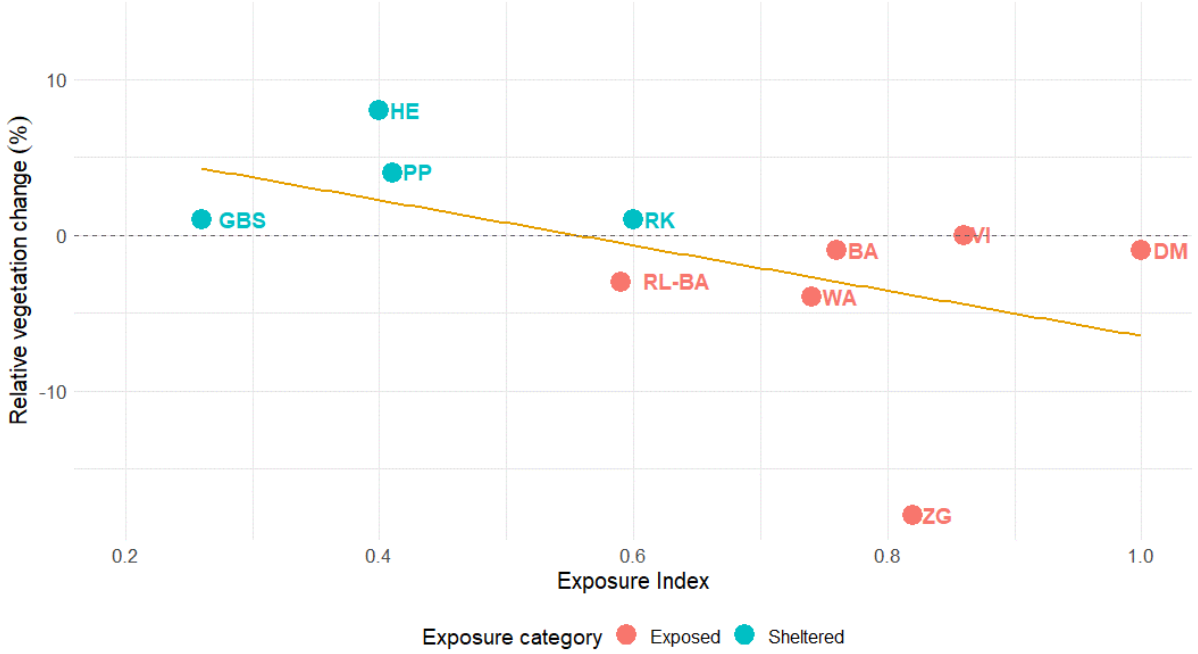

Figure 24 - Correlation between the relative vegetation change (1988 – 2014) and the Exposure Index (r = -0. 501, P=0.14). The data points are coloured by their exposure category.

When comparing the change in saltmarsh, tidal flat and total area, the Eastern Scheldt locations have a significant larger tidal flat and total area compared to the Western Scheldt. Moreover, the exposed sites generally show a larger ratio of saltmarsh versus total area and the fluctuations between the areas per timestep are more pronounced compared to the sheltered sites (figure 25). Comparing the total area with the ratio, often an opposite trend is observed, where an increasing total area and a decreasing ratio are observed in the same time period (e.g. ZG, WA), or a decreasing total area coincides with an increase in ratio (e.g. HE, BA).

Figure 25 - Change in saltmarsh and tidal flat area and the ratio between them per three-year time step from 1985 to 2017. Due to their large extent, RK and VI have a different y-scale. The timesteps are written as 'yy-'yy.

5.2 Short-term Analyses

During the field campaigns, the measured temperature ranged between 0.8 and 8.3°C and the windspeed along the Dutch coast was larger compared to the summer months of 2019. Three storms were measured, which were given the names 'Ciara', 'Dennis' and 'Ellen' (Appendix I). The distance from saltmarsh edge and showed clear resemblance with the inundation time (Appendix J).

5.2.1 Site Specific Tidal Flat Properties

Wet Bulk Density

The WBD data shows that the largest values are found closest to the channels and decrease towards the saltmarsh edge. Moreover, the exposed sites generally show higher values, compared to the sheltered sites (figure 26, Appendix K.i and K.iii). The data is normally distributed (Appendix K.ii), and the Tukey HSD test showed a significant difference between the WBD values collected during December 2019 and January 2020 ($P<0.05$).

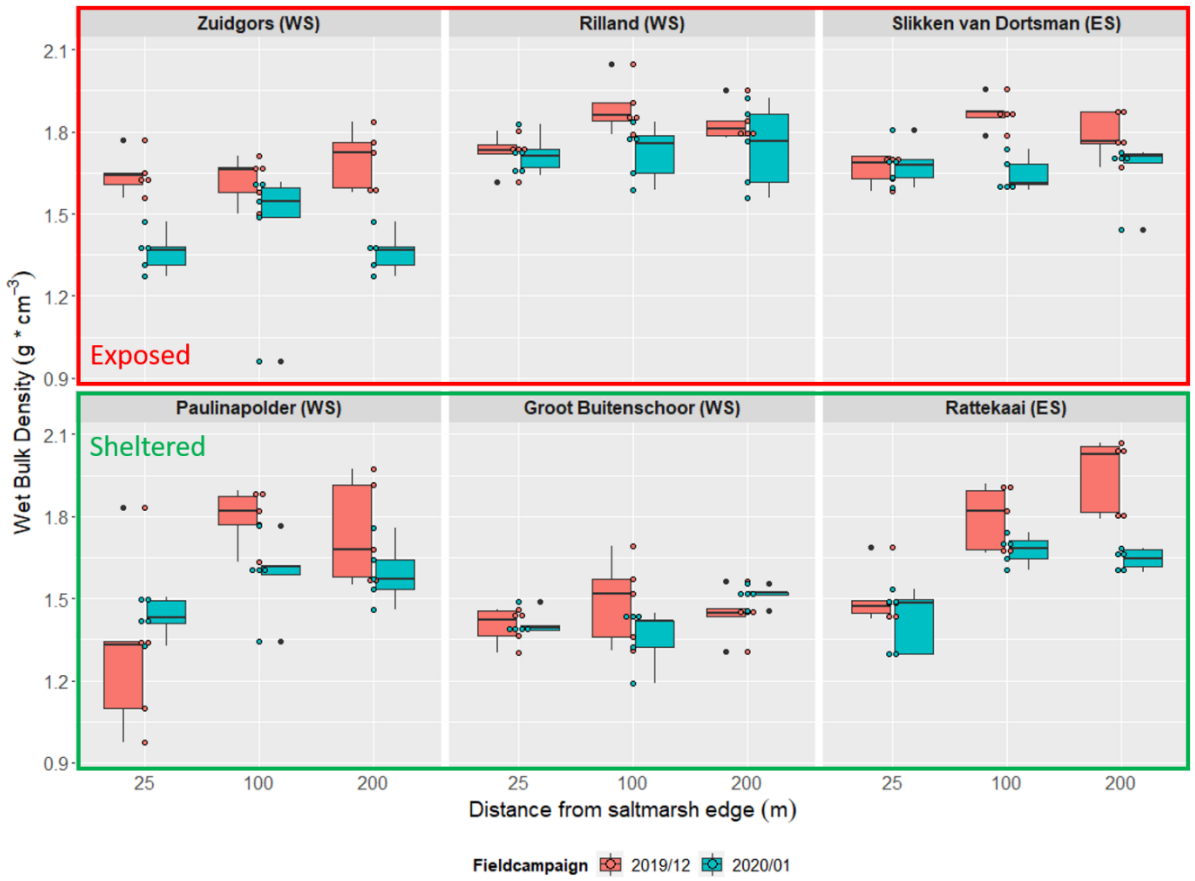

Figure 26 - WBD of the sediment samples taken during two consecutive campaigns, December 2019 (2019/12) and January 2020 (2020/01), divided over the tidal flat and the distance from the saltmarsh. The tidal flats are visually divided over location (Western Scheldt (WS) and Eastern Scheldt (ES)) and exposure category. The coloured dots represent the data points and the black dots outliers in the boxplot.

Dry Bulk Density

The DBD shows to be lowest close to the saltmarsh edge and the highest at 100 m. Moreover, the exposed sites generally show higher values, compared to the sheltered sites (figure 27, Appendix L.i and L.iii). The data is adopted to be normally distributed (Appendix L.ii) and the Tukey HSD test showed a significant effect of the data collection moment on the DBD values with $p<0.05$ between the collection in December 2019 and January 2020.

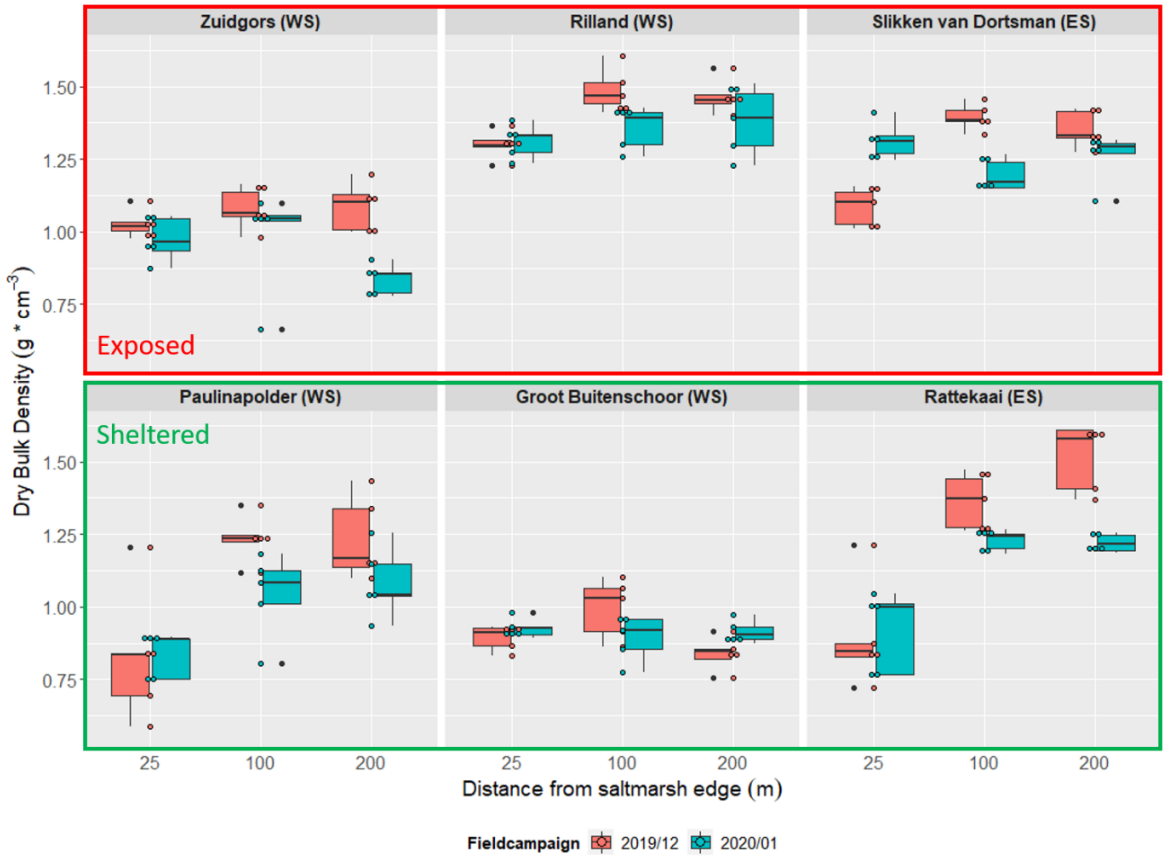

Figure 27 - DBD of the sediment samples taken during two consecutive campaigns, December 2019 (2019/12) and January 2020 (2020/01), divided over the tidal flat and the distance from the saltmarsh. The tidal flats are visually divided over location (Western Scheldt (WS) and Eastern Scheldt (ES)) and exposure category. The coloured dots represent the data points and the black dots outliers in the boxplot

Median Grainsize

The results from the median grainsize analyses showed a decreasing pattern towards the saltmarsh edge. Moreover, the grainsizes at the exposed and the Eastern Scheldt sites where generally larger (figure 28, Appendix M.i and M.iii). GBS and ZG are an exception in the observed fining gradient towards the saltmarsh, where GBS showed similar grainsizes for all three distances and ZG the highest values at 100 m and the lowest values at 200 m. The data is not significantly normally distributed ($P<0.05$) Appendix M.ii). However, combined with the natural occurrence of this data, the Tukey HSD test has been performed, which showed no significant influence of the moment of data collection between two moments during the winter of 2019/ 2020 ($P>0.05$). The average median grainsize over the two campaigns shows a distinction between the silt and sand category (Wentworth scale) for each tidal flat. For the fieldwork locations the distinction between silt and sand appear to be linked to the exposure category. Sediments found at the exposed locations are primarily comprised of the sand fraction whereas at the sheltered sites the sediments are primarily comprised of the silt fraction (Appendix M.i).

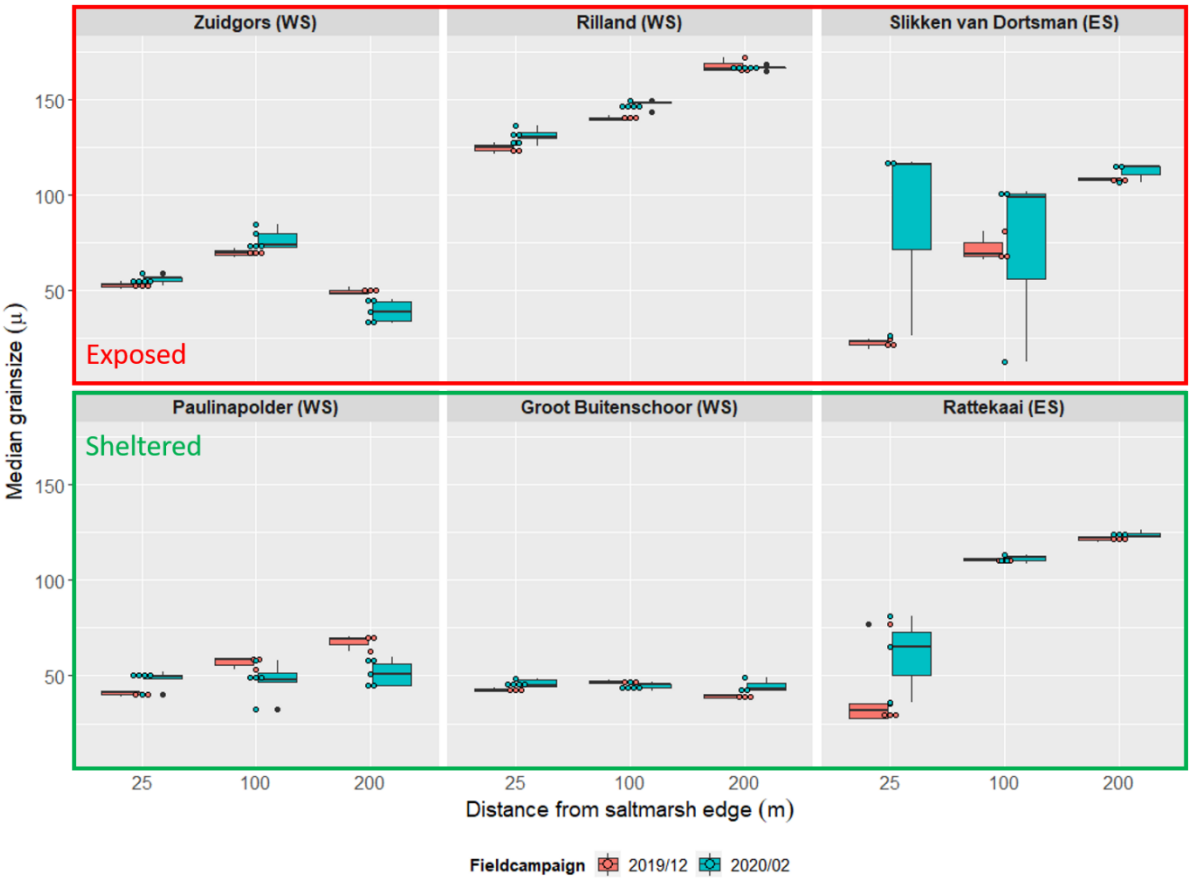

Figure 28 - Median grainsize of the sediment samples taken during two consecutive campaigns, December 2019 (2019/12) and February 2020 (2020/02), divided over the tidal flat and the distance from the saltmarsh. The tidal flats are visually divided over location (Western Scheldt (WS) and Eastern Scheldt (ES)) and exposure category. The coloured dots represent the data points, the black dots outliers in de boxplot.

Correlations Between the Tidal Flat Characteristics

The median grainsize show to be significantly and positively correlated to both the DBD ($r = 0.790$, $P<0.01$) and the WBD ($r=0.641$, $P<0.01$). The WBD and DBD show to have a significant positive correlation ($r=0.949$, $P<2.2e-16$).

5.2.2 Site Specific Short-term Sediment Dynamics

The exposed sites showed to experience more dynamic net change compared to the sheltered sites. The results also show the highest net change at 200 m. For the net change at 100 and 25 m, a different trend is observed between the two exposure categories. The sheltered sites showed higher net erosion at 25 m compared to 100 m, while the exposed locations show an increasing net erosion trend towards 200 m. From all sites, ZG shows the highest net erosion change and PP the least whereas RL shows the highest variability within the measuring period (figure 29).

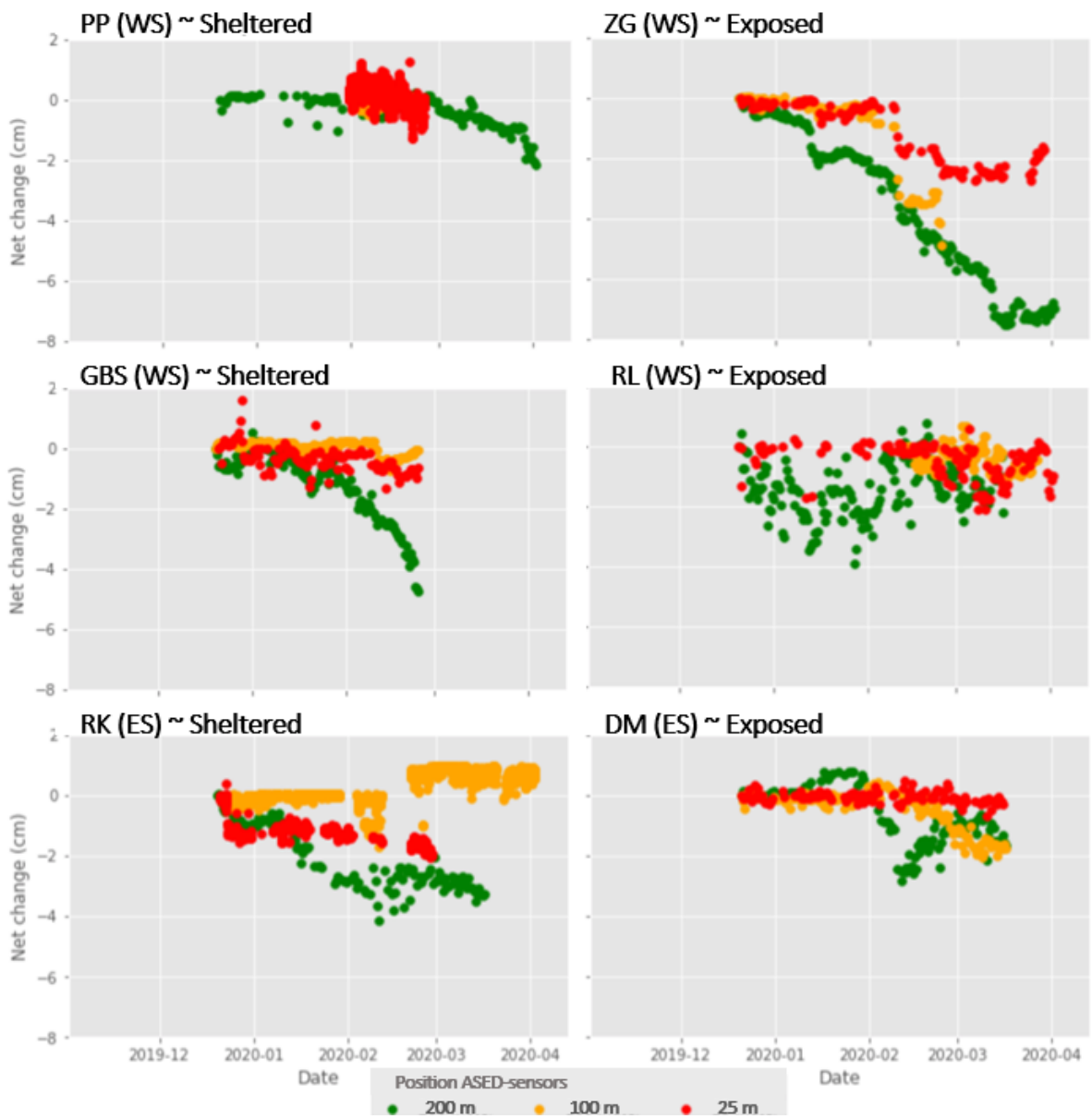

Figure 29 - The net change values as measured by the ASED-sensors at the six different locations. Measurements took place between 20-12-2019 until 18-03-2020. Missing data points in the graphs are the result of (temporal) technical defects in the sensors. The measurements are corrected and visualised by T. Grandjean (2020).

The results from the SEB measurements show a more dynamic bed-level change (higher net change between the consecutive measurements) at the exposed sites compared to the sheltered sites. Also, it is observed how the bed-level dynamics behave different at different distances from the saltmarsh edge, in a similar way as observed for the ASED- sensor results. The highest changes area observed furthest away from the saltmarsh edge (200 m) (figure 30 and 31).

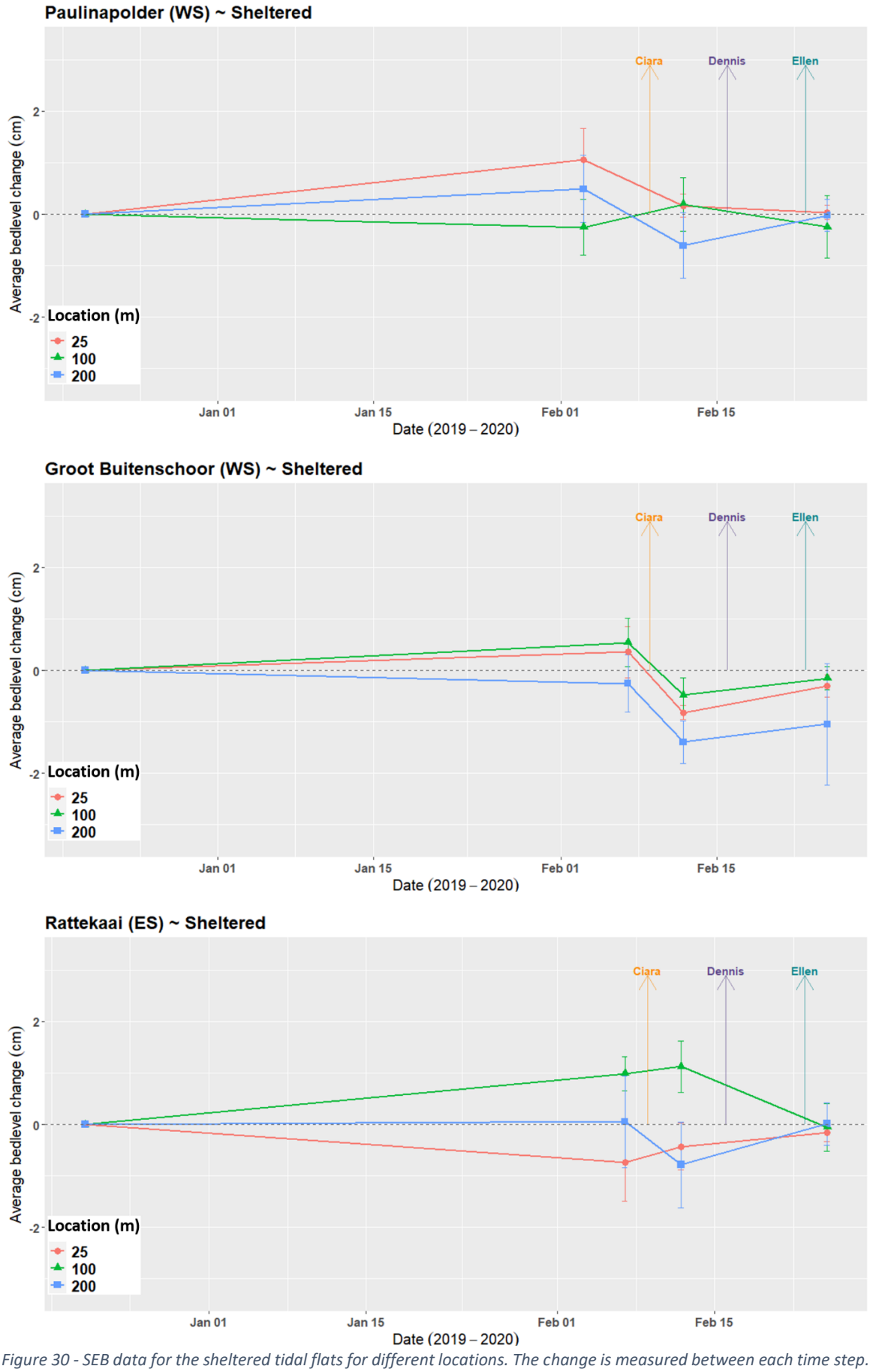

Figure 30 - SEB data for the sheltered tidal flats for different locations. The change is measured between each time step. The moments the three winter storms hit the Netherlands is highlighted by arrows and their name.

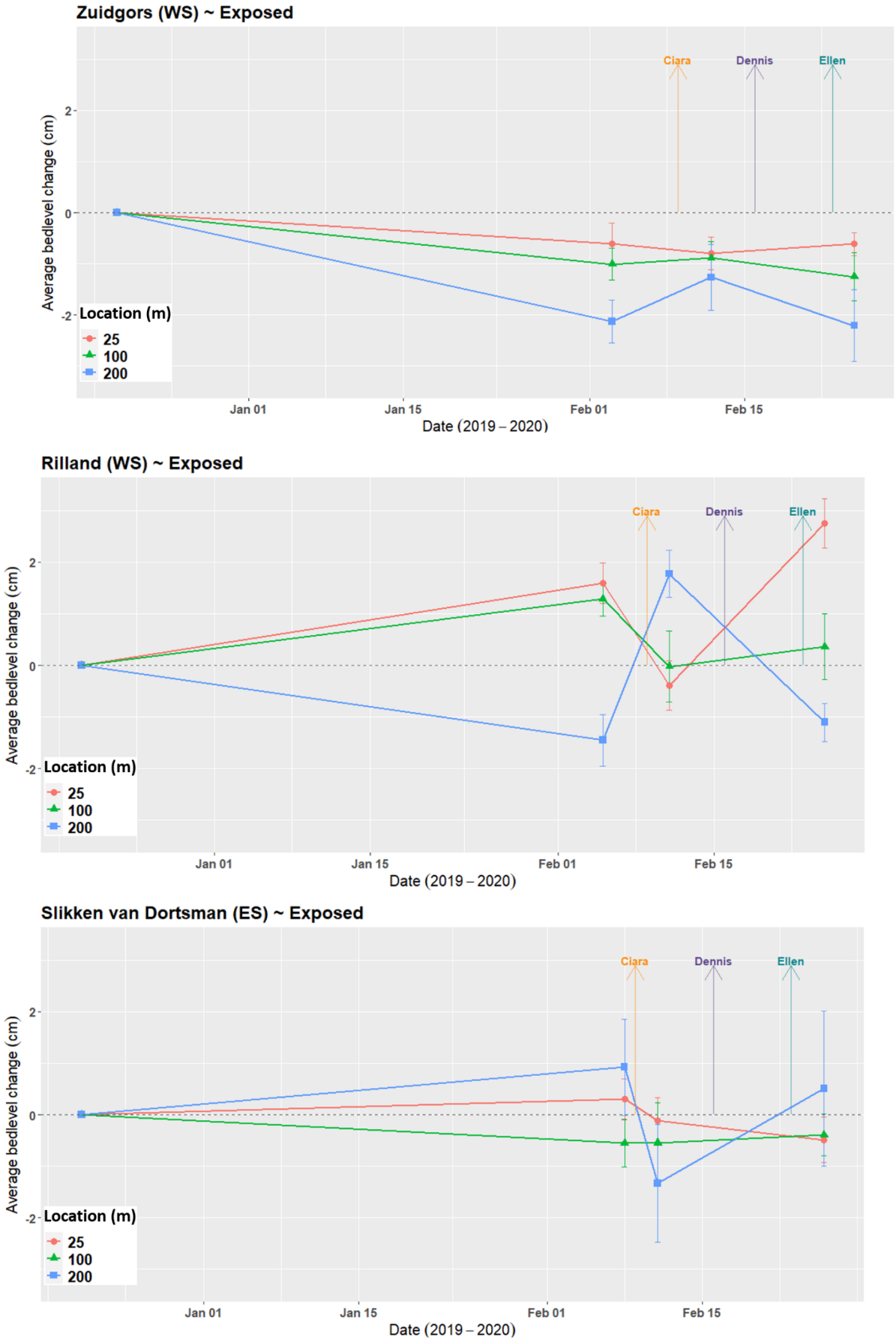

Figure 31 - SEB data for the exposed tidal flats for different locations. The change is measured between each time step. The moments the three winter storms hit the Netherlands is highlighted by arrows and their name.

5.2.3 Site Specific Recovery after Induced Disturbances

Exponential course of the recovery

The results from the exponential fit analyses show that most of the recovery of the induced disturbances follow an exponential approach, although with a different speed for the piles and holes per location. The holes at ZG and the piles at RK formed in exception on the exponential approach. Besides, the recovery has not been completed for most locations within the measured period. Within the measuring period, the exposed sites recovered more often to initial bed-level compared to the sheltered sites. (figure 32 and 33). It is important to note how, after the experiment ended, the recovery furthered for all sites that were not yet recovered within the measured time. PP, ZG and RK/ DM 200 and 100 m were completely recovered relative to the surrounding bed-level. GBS 25 and 100 m showed almost complete recovery. Only DM and RK 25 m were still clearly visible as the disturbances.

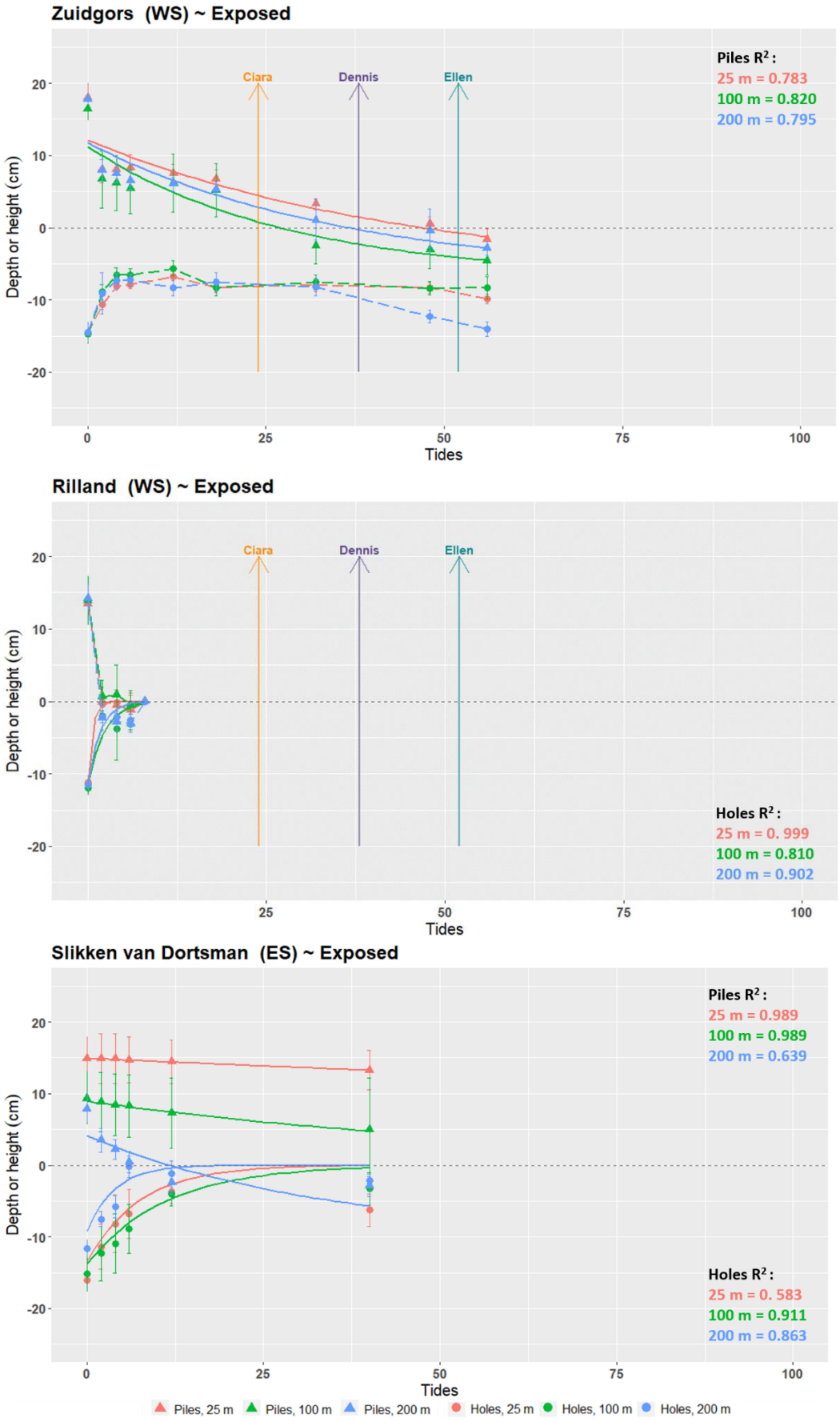

Figure 32 – Erosion of the piles and filling up of the holes for the exposed locations. Height 0 indicates the initial bed-level. An exponential trendline has been plot through the data points. The fit of the models is indicated by the R^2 values.

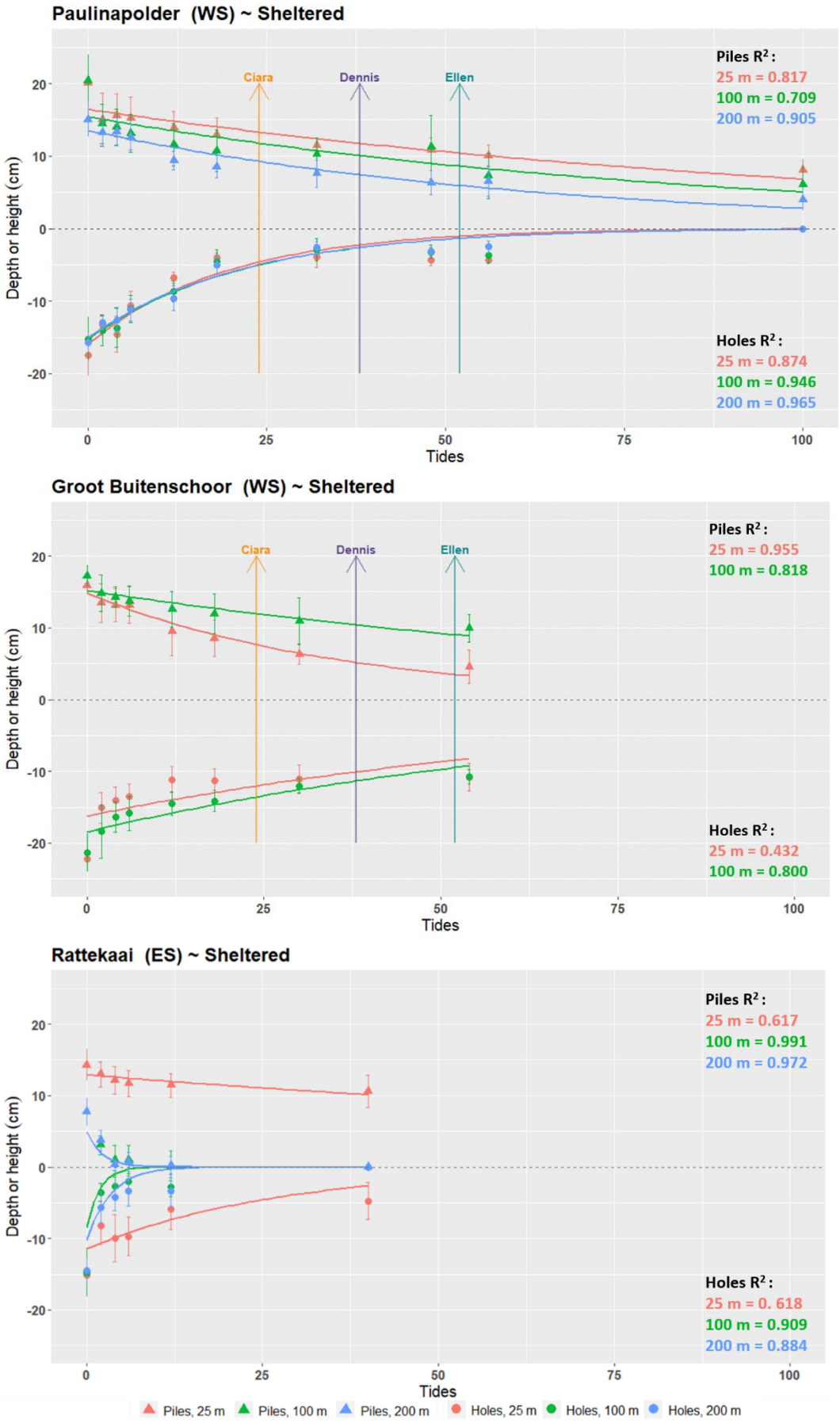

Figure 33 - Erosion of the piles and filling up of the holes for the sheltered locations. Height 0 indicates the initial bed-level. An exponential trendline has been plot through the data points.

Recovery rate after the induced disturbances

The recovery rate data can be found in Appendix O.

Correlations of the recovery rate with the short-term, tidal flat properties

The recovery rate of the piles and the holes show to be significantly correlated (r=0.694, P<0.05) with the piles recovering generally quicker compared to the holes. The median grainsizes showed to be of significant impact to the observed recovery rates for both the piles (r=0.806, P<0.001) and the holes (r=0.837, P<0.001) (Appendix P). It thus shows that locations with a lower grainsize are also the locations were the recovery was slowest.

All tidal flats except GBS show a positive correlation between the recovery rate and the distance (m). Where the recovery rates of the piles and holes are comparable for the Western Scheldt, for the Eastern Scheldt, it is observed that the recovery rates of the holes lie closer to each other while being significantly spread for the piles. The disturbances at the Western Scheldt show a comparable recovery rate between the piles and the holes, while the recovery rates for the holes at the Eastern Scheldt are more spread compared to the piles (figure 34 and 35). A corresponding pattern is observed between the average inundation time and the recovery rates, except for RK, which did show a clear difference for the spreading of the data (Appendix Q). For the Eastern Scheldt, the recovery rate of the piles exceeds the holes for inundation time > 22% , while for inundation time <22%, the holes recover quicker than the piles.

Figure 34 – Relation between the distance from saltmarsh edge (m) and the recovery rate of the piles per individual tidal flat.

Figure 35 - Relation between the distance from saltmarsh edge (m) and the recovery rate of the holes per individual tidal flat.

The DBD shows a positive and significant correlation (P<0.05) to the recovery rates of the piles (r=0.621) and the holes (r=0.729). Between the two systems, the Eastern Scheldt show the best individual correlations and in the Western Scheldt, a large difference in correlation is observed between the piles and holes, whereas the values between the piles and holes in the Eastern Scheldt, are closer to each other (Appendix R).

Correlations with the long-term trends

The exposure to wind related to the recovery of holes and piles shows a general positive trend for both systems. A weak positive correlation between the exposure and the recovery rate was found for the piles (r=0.257, P>0.05), for which the locations being less exposed to wind, showed a smaller rate of recovery (appendix S.i). The correlation for the holes, shows a correlation too close to zero to imply a linear relationship (r=0.059, P>0.05). Dividing the two systems, the EI showed to be significantly positively related to the recovery rate of the piles in the Western Scheldt (r=0.914, P<0.05), the impact of the EI to the recovery of the holes in this system implies no linear relationship, similar to the combined effect (r=0.071, P>0.05) (Appendix S.ii and S.iii). The Eastern Scheldt shows a negative correlation of the EI for both the piles (r=-0.221, P>0.05) and the holes (r=-0.636, P>0.05).

The recovery rates of the piles (r = 0.038, P>0.05) and the holes (r = 0.256, P>0.05) do not show a significant correlation to the vegetation change. A clear distinction is observed between the exposed (negative vegetation change) and sheltered (positive vegetation change) results. A negative relation between the vegetation change and the recovery rate of the piles in the Western Scheldt has been found (r=-0.974, P<0.01). An overall clear and unambiguous trend between the recovery rate and vegetation change of both the Eastern and Western Scheldt was not found from this data (Appendix T).

6. Discussion

6.1 Key Findings

This research aimed for a better prediction of long-term vegetation dynamics on saltmarshes and adjacent tidal flats by studying the short-term sediment dynamics after morphological perturbations to those tidal flats. The impact of long-term exposure to wind and the suspended sediment concentration (SSC) of the system to the short-term saltmarsh (vegetation change) and adjacent tidal flat dynamics (sediment properties and morphology) have been researched. By determining the influences of tidal flat properties, SSC, and exposure to wind on the capacity of tidal flats to recover from disturbances, this research aimed to provide insight into early warning signals for shifts to alternative stable states in complex tidal ecosystems.

The impact of wind exposure suggests that the EI of a tidal flat is indicative for the size of the tidal flat and saltmarsh (larger for higher exposure) and for the dynamics of the saltmarsh area (higher cyclicity and decreasing area over larger time scales for larger exposure). The impact to the recovery showed to be dependant of the system and the hydrodynamic forcing (inundation time), clearly supporting towards the phenomena of critical slowing down in the sediment dynamics of tidal systems. The long-term vegetation change in the two tidal basins suggests towards a relationship between observed saltmarsh trajectories and recovery rate, but no unambiguous trends could be found from this data set.

6.2 Long-term Saltmarsh Trajectories and the Impact of Wind Exposure

The impact of the wind exposure to the recovery did not provide with unambiguous results, yet it has potential to contribute to better understanding of the impact of external energy to the systems' resilience. The recovery rate at the Western Scheldt (positive and stronger for the piles) showed to be opposite to the Eastern Scheldt (negative, and stronger for the holes). These results provide insight in the resulting hydrodynamic influence induced by wind energy. The Western Scheldt, with lower exposure indexes and lower recovery rates shows a quicker recovery at the sites with larger wind exposures whereas the Eastern Scheldt, with overall higher exposure indexes and higher recovery rates, show a quicker recovery for the sites with smaller wind exposures. Connecting this to the daily sediment dynamics, the exposed sites showed more dynamic net change compared to the exposed sites.

Equivalent to the threshold shift for deposition at the exposed sites caused by their higher (wind) energy input, higher flow velocity closer to the tidal channel also brings in more energy to the system. Consequently, the threshold for deposition, and for erosion and transportation of grains changes, depending on the grain diameter (caused by sediment cohesion feedbacks), resulting in increased suspension of sediment and transportation closest to the channel and thereby the highest bed-level change. From the long-term satellite imagery study, it was observed how the exposed sites show a decrease in vegetated area relative to the tidal flat area over time, while the sheltered sites increased or stayed constant in time. Moreover, the area of the exposed locations showed more fluctuations over time, suggesting an alternatingly changing location of the saltmarshes edge, which is in line with the findings of Bouma et al. (2016). The total vegetated area is also generally larger compared to the sheltered ones. This is likely explained through the larger area available for vegetation because of the larger tidal flat area, while the decrease of this area suggests the marsh is experiencing coastal squeeze (Pontee, 2013). This study shows that the EI is associative to the relative vegetation change in the Eastern- and Western Scheldt. Higher levels of exposure to wind result in higher levels of decrease of

saltmarsh area (erosion of the saltmarsh edge) on the long-term.
Differences are observed between the tidal flat and saltmarsh behaviour of the Eastern- and the Western Scheldt. The total saltmarsh and vegetated area of the exposed sites exceeds the area of the sheltered sites in the Western Scheldt, while the opposite is observed between the sheltered and exposed sites at the Eastern Scheldt. Moreover, the cyclicity at the sheltered locations is smaller as opposed to the exposed locations for the Western Scheldt. At the Eastern Scheldt a reversed trend is observed, where the exposed sites remain practically constant and the sheltered site show more dynamic behaviour.

The results showed how exposed sites experienced a landward move of the saltmarsh area and the sheltered sites grew. The EI and vegetation also showed a significant correlation. All these observations suggest how the EI of a tidal flat is indicative for the size of the tidal flat (larger) and for the dynamics of the saltmarsh area (higher cyclicity and decreasing area over larger time scales). A decreasing total area was often accompanied with an increasing saltmarsh to total area ratio. Together with an increasing saltmarsh area, this observation suggests tidal flat erosion. The opposite was also observed, where an increasing area was accompanied with a decrease in saltmarsh to total area ratio and a decreasing saltmarsh area. This suggests the accretion of the tidal flat.

6.3 Influence of the Suspended Sediment Concentration to Recovery

The SSC deficit the Eastern Scheldt experiences showed to be a likely cause for the observed differences in recovery rate between the piles and the holes for the two tidal basins.
The SSC of the Eastern Scheldt has drastically changed after the '*Deltaplan'* was executed, leading to a deficit (Winterwerp et al., 2013), whereas this is not the case for the Western Scheldt. It is therefore expected for the piles to recover quicker compared to the holes, since the tidal flats show overall erosion (Maldegem & Van Pagee, 2005), while the Western Scheldt would show a smaller difference between the two recovery rates. The observed difference between the recovery rates for the piles and the holes between the Eastern- and Western- Scheldt may therefore be the consequence of the SSC, since recovering the piles provide extra sediment to the system in need, whereas the holes are in need for sediment to recover. This would thus explain the smaller difference between the recovery rates for the piles and holes in the Eastern Scheldt. The lower recovery rate for piles compared to holes (Eastern Scheldt) where the average inundation time <22%, is expected to be caused by not receiving enough hydrodynamic forces and therefore show a different trend in recovery compared to the higher inundation times. Their recovery depends more on other factors, but the SSC factor is driven by hydrodynamics, so the lack of hydrodynamic forcing decreases the relative influence of the SSC deficit for those Eastern Scheldt locations.

6.4 Tidal Flat properties determinative for the Recovery Rate

Relations have been found between the properties distinguishing the tidal flats, and the recovery rates. The hydrodynamics showed to be of high and significant importance, as observed from the impact of grainsize and inundation time to the daily bed-level dynamics and the recovery rates in all systems. The tidal bed-level recovery was found to be in line with the phenomena of critical slowing down.
The highest bed-level change was observed furthest away from the saltmarsh edge (200 m). For all locations this coincides with higher inundation times. The recovery rate also showed to increase

further from the saltmarsh edge/ with increased inundation time. The median grainsizes strongly correlate to both these parameters and shows a fining trend from closest to the channel to the saltmarsh edge. These findings were expected, since it is widely recognised that flow velocities at high water levels are largest next to a channel (Friedrichs, 2011). Further away from the channel, the velocity decreases due to friction with the bed resulting in the crossing of the deposition threshold for the largest grains. Consequently, the largest grains are deposited and accumulate close to the tidal channel. With further decreasing flow velocities, the threshold for progressively smaller grainsizes is crossed causing the smaller sediment to be deposited further away from the channel (Friedrichs, 2011). This grainsize fining trend has been significantly observed during the experiment and in line with the relationship as described by the Hjulström diagram (Miedema, 2010). Because tidal systems work in a multidirectional way , the systems' hydrodynamics are complex, which, combined with the availability of smaller grainsizes further landward explains the sediment trend for GBS where the largest grains were found at 25 m and the smallest at 200 m. It is possible that the hydrodynamic forcing at 200 m exceeds the minimal settling velocity, due to the high inundation time (43%), preventing even the larger grainsizes from settling. This is supported by the observations on the daily sediment dynamics, where the bed-level change at 200 m is large considering its location in the Western Scheldt (far inland, low exposure index). Equivalent to the threshold shift for deposition at the exposed sites caused by their higher (wind) energy input, higher flow velocity closer to the tidal channel also brings in more energy to the system. Consequently, the threshold for deposition, and for erosion and transportation of grains changes, depending on the grain diameter (caused by sediment cohesion feedbacks), resulting in increased suspension of sediment and transportation closest to the channel and thereby the highest bed-level change.

The length of the tidal flat to the main tidal channel also affects the hydrodynamic forcing. The tidal flats of the Eastern Scheldt have a larger area than those in the Western Scheldt, accounting for a larger distance between the main tidal channel and the experiment sites. Consequently, more energy is lost to friction with the bed until the water reaches the 200 m location. Due to the stretched elevation gradient, the locations within the Eastern Scheldt have a lower inundation time compared to the Western Scheldt. This resulted in large observed difference within recovery rate between 200 m and 25 m, since 25 m is only rarely inundated (<15%). Moreover, at the 25 m distance at DM, root remains were found in the sediment during the digging as carried out for the disturbance- and recovery experiment. Which in line with the negative vegetation change DM experienced between 1988 and 2014. Although the presence of plants do not significantly reduce marsh edge erosion (Feagin et al., 2009), it does significantly (negatively) correlate to the percentage of coarse material. Due to the incorporation of finer sediment into the soil matrix, it becomes more cohesive. This was observed to be in line with the median grainsizes found at DM, showing a significant difference between 25 m (70.1 µm) and 200 m (111.8 µm). At 25 m, the standard deviation showed grainsizes in the mud fraction (silt), while at 200 m the standard deviation was within the sand fraction (fine sand). The cohesiveness of sediment has been associated with increased resistance of the sediment to wave-induced erosion (Feagin et al., 2009) and could therefore (partially) explain the low recovery rates at DM 25 m, together with the decreased inundation time. The decreased inundation time and consequently hydrodynamic impact is most likely also the explaining factor for the slow recovery at RK 25.

The significant and positive relationship as observed between the DBD and the recovery rates of all the sites is expected since a relation between the density of the sediment and erosion rates for median grainsizes < 222 µm has been found before by previous research (Jacobs et al., 2011; Roberts et al.,

1998). That the individual correlations are lower compared to the inundation time or wet period is also expected. DBD stays vulnerable to changes after deposition (Mahmood, 1987), and due to the nature of the perturbations, the sediment was disturbed, and is expected to have changed to a certain degree from the samples as taken on the undisturbed bed.

The largest recovery rates of both piles and holes are found furthest from the saltmarsh edge. This is in line with the phenomenon of 'critical slowing down', for which Van Belzen et al. (2017) found decreasing biomass recovery rates for increasing inundation stress along the elevation gradient, explaining how the seawater inundation stress slowed down recovery and thereby resilience of tidal marshes. Thus, recovery of saltmarsh vegetation slowed down with increasing inundation by vegetation disturbance. Translating this to tidal bed-level recovery, critical slowing down would show the increase of recovery rate at increased inundation stress. The results from this research enhances the idea of critical slowing down being a generic phenomenon, not only for assessing the resilience of saltmarsh ecosystems but by enhancing it to being a phenomenon which can also be applied to sedimentation resilience.

6.5 Are the short-term sediment dynamics explanatory for the long-term dynamics.

From the results regarding the relative vegetation change, it was observed how locations assigned as exposed experienced negative vegetation change between 1988 and 2014. The sheltered locations experienced positive change, except for VI, showing no change between 1988 and 2014. The results for VI can be explained by the presence of a large manmade structure in front of the tidal flat, inhibiting normal conditions. The correlation between the two factors was calculated to be to moderately negative, meaning lower EI values are linked to positive vegetation change, and higher EI values to negative vegetation change. The vegetation change showed to have a weak correlation with the recovery rate of the holes, while no correlation was found with the recovery rate of the piles. Opposite to this, a weak positive relationship was found between the exposure index and the recovery rate of the piles while no correlation was found with the recovery rate of the holes.

Thus, while a weak correlation is found between the recovery of the piles and the EI, no correlation is found between the vegetation change and the recovery rate of the piles. Opposite to this, no correlation was found between the recovery of the holes and the EI, while a weak correlation was found between the holes' recovery rate and the vegetation change. Contrary to this observation, the vegetation change and the EI did show a correlation. There is thus no significant evidence that the recovery time of the disturbances is linked to the lateral movement of saltmarshes. Moreover, a significant link has been found between the lateral movement of the saltmarsh and the EI during this research

6.6 Recommendations for future research

6.6.1 Adding Wave Energy to the Exposure Index

There are indications that when leaving the wave energy out of the exposure index, and only implementing the wind data, some locations would show different exposure rates (Callaghan et al., 2010). It is therefore proposed to add (long-term) wave logging data to the equation for Exposure Index and compare the results.

6.6.2 Additional field properties analysations

Higher silt content is connected to higher erosion threshold (Jacobs et al., 2011). It would therefore be interesting to see how the silt content correlates to the recovery. It is recommended to take the silt content of the sediment samples into the analyses for future sediment resilience research.
Chlorophyll-a has been sampled during the field campaigns, but not analysed due to time constrains following from the COVID-19 Pandemic. It is therefore recommended to analyse those samples. Additionally, it is recommended to redo this experiment during the summer months, to increase the understanding of the biotic impact versus the hydro- and sediment dynamics. The two-yearly experiment, possibly on a smaller spatial scale due to the labour intensity of the field work, it is also recommended to repeat yearly or two yearly, depending on the available recourses. This accounts for gaining a long-term data set in which resilience can be observed and relative changes leaning to reaching a critical tipping point can be noticed prematurely. Since RL recovered too fast in this experiment to be taken into further analyses, it is proposed for a next experiment to increase the size of the perturbations at this tidal flat.

6.6.3 Improving the satellite data set

The used satellite data has a large spatial resolution (30 m). As a consequence of this larger grid size, the results fail to explain internal vegetation characteristics, for example the density and health of the vegetation. Van der Wal et al., 2008 also studied saltmarsh development in its spatial context, over a 30-year period, used high resolution (25 cm) imagery. Although the scope of this research was different, it shows how primarily looking at changes in total area when considering saltmarsh vegetation, misses local feedback mechanisms between plant growth, morphology and hydrodynamics of both saltmarshes and the tidal flats. This article also shows a small decline in RL's vegetation cover over the 30-year period, however where it becomes clear from the article that the salt marshes edge suffered from erosion, the internal vegetation grew over this period. This is not visible from the lower resolution imagery. It is therefore recommended for future research to combine the fieldwork on the same locations with NDVI research on imagery with a resolution 30 cm

6.6.4 Quantify the relation between the Suspended Sediment Concentration, tidal flat properties and recovery rates

To further understand the impact of the SSC deficit to the tidal flat properties and the recovery rate of a tidal system, further field research, using a field flume (figure 36) is proposed comparing the Eastern- and the Western Scheldt. The differences within SSC between the two proposed systems provide insight in the effect of wave- and tidal force on tidal flats and salt marshes with different underlying sediment concentration states. Combined with the sediment characteristics and the recovery rates from the research in this report, more quantified insight can be gained about the correlations between the D50, WBD, DBD, shear strength and how this affects the ease of sediment getting into suspension. The outcome might provide more insight in the magnitude of correlation between the SSC and the recovery.

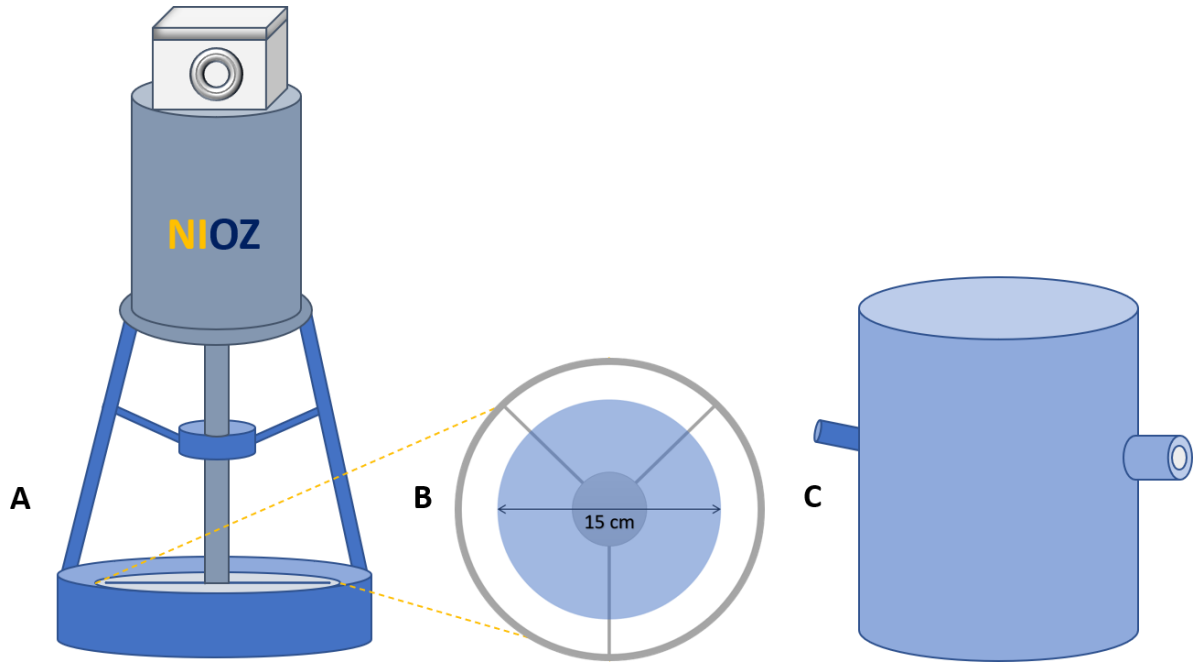

Figure 36 - The rotator used to set the sediment into suspension (A) the bottom view of the disc (B) bringing the sediment into suspension during the experiment and the flume (C).During the measurements, the flume is placed under the rotator. (designed by T.J. Bouma).

7. Conclusion

This study provides new understanding of predicting long-term vegetation dynamics on tidal flats and adjacent saltmarshes by studying the resilience and short-term sediment dynamics of those tidal flats. It aimed to determine whether early warning signals can be found as indicator for resilience for complex tidal ecosystems.

Based on the results from this study, it was found that exposed sites with larger median grainsizes and bulk densities are more resilient to changes in their environment and will likely survive more extreme weather and rising sea levels longer. Over a 30-year time scale the exposed sites were generally larger, while showing a decrease in area over time, resulting from coastal squeeze. There is evidence that this is true in the Eastern- and Western Scheldt, but further research on other systems is required to increase the understanding of the internal feedback mechanisms for intertidal ecosystems. The equilibrium state of the system also showed to be of importance for the recovery of the system. For which a state with an SSC deficit accounts for larger differences between the recovery of different types of perturbations, being in need of sediment (holes) or having an excess of sediment (piles).

The recovery rate showed to be dependant of the system and the hydrodynamic forcing, clearly supporting towards the phenomena of critical slowing down in the sediment dynamics of tidal systems. The long-term vegetation change in the two tidal basins suggests towards a relationship between observed saltmarsh trajectories and recovery rate, but no unambiguous trends could be found from this data set. The results from this research enhances the idea of critical slowing down being a generic phenomenon, which can also be applied to the resilience of sedimentation perturbations. In conclusion, the exposed sites with the highest median grainsizes are most resilient to external forcing, they show more internal dynamics and show more erosion compared to the sheltered sites. However, they can overcome erosion easier compared to sheltered sites with lower median grainsizes. Their erosion is often less in terms of net change, but the erosion takes much longer to be recovered.

The resilience of the tidal flat helps us better understand the response of the tidal flats to rising sea levels and increased frequency of erosive events like storms. An attempt has been made to apply theoretical approaches of complex systems to real-world wetlands. The complexity of the system in terms of their interrelatedness, is emphasised again. It is therefore recommended to build on this research, by measuring the recovery rate of the tidal flats, monitoring the change in resilience and providing the possibility to intervene when the recovery rate shows indications of reaching a critical tipping point.

References

Allen, J. R. L. (2000). Morphodynamics of Holocene salt marshes: a review sketch from the Atlantic and Southern North sea coasts of Europe. *Quaternary Science Reviews*, *19*(17–18), 1155–1231. https://doi.org/10.1016/S0277-3791(00)00157-8

Andersen, T. J., Lund-Hansen, L. C., Pejrup, M., Jensen, K. T., & Mouritsen, K. N. (2005). Biologically induced differences in erodibility and aggregation of subtidal and intertidal sediments: a possible cause for seasonal changes in sediment deposition. *Journal of Marine Systems*, *55*, 123–138. https://doi.org/10.1016/j.jmarsys.2004.09.004

Arshad, M. A. C., Lowery, B., & Grossman, B. (1997). *Physical Tests for Monitoring Soil Quality* (pp. 123–141). John Wiley & Sons, Ltd. https://doi.org/10.2136/sssaspecpub49.c7

Baeyens, W., van Eck, B., Lambert, C., Wollast, R., & Goeyens, L. (1998). General description of the Scheldt estuary. In *Hydrobiologia* (Vol. 366).

Balke, T., Herman, P. M. J., & Bouma, T. J. (2014). Critical transitions in disturbance-driven ecosystems: Identifying windows of opportunity for recovery. *Journal of Ecology*, *102*(3), 700–708. https://doi.org/10.1111/1365-2745.12241

Bassoullet, P., Le Hir, P., Gouleau, D., & Robert, S. (2000). Sediment transport over an intertidal mudflat: Field investigations and estimation of fluxes within the “Baie de Marennes-Oleron” (France). *Continental Shelf Research*, *20*(12–13), 1635–1653. https://doi.org/10.1016/S0278-4343(00)00041-8

Bennett, E. M., Cumming, G. S., & Peterson, G. D. (2005). A Systems Model Approach to Determining Resilience Surrogates for Case Studies. *Ecosystems*, *8*(8), 945–957. https://doi.org/10.1007/s10021-005-0141-3

Blew, J., Eskildsen, K., Günter, K., Laursen, K., Potel, P., Rösner, H.-U., van Roomen, M., & Südbeck, P. (2005). 12.2 Migratory Birds. In *Wadden Sea Ecosystem* (19th ed.).

Bouma, T. J., van Belzen, J., Balke, T., van Dalen, J., Klaassen, P., Hartog, A. M., Callaghan, D. P., Hu, Z., Stive, M. J. F., Temmerman, S., & Herman, P. M. J. (2016). Short-term mudflat dynamics drive long-term cyclic salt marsh dynamics. *Limnology and Oceanography*, *61*(6), 2261–2275. https://doi.org/10.1002/lno.10374

Bouma, T. J., van Belzen, J., Balke, T., Zhu, Z., Airoldi, L., Blight, A. J., Davies, A. J., Galvan, C., Hawkins, S. J., Hoggart, S. P. G., Lara, J. L., Losada, I. J., Maza, M., Ondiviela, B., Skov, M. W., Strain, E. M., Thompson, R. C., Yang, S., Zanuttigh, B., … Herman, P. M. J. (2014). Identifying knowledge gaps hampering application of intertidal habitats in coastal protection: Opportunities & steps to take. *Coastal Engineering*, *87*, 147–157. https://doi.org/10.1016/j.coastaleng.2013.11.014

Buchele, W. F. (1984). *Means and method for soil testing* (Patent No. 4,480,481). http://lib.dr.iastate.edu/patents/6

Callaghan, D. P., Klaassen, P. C., Stive, M., Callaghan, D. P., Bouma, T. J., Klaassen, P., Van Der Wal, D., Stive, M. J. F., & Herman, P. M. J. (2010). *Hydrodynamic forcing on salt marsh development: distinguishing the relative importance of waves vs. tidal flow Vegetation modelling HPP (VNSC project) View project Coping with Deltas in Transition-Within the framework of The Programme Strategic Scientific*. https://doi.org/10.1016/j.ecss.2010.05.013

Cao, H., Zhu, Z., Balke, T., Zhang, L., & Bouma, T. J. (2018). Effects of sediment disturbance regimes on Spartina seedling establishment: Implications for salt marsh creation and restoration. *Limnology and Oceanography*, *63*(2), 647–659. https://doi.org/10.1002/lno.10657

Carpenter, S. R., & Brock, W. A. (2006). Rising variance: a leading indicator of ecological transition. *Ecology Letters*. https://doi.org/10.1111/j.1461-0248.2005.00877.x

Carpenter, S., Walker, B., Anderies, J. M., & Abel, N. (2001). From Metaphor to Measurement: Resilience of What To What? *Ecosystems*, *4*(8), 756–781. https://doi.org/10.1007/s10021-001-0045-9

Cleveringa, J. (2014). Ecotopen in de Westerschelde. *LTV - Veiligheid En Toegankelijkheid*, *april*.

Davidson, N. C. (2014). How much wetland has the world lost? Long-term and recent trends in global wetland area. *Marine and Freshwater Research*, *65*, 934–941. https://doi.org/10.1071/MF14173

De Brouwer, J. F. C., Bjelic, S., De Deckere, E. M. G. T., & Stal, L. J. (2000). Interplay between biology and sedimentology in a mudfat (Biezelingse Ham, Westerschelde, The Netherlands). *Continental Shelf Research*, *20*, 1159–1177.

De Vriend, H. J., Wang, Z. B., Ysebaert, T., Herman, P. M. J., & Ding, P. (2011). Eco-morphological problems in the yangtze estuary and the western scheldt. *Wetlands*, *31*(6), 1033–1042. https://doi.org/10.1007/s13157-011-0239-7

Dijkema, K., Nicolai, A., de Vlas, J., Smit, C., Jongerius, H., & Nauta, H. (2001). *Van landaanwinning naar kwelderwerken*.

Duarte, C. M., Losada, I. J., Hendriks, I. E., Mazarrasa, I., & Marbà, N. (2013). The role of coastal plant communities for climate change mitigation and adaptation. In *Nature Climate Change* (Vol. 3, Issue 11, pp. 961–968). Nature Publishing Group. https://doi.org/10.1038/nclimate1970

Dyer, K. R., Christie, M. C., & Wright, E. W. (2000). The classification of intertidal mudflats. *Continental Shelf Research*, *20*(10–11), 1039–1060. https://doi.org/10.1016/S0278-4343(00)00011-X

Eelkema, M., Wang, Z. B., Hibma, A., & Stive, M. J. F. (2013). Morphological effects of the eastern scheldt storm surge barrier on the ebb-tidal delta. *Coastal Engineering Journal*, *55*(3). https://doi.org/10.1142/S0578563413500101

Feagin, R. A., Lozada-Bernard, S. M., Ravens, T. M., Möller, I., Yeager, K. M., & Baird, A. H. (2009). *Does vegetation prevent wave erosion of salt marsh edges?* (Vol. 106).

Friedrichs, C. T. (2011). *Tidal flat morphodynamics: a synthesis*. https://scholarworks.wm.edu/presentations

Friedrichs, C. T., & Aubrey, D. G. (1996). Uniform bottom shear stress and equilibrium hyposometry of intertidal flats. *Coastal and Estuarine Studies*, *50*, 405–429. https://doi.org/10.1029/ce050p0405

Geurts van Kessel, A. J. M. (2004). *Verlopend tij*.

Gleason, M. (2018). *Algorithm Prototyping Coastline Extraction*. https://notebooks.geobigdata.io/hub/tutorials/5c006459f3acbc49e7a459f4?tab=code

Grabemann, H., Grabemann, I., & Eppel, D. P. (2004). Climate change and hydrodynamic impact in the Jade-Weser area : a case study. *Coastline Reports*, *1*, 83–91.

Grabowski, R. C. (2014). Measuring the shear strength of cohesive sediment in the field. In *British Society for Geomorphology Geomorphological Techniques*.

Holling, C. S. (1973). Resilience and stability of ecological systems. *Annual Review of Ecology and*

Systematics, *4*, 1–23.

Hu, Z., Van Belzen, J., Van Der Wal, D., Balke, T., Wang, Z. B., Stive, M., & Bouma, T. J. (2015). Windows of opportunity for salt marsh vegetation establishment on bare tidal flats: The importance of temporal and spatial variability in hydrodynamic forcing. *Journal of Geophysical Research G: Biogeosciences*, *120*(7), 1450–1469. https://doi.org/10.1002/2014JG002870

Hu, Z., Yao, P., Van Der Wal, D., & Bouma, T. J. (2017). Patterns and drivers of daily bed-level dynamics on two tidal flats with contrasting wave exposure. *Scientific Reports*, *7*(1), 1–9. https://doi.org/10.1038/s41598-017-07515-y

Huisman, B. J. A., & Luijendijk, A. P. (2009). *Sand demand of the Eastern Scheldt morphology around the barrier*.

Jacobs, W., Le Hir, P., Van Kesteren, W., & Cann, P. (2011). Erosion threshold of sand-mud mixtures. *Continental Shelf Research*, *31*(10, Supplement), S14–S25. https://doi.org/10.1016/j.csr.2010.05.012

Jadhav, B. D., & Patil, P. M. (2014). Hyperspectral Remote Sensing For Agricultural Management: A Survey. *International Journal of Computer Applications*, *106*(7), 38–43.

Jesus, B., Brotas, V., Ribeiro, L., Mendes, C. R., Cartaxana, P., & Paterson, D. M. (2009). Adaptations of microphytobenthos assemblages to sediment type and tidal position. *Continental Shelf Research*, *29*(13), 1624–1634. https://doi.org/10.1016/j.csr.2009.05.006

Keddy, P. A. (1982). Quantifying within-lake gradients of wave energy: Interrelationships of wave energy, substrate particle size and shoreline plants in axe lake, Ontario. *Aquatic Botany*, *14*, 41–58. https://doi.org/https://doi.org/10.1016/0304-3770(82)90085-7

Kirwan, M. L., Guntenspergen, G. R., D'Alpaos, A., Morris, J. T., Mudd, S. M., & Temmerman, S. (2010). Limits on the adaptability of coastal marshes to rising sea level. *Geophysical Research Letters*, *37*(23), 1–5. https://doi.org/10.1029/2010GL045489

Kirwan, M. L., & Megonigal, & J. P. (2013). Tidal wetland stability in the face of human impacts and sea-level rise. *Nature*, *504*, 53–60. https://doi.org/10.1038/nature12856

Kirwan, M. L., Temmerman, S., Skeehan, E. E., Guntenspergen, G. R., & Fagherazzi, S. (2016). Overestimation of marsh vulnerability to sea level rise. *Nature Climate Change*, *6*(3), 253–260. https://doi.org/10.1038/nclimate2909

KNMI. (2019). *Klimatologie - Daggegevens van het weer in Nederland*. http://projects.knmi.nl/klimatologie/daggegevens/selectie.cgi

KNMI. (2020). *Klimatologie - Daggegevens van het weer in Nederland*. http://projects.knmi.nl/klimatologie/daggegevens/selectie.cgi

Laegdsgaard, P. (2006). Ecology, disturbance and restoration of coastal saltmarsh in Australia: A review. *Wetlands Ecology and Management*, *14*(5), 379–399. https://doi.org/10.1007/s11273-005-8827-z

Laengner, M. L., Siteur, K., & van der Wal, D. (2019). Trends in the Seaward Extent of Saltmarshes across Europe from Long-Term Satellite Data. *Remote Sensing*, *11*(14), 1653. https://doi.org/10.3390/rs11141653

Le Hir, P., Roberts, W., Cazaillet, O., Christie, M., Bassoullet, P., & Bacher, C. (2000). Characterization of intertidal flat hydrodynamics. *Continental Shelf Research*, *20*(12–13), 1433–1459. https://doi.org/10.1016/S0278-4343(00)00031-5

Mahmood, K. (1987). Reservoir Sedimentation: Impact, Extent, and Mitigation. *World Bank Tech. Pap.*, *71*, 45–48.

Maldegem, D. C., & Van Pagee, J. A. (2005). *Zandhonger Oosterschelde : een verkenning naar mogelijke maatregelen | Hydrotheek*. Rijksinstituut voor Kust en Zee (RIKZ). https://library.wur.nl/WebQuery/hydrotheek/1877573

Mason, L. A., Riseng, C. M., Layman, A. J., & Jensen, R. (2018). Effective fetch and relative exposure index maps for the Laurentian Great Lakes. *Scientific Data*, *5*, 1–7. https://doi.org/10.1038/sdata.2018.295

Menge, B. A., Caselle, J. E., Milligan, K., Gravem, S. A., Gouhier, T. C., Wilson White, J., Barth, J. A., Blanchette, C. A., Carr, M. H., Chan, F., Lubchenco, J., McManus, M. A., Novak, M., Raimondi, P. T., & Washburn, L. (2019). Integrating coastal oceanic and benthic ecological approaches for understanding large-scale meta-ecosystem dynamics. *Oceanography*, *32*(3), 38–49.

Miedema, S. A. (2010). *Constructing the Shields Curve, a new theoretical approach and its applications*. https://www.researchgate.net/publication/228750218

Murray, N., Phinn, S. R., Clemens, R. S., Roelfsema, C. M., & Fuller, R. A. (2012). Continental Scale Mapping of Tidal Flats across East Asia Using the Landsat Archive. *Remote Sensing*, *4*(11), 3417–3426. https://doi.org/10.3390/rs4113417

Mus, A. (2019). *The applicability of the ASED-sensor for measuring bed level changes in intertidal areas*. University of Twente and NIOZ.

Nolte, S., Koppenaal, E. C., Esselink, P., Dijkema, K. S., Schuerch, M., De Groot, A. V, Bakker, J. P., & Temmerman, S. (2013). Measuring sedimentation in tidal marshes: a review on methods and their applicability in biogeomorphological studies. *Journal of Coastal Conservation*, *17*, 301–325. https://doi.org/10.1007/s11852-013-0238-3

Perillo, G. M. E. (1995). Definitions and geomorphologic classifications of estuaries. *Developments in Sedimentology*, *53*(C), 17–47. https://doi.org/10.1016/S0070-4571(05)80022-6

Pimm, S. L. (1984). The complexity and stability of ecosystems. *Nature*, *307*, 321,326. http://www.biosym.uzh.ch/modules/models/ETHZ/StabilityAndComplexity/pimm.pdf

Pontee, N. (2013). Defining coastal squeeze: A discussion. *Ocean & Coastal Management*, *84*, 204–207. https://doi.org/10.1016/j.ocecoaman.2013.07.010

Rijkswaterstaat. (2017). *Toelichting op de zoute ecotopenkaart Westerschelde 2016*.

Roberts, J., Jepsen, R., Gotthard, D., & Lick, W. (1998). Effects of particle size and bulk density on erosion of quartz particles. *Journal of Hydraulic Engineering*, *124*(12), 1261–1267. https://doi.org/10.1061/(ASCE)0733-9429(1998)124:12(1261)

Scheffer, M., Bascompte, J., Brock, W. A., Brovkin, V., Carpenter, S. R., Dakos, V., Held, H., Van Nes, E. H., Rietkerk, M., & Sugihara, G. (2009). Early-warning signals for critical transitions. *Nature*, *461*, 53–59. https://doi.org/10.1038/nature08227

Scheffer, M., Carpenter, S., Foley, J. A., Folke, C., & Walker, B. (2001). Catastrophic shifts in ecosystems. In *NATURE* (Vol. 413). www.nature.com591

Schwarz, C., Gourgue, O., van Belzen, J., Zhu, Z., Bouma, T. J., van de Koppel, J., Ruessink, G., Claude, N., & Temmerman, S. (2018). Self-organization of a biogeomorphic landscape controlled by plant life-history traits. *Nature Geoscience*, *11*(9), 672–677. https://doi.org/10.1038/s41561-018-0180-y

Serota, S., & Jangle, A. (1972). Direct-Reading Pocket Shear Vane. *Civil Engineering*, *42*, 73–74. https://doi.org/10.1016/B978-0-08-100142-4.00004-X

Silinski, A., van Belzen, J., Fransen, E., Bouma, T. J., Troch, P., Meire, P., & Temmerman, S. (2016). Quantifying critical conditions for seaward expansion of tidal marshes: A transplantation experiment. *Estuarine, Coastal and Shelf Science*, *169*, 227–237. https://doi.org/10.1016/j.ecss.2015.12.012

Smaal, A. C., & Nienhuis, P. H. (1992). The Eastern Scheldt (The Netherlands), from an estuary to a tidal bay: a review of responses at the ecosystem level*. In *Netherlands Journal of Sea Research* (Vol. 30).

Temmerman, S., Meire, P., Bouma, T. J., Herman, P. M. J., Ysebaert, T., & De Vriend, H. J. (2013). Ecosystem-based coastal defence in the face of global change. *Nature*, *504*, 79–83. https://doi.org/10.1038/nature12859

Tucker, C. J. (1979). Red and Photographic Infrared linear Combinations for Monitoring Vegetation. *Remote Sensing of Environment*, *8*, 127–150.

U.S. Geological Survey. (2020). Landsat—Earth observation satellites. In *U.S. Geological Survey Fact Sheet 2015–3081*. https://doi.org/10.3133/fs20153081

van Belzen, J., van de Koppel, J., Kirwan, M. L., Guntenspergen, G. R., & Bouma, T. J. (2017). Disturbance-recovery experiments to assess resilience of ecosystems along a stress gradient. *Protocol Exchange*. https://doi.org/10.1038/protex.2017.028

Van Belzen, J., Van De Koppel, J., Kirwan, M. L., Van Der Wal, D., Herman, P. M. J., Dakos, V., Kéfi, S., Scheffer, M., Guntenspergen, G. R., & Bouma, T. J. (2017). Vegetation recovery in tidal marshes reveals critical slowing down under increased inundation. *Nature Communications*, *8*, 1–7. https://doi.org/10.1038/ncomms15811

Van der Wal, D., Wielemaker-van den Dool, A., & Herman, P. M. J. (2010). Spatial synchrony in intertidal benthic algal biomass in temperate coastal and estuarine ecosystems. *Ecosystems*, *13*(2), 338–351. https://doi.org/10.1007/s10021-010-9322-9

Van der Wal, D., Wielemaker-Van den Dool, A., & Herman, P. M. J. (2008). Spatial patterns, rates and mechanisms of saltmarsh cycles (Westerschelde, The Netherlands). *Estuarine, Coastal and Shelf Science*, *76*(2), 357–368. https://doi.org/10.1016/j.ecss.2007.07.017

Van Eerden, M. R., Drent, R. H., Stahl, J., & Bakker, J. P. (2005). Connecting seas: Western Palaearctic continental flyway for water birds in the perspective of changing land use and climate. *Global Change Biology*, *11*(6), 894–908. https://doi.org/10.1111/j.1365-2486.2005.00940.x

van Nes, E. H., & Scheffer, M. (2007). Slow Recovery from Perturbations as a Generic Indicator of a Nearby Catastrophic Shift. *The American Naturalist*, *169*(6), 738–747. https://doi.org/10.1086/516845

Van Wijnen, H. J., & Bakker, J. P. (2001). Long-term Surface Elevation Change in Salt Marshes: a Prediction of Marsh Response to Future Sea-Level Rise. *Estuarine, Coastal and Shelf Science*, *52*, 381–390. https://doi.org/10.1006/ecss.2000.0744

Veihe, A., Jensen, N. H., Schiøtz, I. G., & Nielsen, S. L. (2011). Magnitude and processes of bank erosion at a small stream in Denmark. *Hydrological Processes*, *25*(10), 1597–1613. https://doi.org/10.1002/hyp.7921

Vuik, V., Jonkman, S. N., Borsje, B. W., & Suzuki, T. (2016). Nature-based flood protection: The efficiency of vegetated foreshores for reducing wave loads on coastal dikes. *Coastal*

Engineering, *116*, 42–56. https://doi.org/10.1016/j.coastaleng.2016.06.001

Wang, Z. B., & Winterwerp, J. C. (2001). Impact of dredging and dumping on the stability of ebb-flood channel systems. *Proceedings of the 2nd IAHR Symposium on River, Coastal and Estuarine Morphodynamics*, 515–524.

Widdows, J., Brinsley, M. D., Salkeld, P. N., & Lucas, C. H. (2000). Influence of biota on spatial and temporal variation in sediment erodability and material flux on a tidal flat (Westerschelde, The Netherlands). *Marine Ecology Progress Series*, *194*, 23–37.

Willemsen, P. W. J. M., Borsje, B. W., Hulscher, S. J. M. H., Van der Wal, D., Zhu, Z., Oteman, B., Evans, B., Möller, I., & Bouma, T. J. (2018). Quantifying Bed Level Change at the Transition of Tidal Flat and Salt Marsh: Can We Understand the Lateral Location of the Marsh Edge? *Journal of Geophysical Research: Earth Surface*, *123*(10), 2509–2524. https://doi.org/10.1029/2018JF004742

Winterwerp, J. C., Wang, Z. B., Van Braeckel, A., Van Holland, G., & Kösters, F. (2013). Man-induced regime shifts in small estuaries - II: A comparison of rivers. *Ocean Dynamics*, *63*(11–12), 1293–1306. https://doi.org/10.1007/s10236-013-0663-8

Wissel, C. (1984). A universal law of the characteristic return time near thresholds. *Oecologica*, *65*, 101–107.

Yang, S. L., Friedrichs, C. T., Shi, Z., Ding, P. X., Zhu, J., & Zhao, Q. Y. (2003). Morphological Response of Tidal Marshes, Flats and Channels of the Outer Yangtze River Mouth to a Major Storm. *Estuaries*, *26*(6), 1416–1425. https://doi.org/10.1007/BF02803650

Zhu, Z., van Belzen, J., Zhu, Q., van de Koppel, J., & Bouma, T. J. (2019). Vegetation recovery on neighboring tidal flats forms an Achilles' heel of saltmarsh resilience to sea level rise. *Limnology and Oceanography*, *9999*, 1–12. https://doi.org/10.1002/lno.11249

Appendix

Appendix A – Landsat Satellites deployment and band widths of Landsat 5 and 7

Figure A1 - Landsat Missions Timeline (U.S. Geological Survey, 2020)

Satellite images from Landsat 5 and 7 were deployed. Landsat 5 carried both the multispectral Scanner (MSS) and Thematic Mapper (TM) sensors. Landsat 7 carried the Enhanced Thematic Mapper (ETM+) sensor *(U.S. Geological Survey, 2020)* . The Landsat Satellite sensors are a passive type of remote sensing, meaning that the sensors measure light energy from an existing source (the sun) instead of emitting it actively. The bandwidths of these sensors are found in table A1.

Table A1 - Band designations for Landsat satellites 5 and 7 (U.S. Geological Survey, 2020)

Landsat 5 (TM)			Landsat 7 (ETM+)	
Band name	**Bandwidth (µm)**	**Resolution (m)**	**Bandwidth (µm)**	**Resolution (m)**
1 – Blue	0.45-0.52	30	0.45–0.52	30
2 – Green	0.52-0.60	30	0.52–0.60	30
3 - Red	0.63-0.69	30	0.63–0.69	30
4 – NIR	0.76-0.90	30	0.77–0.90	30
5 – SWIR1	1.55-1.75	30	1.55–1.75	30
7 – SWIR2	2.08-2.35	30	2.09–2.35	30
8 - Panchromatic			0.52–0.90	15
6 – TIR	10.4-12.50	120 (30)	10.4–12.50	60 (30)

Appendix B - ASED-sensor locations in coordinate system RD new

Table A2 – Locations of the deployed ASED-sensors in RD new

Mudflat	Distance	Easting	Northing
PP	25m	38867.477	374860.21
PP	100m	38923.187	374913.744
PP	200m	38987.951	374994.662
ZG	25m	46245.444	378693.071
ZG	100m	46210.784	378621.152
ZG	200m	46171.262	378525.399
RL	25m	69807.152	379372.595
RL	100m	69818.487	379310.411
RL	200m	69846.917	379214.568
GBS	25m	75555.806	375622.348
GBS	100m	75486.363	375600.731
GBS	200m	75387.145	375576.271
DM	25m	60670.994	398230.699
DM	100m	60615.698	398185.166
DM	200m	60542.732	398116.606
RK	25m	70641.677	384263.159
RK	100m	70581.826	384317.273
RK	200m	70492.929	384372.919

Appendix C – Method for Sampling and Analysing the Shear Strength

A pocket shear vane tester or torvane from Eijkelkamp, with custom vanes, has been used for the shear strength measurements of the sediments. The maximum measuring range (MR_{max}) for the custom vanes are based on a calculation in the torvane patent description (Buchele, 1984). It measures the undrained shear strength of cohesive sediment and is widely used for shear strength analyses in soils (Grabowski, 2014; Serota & Jangle, 1972). The values gained by the Read Out (RO) measurements ([kg/cm^2]) were used as input for equation (A1), used to calculate the shear strength (τ) [kPa = kN/m^2]. For the MR_{max} value, a custom vane of 0.032314 kg/cm^2 has been used (NIOZ, internal communication).

$$\tau = RO \cdot MR_{max} \cdot 10 \quad \text{(A1)}$$

The shear vane tester is used in the field by placing the bulges of the vane in the sediment, while placing the arrow to the RO value of '0'. The top of the torvane is now turned until the sediment cannot hold the bulges anymore. This has been repeated randomly five times per site, at the area besides or behind the ASED-sensors to minimize disturbance to the sensor. The measures where always taken by the same person, to minimize personal force differences reflecting in the measurements.

The results from the shear strength were analysed yet showed no significant trends with the location, distance, and/ or the exposure category. Therefore, it was deemed not suitable for further analyses and the results can be found in Appendix N.

Appendix D – Method for the executed 'resilience' Pilot studies

Following from the two pilot studies is was determined early on how to execute the main experiment. Consequently, the results were not used for further analyses.

Before starting the main experiment, the best research set up has been investigated by performing two pilot studies in January 2020. These studies have been carried out to explore the best dimensions for the piles/ holes in terms of them not going back to their original state between one tidal cycle, and also being small enough to make it physically manageable and staying as close as possible to the ASED-sensor. For the first pilot study, holes of two m wide where dug and with this retrieved sediment, piles (of the same length) where made (figure A2.A). This was done at two locations, namely RK (Eastern Scheldt) and RL (Western Scheldt), along the 25m, 100m and 200m transect. The width to depth ratio was assigned as 3x the depth and the depth was assigned to exceed the average sedimentation rate in the area (Willemsen et al., 2018). Due to the scouring effect, the pile and the hole can influence each other, when placed close enough to each other. Therefore, they were placed with a 5 m interval from each other. In between the following tidal cycles, the relative height of the holes and piles where measured, using the SEB.

The second pilot study was performed because the practicability of the first pilot study was not sufficient to apply at all six locations, due to the high amount of sediment. Moreover, it was impossible to equalize the depth and height of the piles/ holes due to the quantity of the sediment. Consequently, a second pilot study (figure A2.B) has been performed at the same locations. For this study, a smaller amount of sediment wat used. By sticking a pole in the piles/ holes, the relative height has been measured at the beginning and after tidal cycles. This experiment showed that the amount of sediment wat sufficient to sustain multiple tidal cycles, being a prerequisite for using less sediment.

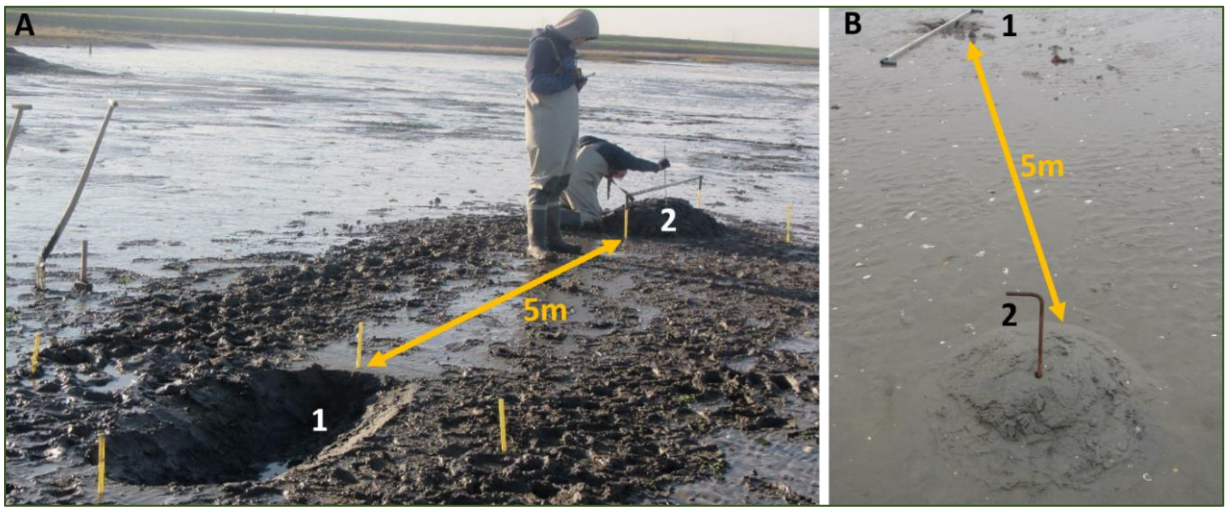

Figure A2 - Pilot studies for the disturbance and recovery experiment;(A) shows the first pilot study. A hole (1) and a pile(2) of sediment at Rattekaai (25m). The relative height of the pile is measured by means of a SEB. (B) shows the second pilot study with a smaller hole (1) and pile (2) of sediment. The relative height is measured by the height of a stick

Appendix E - Wind roses of the Eastern- and Western Scheldt 1989-2019

Figure A3 – Wind roses for the Eastern- and Western Scheldt, providing with the speed and frequency from 30 year of data. The Western Scheldt data is derived from station 310 (*Vlissingen) and from 312 (Oosterschelde) for the Eastern Scheldt. The total average data is provided (**A, D**), and the winter (**B, E**) and summer data (**C, F**).*

Appendix F – Exposure Index values

Table A3- Average Exposure Index values for the Eastern and the Western Scheldt, with their assigned category (sheltered or exposed). The difference is calculated between the winter and the summer EI values.

Mudflat	EI winter	EI summer	Difference	EI total	Winter Category
PP (WS)	0.41	0.40	0.02	0.54	Sheltered
ZG (WS)	0.82	0.52	0.30	0.77	Exposed
BA (WS)	0.76	0.44	0.33	0.69	Exposed
HE (WS)	0.40	0.45	- 0.05	0.53	Sheltered
WA (WS)	0.74	0.48	0.26	0.71	Exposed
RL-BA (WS)	0.59	0.39	0.20	0.56	Exposed
GBS (WS)	0.26	0.21	0.04	0.27	Sheltered
VI (ES)	0.86	0.64	0.22	0.84	Exposed
DM (ES)	1.00	0.80	0.20	1.00	Exposed
RK (ES)	0.60	0.74	- 0.13	0.81	Sheltered

Appendix G - Vegetation trajectories for the research sites (1985-2017)

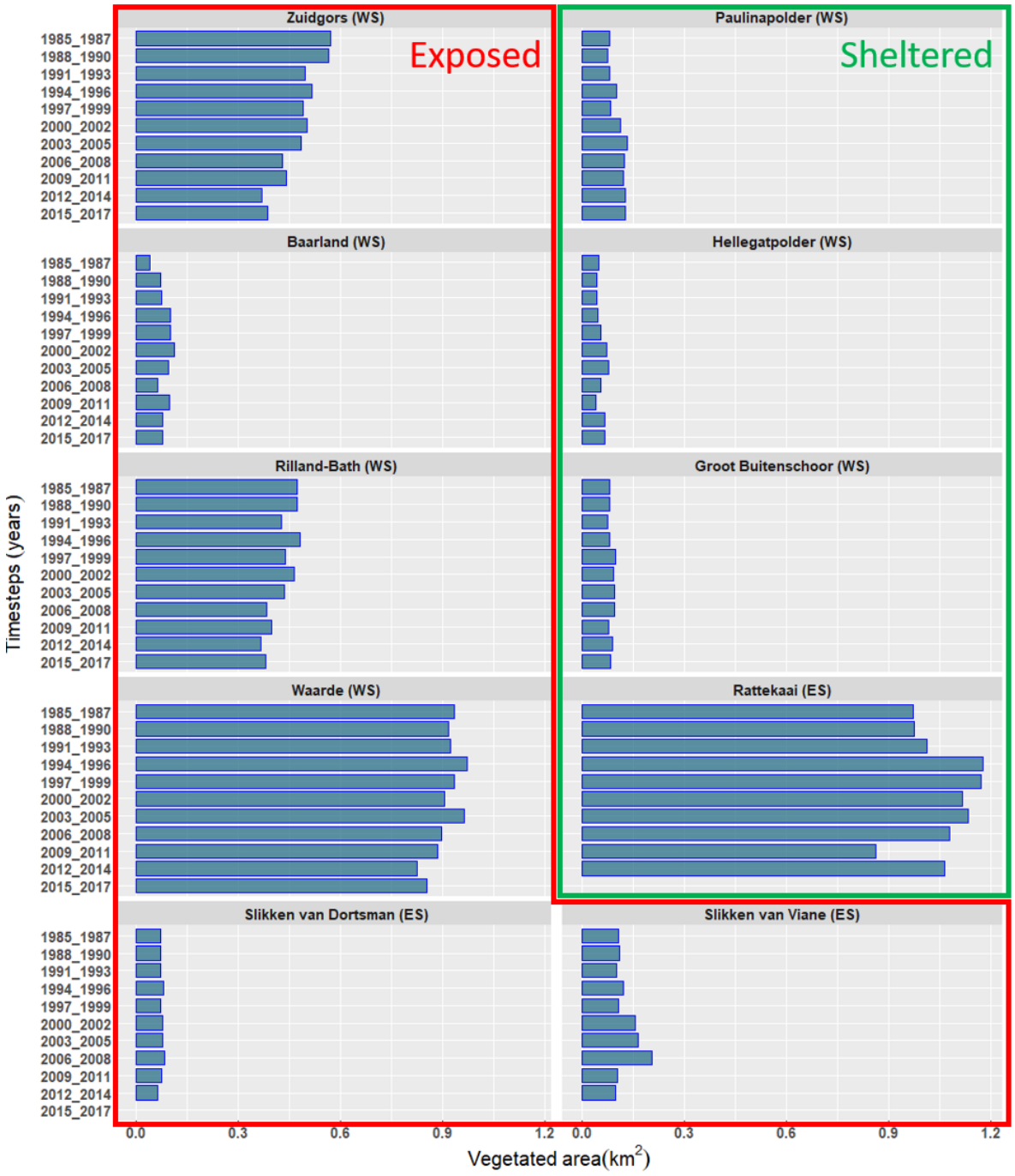

Figure A4 - Absolute vegetated area per three-year timestep. The locations are divided on their assigned exposure category.

Appendix H - Exposure Index versus Vegetation Change in the Western- and Eastern Scheldt

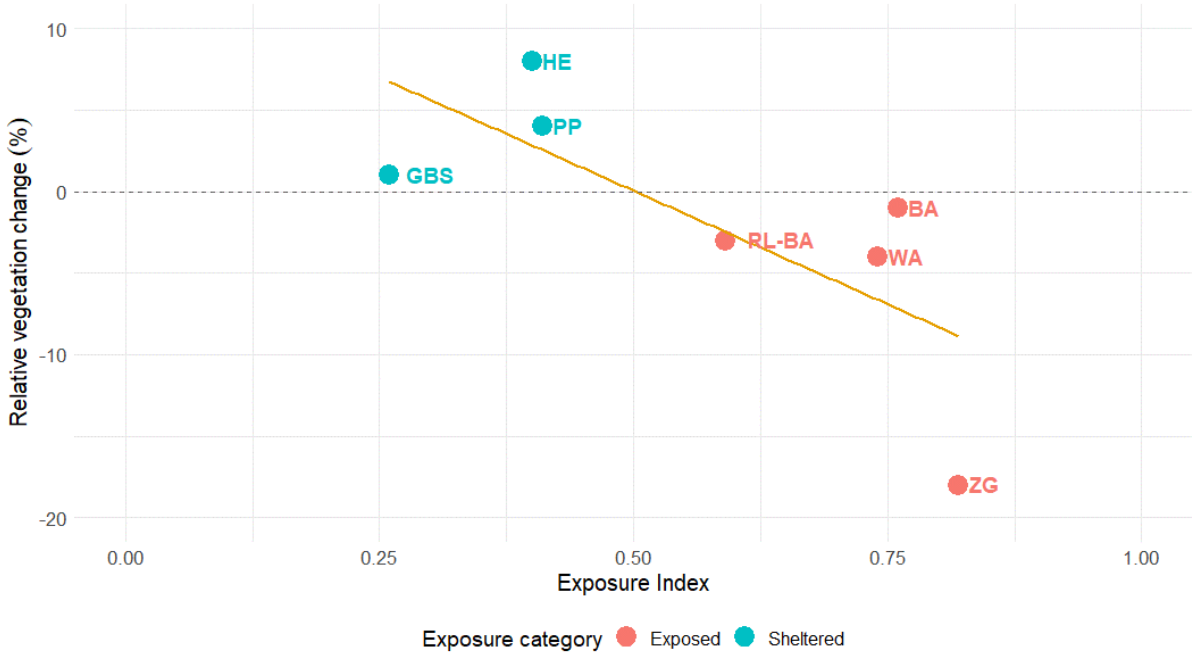

Figure A5 – Exposure Index versus the relative vegetation change in the Western Scheldt between 1988-2014. (r=-0.729, P=0.06)

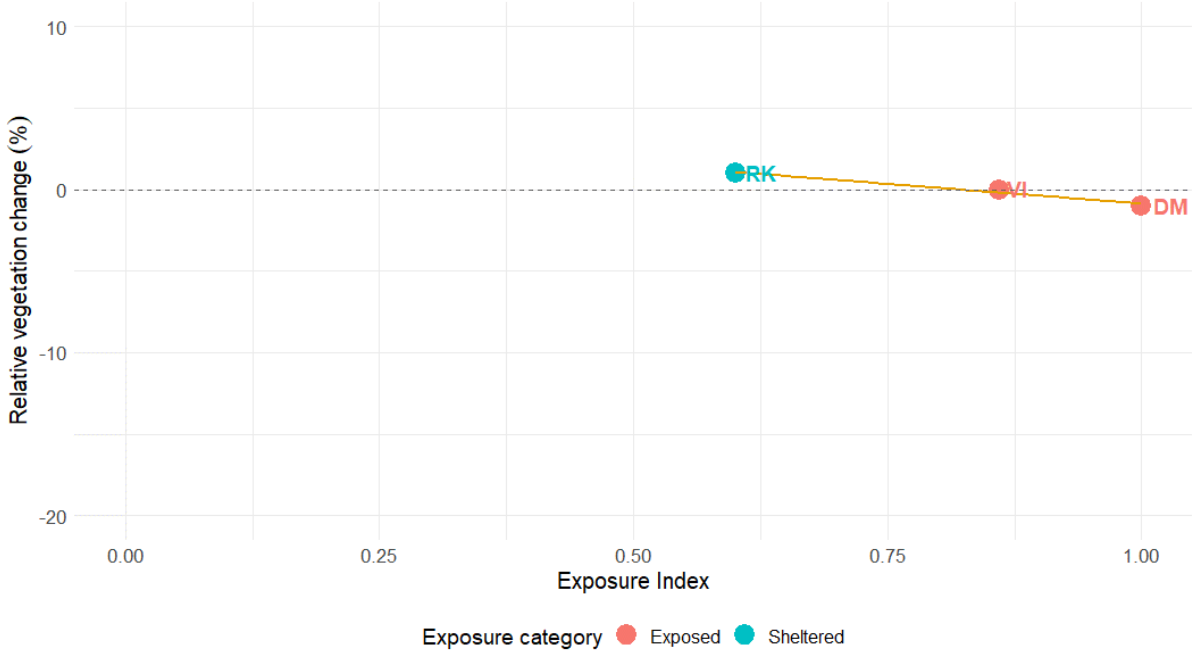

Figure A6 – Exposure Index versus the relative vegetation change in the Eastern Scheldt between 1988-2014. (r=-0.985, P>0.05)

Appendix I - Wind Speed and Temperature during the Measurements

The temperature during the experiment ranged between 0.8 and 8.3°C. The windspeed along the Dutch coast showed to be larger compared to the rest of the year 2019. Three storms have been measured during the winter of 2019/ 2020: Ciara, Dennis and Ellen (figure A7). Only the data measured at the Vlissingen KNMI station (western Scheldt) has been used since the data from the Oosterschelde KNMI station missed a significant amount of days during the past year (KNMI, 2020). The magnitude of the wind speed is expected to slightly differ between the two stations, but the temperature is expected to be generally similar.

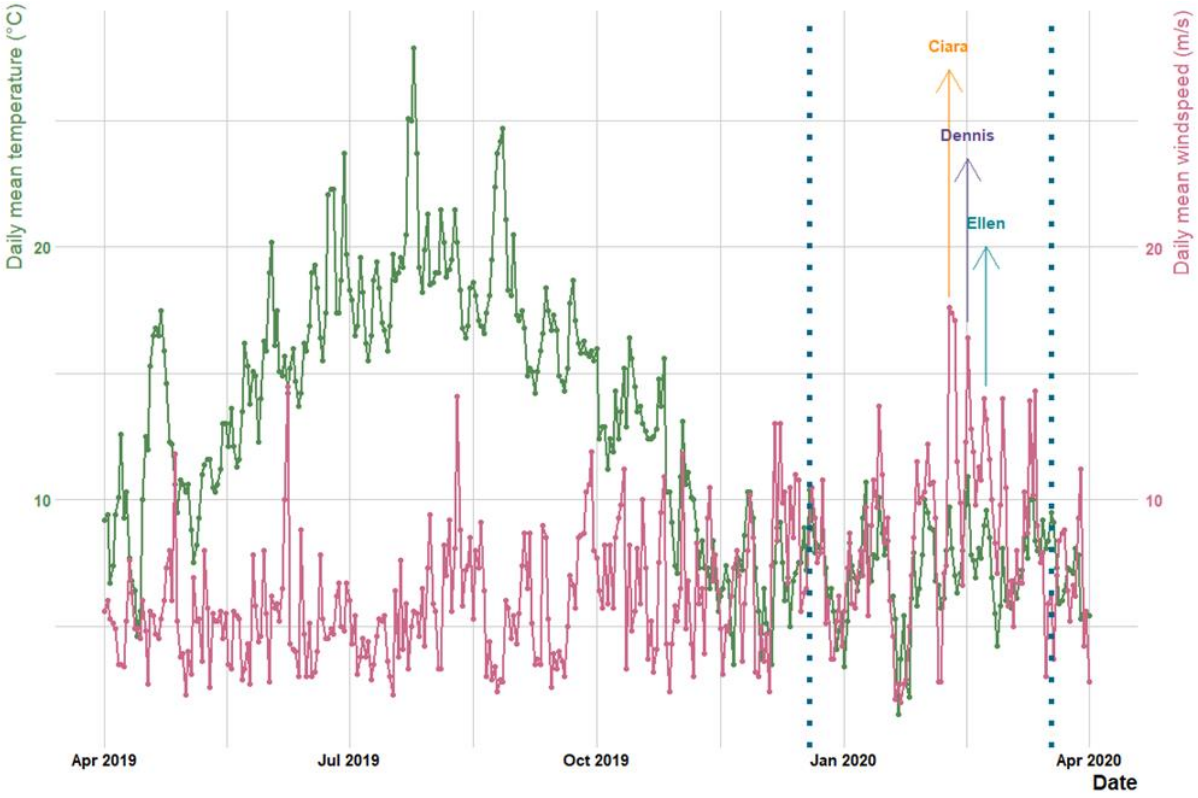

Figure A7 – Daily mean temperature and mean windspeed between April 2019 to April 2020, for the KNMI location of Vlissingen. The blue dotted lines indicate the period in which the measurements used for this research are executed. The arrows show the dates within the measure period, on which storms took place, with their names indicated above the arrows.

Appendix J - Relation between the Distance from Saltmarsh Edge and the Inundation Time (%)

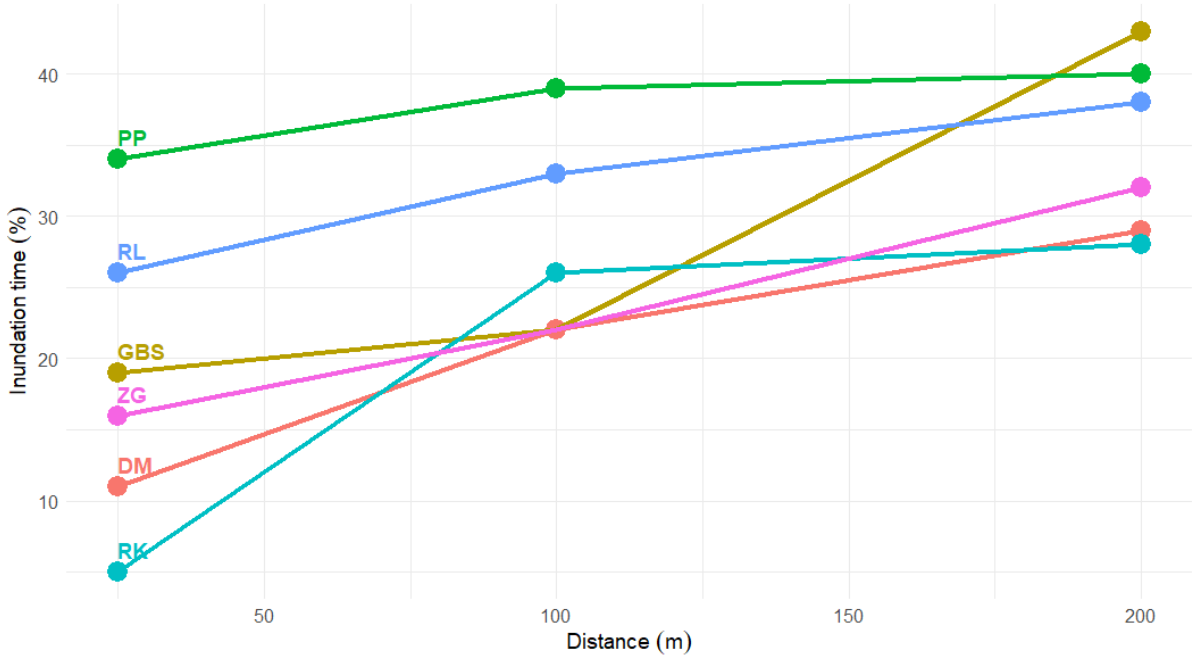

Figure A8 – Relation between the individual fieldwork locations and distances from saltmarsh edge with the average inundation time (%).

Appendix K – Results Wet Bulk Density Analyses

i. Median Wet Bulk Density Data

Table A2 – The average data resulting from the WBD data analyses. The Average values of the two campaigns is also provided

Mudflat	Distance (m)	Median 2019/12 WBD (g*cm^3)	Median 2020/01 WBD (g*cm^3)	Average median WBD (g*cm^3)
PP (WS)	25	1.33	1.43	1.38
PP (WS)	100	1.82	1.62	1.72
PP (WS)	200	1.68	1.57	1.63
ZG (WS)	25	1.64	1.37	1.51
ZG (WS)	100	1.66	1.55	1.60
ZG (WS)	200	1.72	1.37	1.55
RL (WS)	25	1.73	1.71	1.72
RL (WS)	100	1.86	1.76	1.81
RL (WS)	200	1.81	1.77	1.79
GBS (WS)	25	1.42	1.39	1.41
GBS (WS)	100	1.52	1.42	1.47
GBS (WS)	200	1.45	1.52	1.48
DM (ES)	25	1.69	1.68	1.68
DM (ES)	100	1.87	1.61	1.74
DM (ES)	200	1.77	1.71	1.74
RK (ES)	25	1.47	1.48	1.48
RK (ES)	100	1.82	1.69	1.75
RK (ES)	200	2.03	1.64	1.83

ii. Normality test of the Wet Bulk Density Data

A QQ-plot showed how the data points lie along the normal distribution line within the 95% significance level meaning the data can be interpreted as being normally distributed (figure A9). The Shapiro-Wilk normality test result are in line with this ($p > 0.05$) indicating the dataset to be normally distributed. The Tukey HSD test showed that the moment of data collection was of significant impact to the WBD values ($P<0.05$).

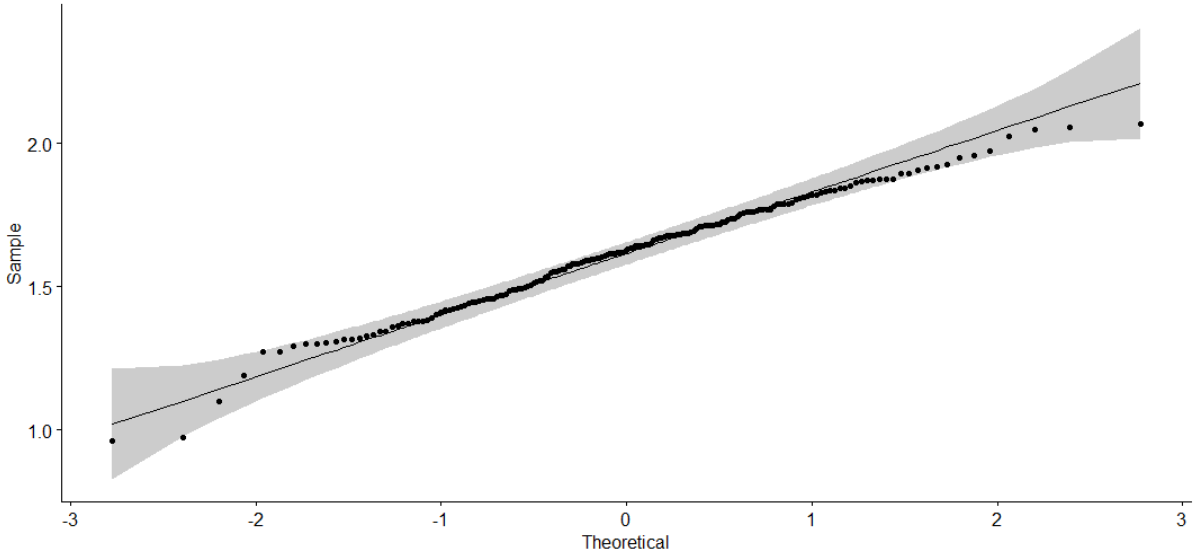

Figure A9 – Result of the QQ-plot for the WBD dataset of the two campaigns.

iii. Outcome of the Wet Bulk Density model

External factors (the location, distance from the saltmarsh edge and the field campaign) showed to be of significant impact for the outcome of the WBD data (table A5). This model provides with an adjusted R^2 of 0.509 (p-value < 2.2e-16), and thus an explanatory value of the observations of 51%.

*Table A3 - Outcome of the WBD model explaining the measured values for 50.9%. The intercept provides with the reference values to which the other estimate values are calculated. The Intercept stands for RL, Distance 25 m and Field campaign 2019/12. Significant. codes: 0 '***' 0.001 '**' 0.01 '*' 0.05 '.' 0.1 ' ' 1*

	Estimate	Std Error	Significance
(Intercept)	1.876894	0.031509	***
ZG (WS)	-0.250333	0.036384	***
DM (ES)	-0.054600	0.036384	
PP (WS)	-0.194833	0.036384	***
GBS (WS)	-0.337200	0.036384	***
RK (ES)	-0.106967	0.036384	**
Distance 100 m	0.13535	0.02573	***
Distance 200 m	0.14068	0.02573	***
Field campaign 2020/01	-0.122311	0.021006	***

Appendix L – Results of the Dry Bulk Density Analyses

i. Median Dry Bulk Density Data

Table A4 - The average data resulting from the DBD data analyses. The Average values of the two campaigns is also provided

Mudflat	Distance (m)	Median 2019/12 DBD (g*cm^3)	Median 2020/01 DBD (g*cm^3)	Average median DBD (g*cm^3)
PP (WS)	25	0.84	0.89	0.86
PP (WS)	100	1.23	1.08	1.16
PP (WS)	200	1.17	1.04	1.11
ZG (WS)	25	1.02	0.96	0.99
ZG (WS)	100	1.06	1.04	1.05
ZG (WS)	200	1.10	0.86	0.98
RL (WS)	25	1.30	1.33	1.31
RL (WS)	100	1.47	1.39	1.43
RL (WS)	200	1.45	1.39	1.42
GBS (WS)	25	0.91	0.93	0.92
GBS (WS)	100	1.03	0.92	0.97
GBS (WS)	200	0.85	0.91	0.88
DM (ES)	25	1.10	1.31	1.21
DM (ES)	100	1.39	1.17	1.28
DM (ES)	200	1.33	1.29	1.31
RK (ES)	25	0.85	1.00	0.92
RK (ES)	100	1.37	1.24	1.31
RK (ES)	200	1.58	1.22	1.40

ii. Normality test of the Dry Bulk Density Data

A QQ-plot analyses shows the datapoints fitting to the normal distribution line (figure A10). A Shapiro-test shows that the 2019 dataset is normally distributed, but not the 2020 dataset. Keeping in mind the natural source of the data, the data is adopted to be normally distributed.

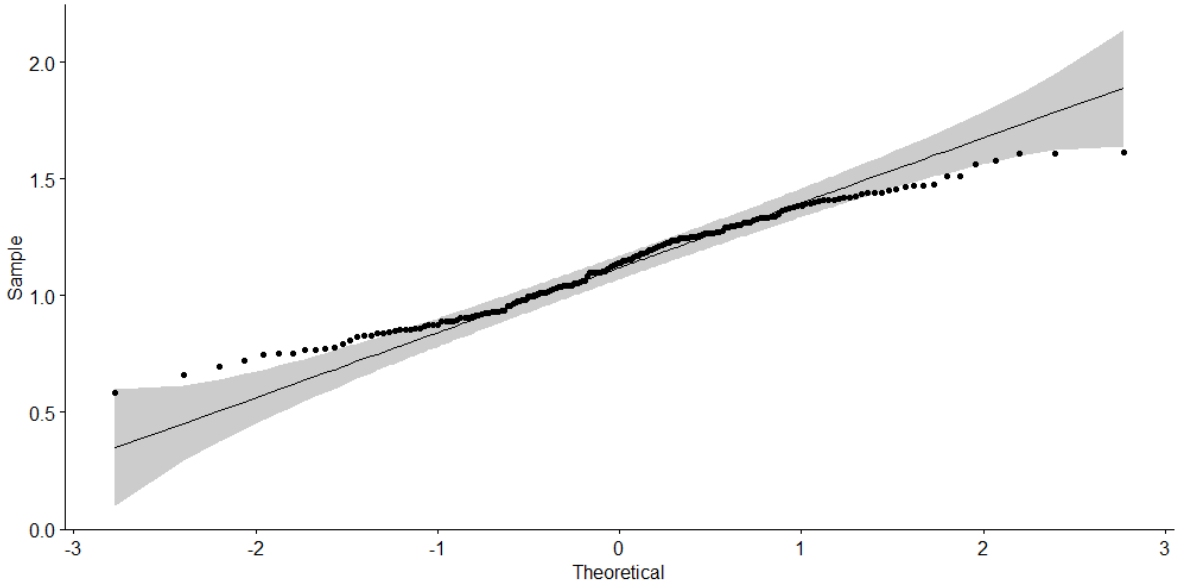

Figure A10 - Result of the QQ-plot for the DBD dataset of the two campaigns.

iii. Outcome of the Dry Bulk Density model

External factors (the location, distance from the saltmarsh edge and the field campaign) showed to be of significant impact for the outcome of the DBD data (table A7). This model provides with an adjusted R^2 of 0.644 (p-value < 2.2e-16), and thus an explanatory value of the observations of 64%.

*Table A7 - Outcome of the DBD model explaining the measured values for 64.4%. The intercept provides with the reference values to which the other estimate values are calculated. The Intercept stands for RL, Distance 25m and Field campaign 2019/12. Significant. codes: 0 '***' 0.001 '**' 0.01 '*' 0.05 '.' 0.1 ' ' 1*

	Estimate	Std. Error	Significance
(Intercept)	1.31714	0.03028	***
ZG (WS)	-0.38633	0.03497	***
DM (ES)	-0.11697	0.03497	**
PP (WS)	-0.33987	0.03497	***
GBS (WS)	-0.47383	0.03497	***
RK (ES)	-0.19337	0.03497	***
Distance 100 m	0.16138	0.02473	***
Distance 200 m	0.15603	0.02473	***
Field campaign 2020/01	-0.07877	0.02019	***

Appendix M – Results of the Median Grainsize Analyses

i. Median Grainsizes and corresponding Wentworth scale category

Table A8 - The Wentworth category belonging to each of the fieldwork and satellite locations median values. The last four columns represent the satellite locations. The Wentworth categories as found in the ecotope maps (chapter 3) correspond to values found in literature(Zhu et al., 2019)

Mudflat	Distance	Average median grainsize (µm)	Category (Wentworth (1922))
PP (WS)	25	45.5	Coarse silt
PP (WS)	100	53.3	Coarse silt
PP (WS)	200	60.2	Coarse silt
ZG (WS)	25	54.8	Coarse silt
ZG (WS)	100	72.2	Very fine sand
ZG (WS)	200	43.9	Coarse silt
RL (WS)	25	127.8	Fine sand
RL (WS)	100	144.2	Fine sand
RL (WS)	200	166.6	Fine sand
GBS (WS)	25	43.7	Coarse silt
GBS (WS)	100	46.0	Coarse silt
GBS (WS)	200	41.3	Coarse silt
DM (ES)	25	70.1	Very fine sand
DM (ES)	100	84.3	Very fine sand
DM (ES)	200	111.8	Very fine sand
RK (ES)	25	48.4	Coarse silt
RK (ES)	100	111.6	Very fine sand
RK (ES)	200	122.6	Very fine sand
BA (WS)	-	-	Silt
HE (WS)	-	-	Fine sand
WA (WS)	-	-	Silt to fine sandy
VI (WS)	-	-	Fine sandy

ii. QQ-plot Median Grainsize

From a QQplot analyses for the median grainsize data it can be observed how the data does not follow the normal distribution line (figure A11). The Shapiro-Wilk normality test also implies no normal distribution ($p<0.05$).

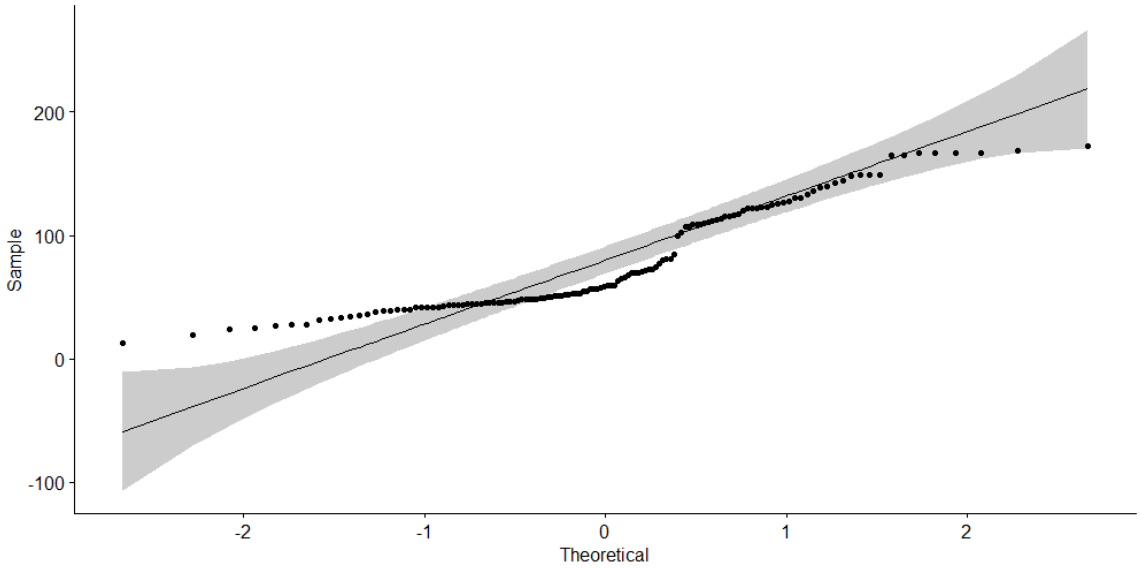

Figure A11 - Result of the QQ-plot for the median grainsize dataset of the two campaigns.

iii. Outcome of the Median Grainsize model

The location, distance from the saltmarsh edge and the field campaign showed to be strongly determinative for the outcome of the found grainsizes (table A9). shows a high explanatory value (adjusted R^2=0.786, P<2.2e-16), meaning that almost 80% of the data distribution can be explained by the location, distance, and campaign.

*Table A9 – Outcome of the model explaining the median grainsize for 78.9%. The intercept provides with the reference values to which the other estimate values are calculated. The Intercept stands for RL, Distance 25m and Field campaign 2019/12. Significant. codes: 0 '***' 0.001 '**' 0.01 '*' 0.05 '.' 0.1 ' ' 1*

	Estimate	Std. Error	Significance
Intercept	127.999	5.229	***
ZG (WS)	-89.54	5.763	***
DM (ES)	-67.251	6.24	***
PP (WS)	-95.803	5.763	***
GBS (WS)	-101.581	5.898	***
RK (ES)	-55.164	6.08	***
Distance 100 m	19.742	4.214	***
Distance 200 m	26.246	4.267	***
Field campaign 2020/02	5.808	3.549	

Appendix N – Results of the Shear Strength Analyses

i. Average Median Shear Strength Data

Table A10 - The average data resulting from the shear strength data analyses.

Mudflat	Exposure	Distance	Average shear strength (kPa)
PP (WS)	Sheltered	25	2.21
PP (WS)	Sheltered	100	2.09
PP (WS)	Sheltered	200	1.74
ZG (WS)	Exposed	25	2.43
ZG (WS)	Exposed	100	2.55
ZG (WS)	Exposed	200	2.72
RL (WS)	Exposed	25	2.57
RL (WS)	Exposed	100	2.48
RL (WS)	Exposed	200	2.68
GBS (WS)	Sheltered	25	2.67
GBS (WS)	Sheltered	100	2.93
GBS (WS)	Sheltered	200	2.17
DM (ES)	Exposed	25	2.50
DM (ES)	Exposed	100	2.58
DM (ES)	Exposed	200	2.57
RK (ES)	Sheltered	25	2.86
RK (ES)	Sheltered	100	2.32
RK (ES)	Sheltered	200	2.27

The shear strength results show that the shear strength is significantly smallest at 200 m and shows no resemblance to the exposure category (table A11). The data is not normally distributed (figure A13). A Tuskey HSD test showed no significant effect of the data collection moment on the shear strength values with $p>0.05$ between the collection at different moments throughout January and February of 2020. The shear strength values also showed to be very poorly dependent on the mudflat, distance, and the campaign (adjusted $R^2 = 0.194$, p-value < 3.7e-16) (table A13).

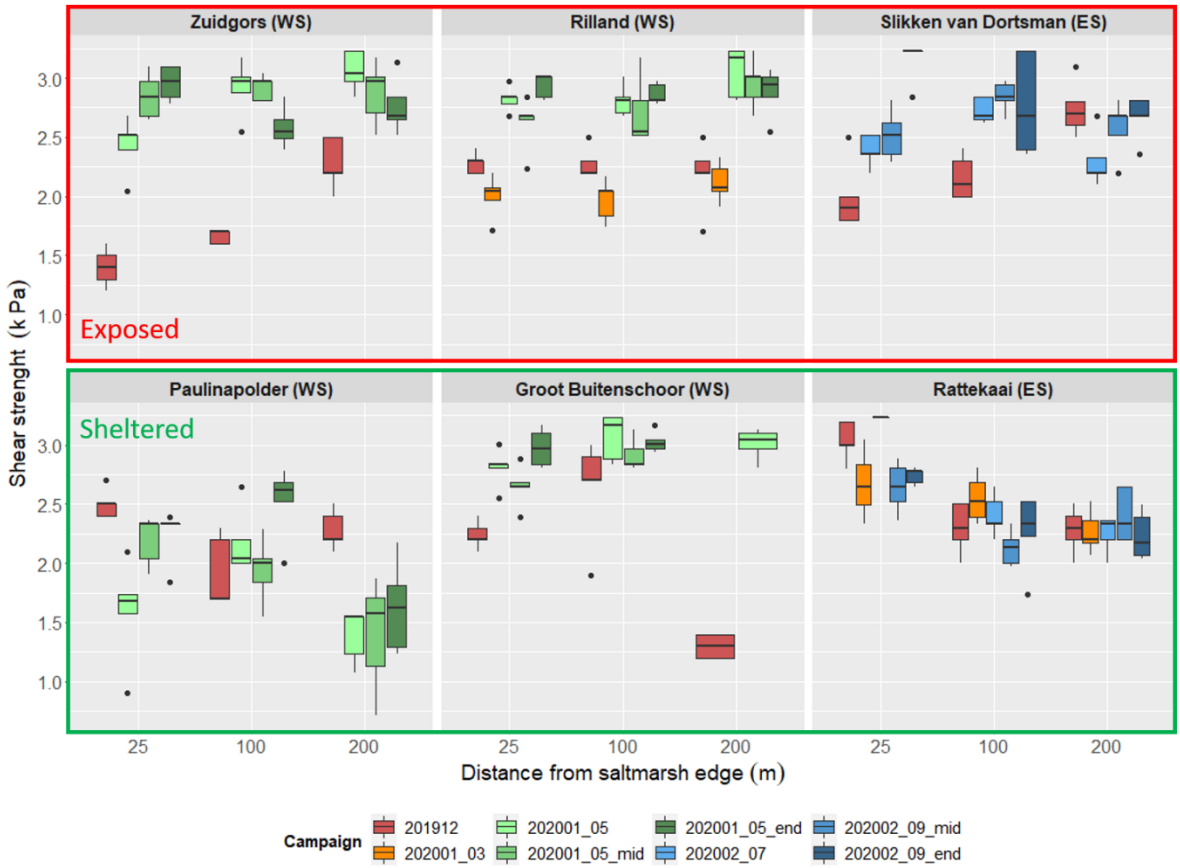

Figure A12 - Shear strength values as measured during different field campaigns (yyyymm_ww). Mid and end values have been measured during the disturbance and recovery experiment, consecutively between hole and pile 3 and 5. The black dots represent outliers in the boxplot.

ii. Normality test of the Shear Strength Data

The QQ-plot analyses show the fit of the data points to the normal distribution line (figure A13). Keeping in mind the natural source of the data, the distribution is interpreted as being a normal distribution. However, the Shapiro-Wilk normality test implies a data distribution being significantly different from a normal distribution (P<0.05) (p-value = 1.154e-8) .

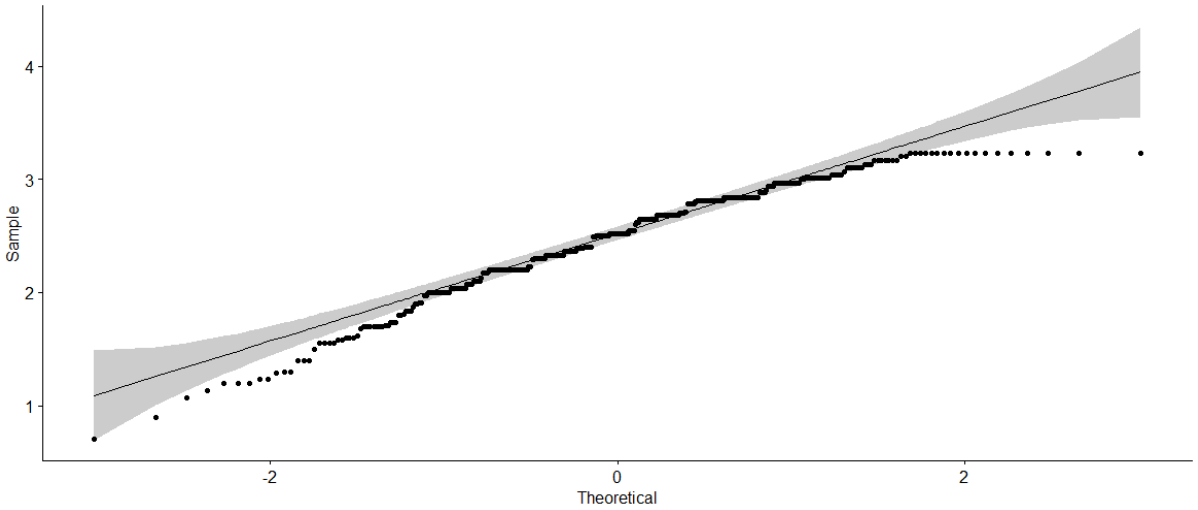

Figure A13 – QQ-plot of the shear strength data set from all the campaigns.

A Tukey HSD test has been conducted between all the campaigns to compare the effect of different campaigns to the shear strength of the sediments. There was no significant effect of the data collection moment on the shear strength values with $p>0.05$ between the collection at different moments throughout January and February of 2020. There was however found a significant difference between campaigns in week 5, 7 and 9 to the measurements done in December 2019 ($p<0.05$). Notable is the significance within both campaign 5 and 7 between the locations measured next to the ASED-sensor and between the holes and piles (mid and end measurements) from the disturbance and recovery experiment.

*Table A11- Outcome of the shear vane model explaining the measured values for 19.4%. The intercept provides with the reference values to which the other estimate values are calculated. The Intercept stands for ZG, Distance 25. Significant. codes: 0 '***' 0.001 '**' 0.01 '*' 0.05 '.' 0.1 ' ' 1*

	Estimate	Std. Error	Significance
(Intercept)	2.618367	0.065822	***
Rilland (WS)	0.006633	0.077076	
Slikken van Dortsman (ES)	0.013333	0.081245	
Paulinapolder (WS)	-0.575333	0.081245	***
Groot Buitenschoor (WS)	0.088199	0.085464	
Rattekaai (ES)	-0.0647	0.077076	
distance100	-0.031231	0.055195	
distance200	-0.149369	0.056536	**

Appendix O - Recovery Rate Data

Table A12 – Recovery data as used for all the statistical analyses. Δt is in tides and λ in tides^{-1}.

SM	Dist	P / H	Δt	Date start	Date end	Initial height/ depth disturbance (cm)	Final height/ depth disturbance (cm)	Z(dist. 0) SED	Z(dist.end)SED	ΔSED (cm)	Z(dist.end)	Recovery (cm)	Dist.z.end (fractie)	recovery.z.end. fractie (=f)	λ
PP	25	H	56	28/01	25/02	-17.48	-4.3	0.208	0.223	-1.481	-2.819	-14.661	0.161	0.839	0.014
PP	25	P	100	28/01	18/03	20.1	8.12	0.208	0.228	-2.044	10.164	9.936	0.506	0.494	0.003
PP	100	H	56	28/01	25/02	-15.24	-3.68	0.125	0.131	-0.590	-3.090	-12.150	0.203	0.797	0.012
PP	100	P	100	28/01	18/03	20.4	6.1	0.125	0.136	-1.040	7.140	13.260	0.350	0.650	0.005
PP	200	H	56	28/01	25/02	-15.74	-2.52	0.155	0.162	-0.675	-1.845	-13.895	0.117	0.883	0.017
PP	200	P	100	28/01	18/03	15.04	4.04	0.155	0.171	-1.566	5.606	9.434	0.373	0.627	0.004
ZG	25	H	56	28/01	25/02	-14.74	-9.88	0.127	0.152	-2.533	-7.347	-7.393	0.498	0.502	0.005
ZG	25	P	48	28/01	21/02	18	0.52	0.127	0.141	-1.463	1.983	16.017	0.110	0.890	0.020
ZG	100	H	56	28/01	25/02	-14.72	-8.32	0.128	0.187	-5.888	-2.432	-12.288	0.165	0.835	0.014
ZG	100	P	18	28/01	06/02	16.5	5.18	0.128	0.133	-0.478	5.658	10.842	0.343	0.657	0.026
ZG	200	H	32	28/01	13/02	-14.5	-8.18	0.169	0.185	-1.556	-6.624	-7.876	0.457	0.543	0.011
ZG	200	P	32	28/01	13/02	17.82	1.06	0.169	0.185	-1.556	2.616	15.204	0.147	0.853	0.026
RL	25	H	6	28/01	31/01	-11.24	-0.36	0.124	0.126	-0.263	-0.097	-11.143	0.009	0.991	0.344
RL	25	P	2	28/01	29/01	13.48	-0.08	0.124	0.124	-0.028	-0.052	13.532	-0.004	1.004	Error
RL	100	H	6	28/01	31/01	-11.94	-3.1	error	error	error	error	error	error	error	Error
RL	100	P	4	28/01	30/01	13.92	0.96	error	error	error	error	error	error	error	Error
RL	200	H	6	28/01	31/01	-11.525	-2.6	0.219	0.220	-0.019	-2.581	-8.944	0.224	0.776	0.108
RL	200	P	2	28/01	29/01	14.22	-2.34	0.219	0.214	0.553	-2.893	17.113	-0.203	1.203	Error
GBS	25	H	54	29/01	25/02	-22.26	-10.82	0.152	0.159	-0.760	-10.060	-12.200	0.452	0.548	0.006
GBS	25	P	54	29/01	25/02	15.86	4.58	0.152	0.159	-0.760	5.340	10.520	0.337	0.663	0.009
GBS	100	H	54	29/01	25/02	-21.34	-10.78	0.127	0.131	-0.440	-10.340	-11.000	0.485	0.515	0.006

SM	Dist	P / H	Δt	Date start	Date end	Initial height/ depth disturbance (cm)	Final height/ depth disturbance (cm)	Z(dist. 0) SED	Z(dist.end)SED	ΔSED (cm)	Z(dist.end)	Recovery (cm)	Dist.z.end (fractie)	Recovery.z.end. fractie (=f)	λ
GBS	100	P	54	29/01	25/02	17.2	9.9	0.127	0.131	-0.440	10.340	6.860	0.601	0.399	0.004
DM	25	H	40	26/02	17/03	-16	-6.275	0.189	0.196	-0.778	-5.497	-10.503	0.344	0.656	0.012
DM	25	P	40	26/02	17/03	14.875	13.275	0.189	0.196	-0.778	14.053	0.822	0.945	0.055	0.001
DM	100	H	40	26/02	17/03	-15.18	-3.3	0.187	0.199	-1.219	-2.081	-13.099	0.137	0.863	0.022
DM	100	P	40	26/02	17/03	9.34	4.98	0.187	0.199	-1.219	6.199	3.141	0.664	0.336	0.004
DM	200	H	40	26/02	17/03	-11.64	-2.18	0.153	0.157	-0.328	-1.852	-9.788	0.159	0.841	0.020
DM	200	P	4	26/02	28/02	7.88	2.2	0.153	0.153	0.056	2.144	5.736	0.272	0.728	0.141
RK	25	H	40	26/02	17/03	-15.2	-4.74	0.157	0.158	-0.019	-4.721	-10.479	0.311	0.689	0.013
RK	25	P	40	26/02	17/03	14.28	10.58	0.157	0.158	-0.019	10.599	3.681	0.742	0.258	0.003
RK	100	H	12	26/02	03/03	-14.78	-2.76	0.126	0.125	0.178	-2.938	-11.842	0.199	0.801	0.058
RK	100	P	6	26/02	29/02	7.76	1.04	0.126	0.125	0.141	0.899	6.861	0.116	0.884	0.156
RK	200	H	12	26/02	03/03	-14.14	-3.34	0.185	0.192	-0.750	-2.590	-11.550	0.183	0.817	0.061
RK	200	P	12	26/02	03/03	7.7	0.24	0.185	0.192	-0.750	0.990	6.710	0.129	0.871	0.074

Appendix P – Grainsize versus Recovery Rate of the Piles and Holes

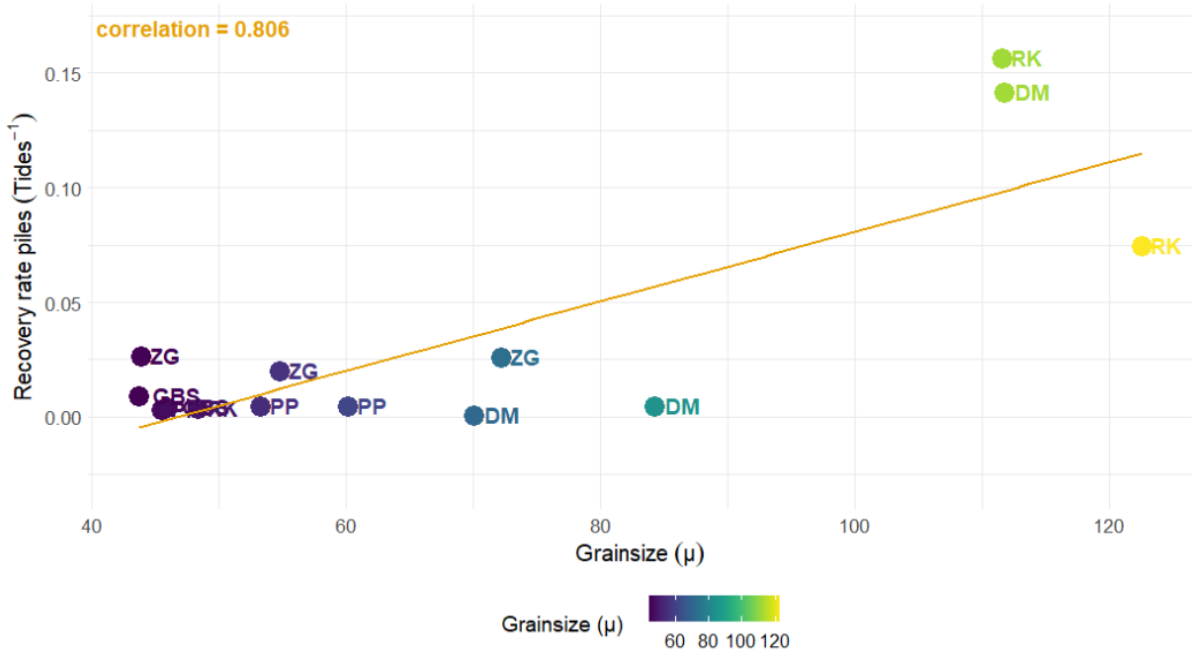

Figure A14 – Average median grainsize versus the recovery rates of the piles for all locations with their correlation coefficient (r=0.806, P<0.001)

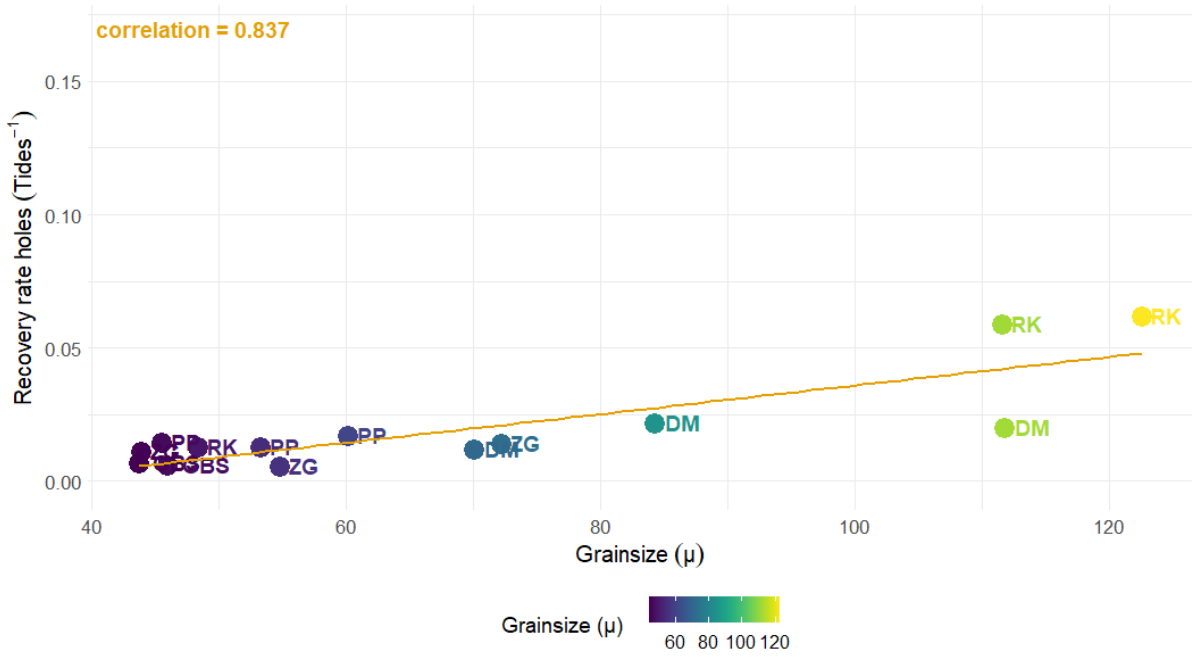

Figure A15 - Average median grainsize versus the recovery rates of the holes for all locations with their correlation coefficient (r=0.837, P<0.001)

Appendix Q - Inundation Time versus the Recovery time of the Piles and Holes

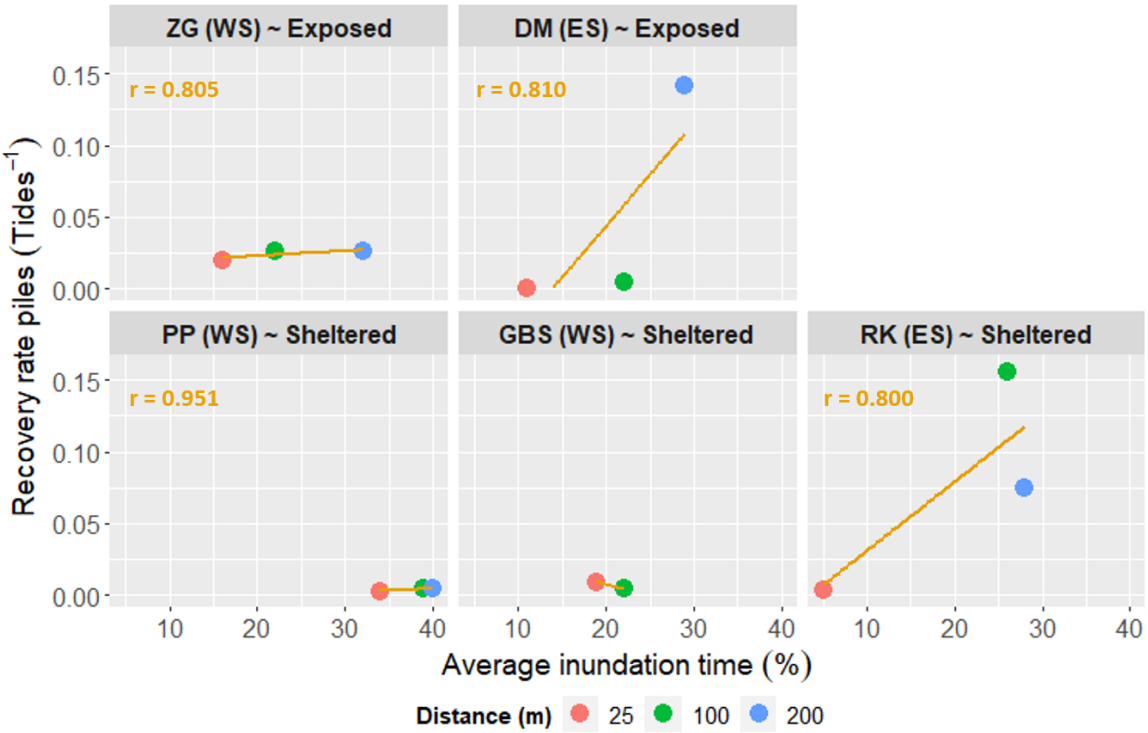

Figure A16 – Average Inundation Time (%) versus the recovery time of the piles per tidal flat. The correlation coefficient in shown for each tidal flat, all the correlations are not significant (P>0.05).

Figure A17 - Average Inundation Time (%) versus the recovery time of the holes per tidal flat. The correlation coefficient in shown for each tidal flat, all the correlations are not significant (P>0.05).

Appendix R – Dry Bulk Density versus the Recovery time of the Piles and Holes

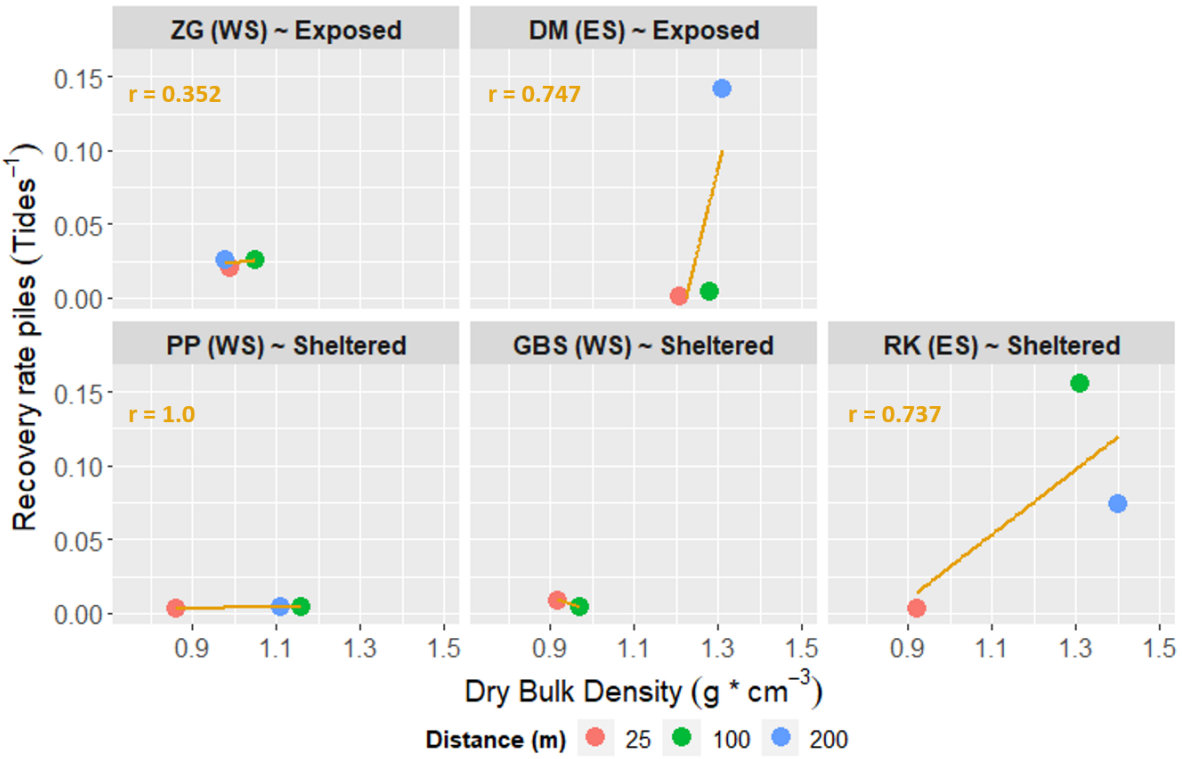

Figure A18 – Average median DBD versus the recovery time of the piles per tidal flat. The correlation coefficient in shown for each tidal flat, all the correlations are not significant (P>0.05).

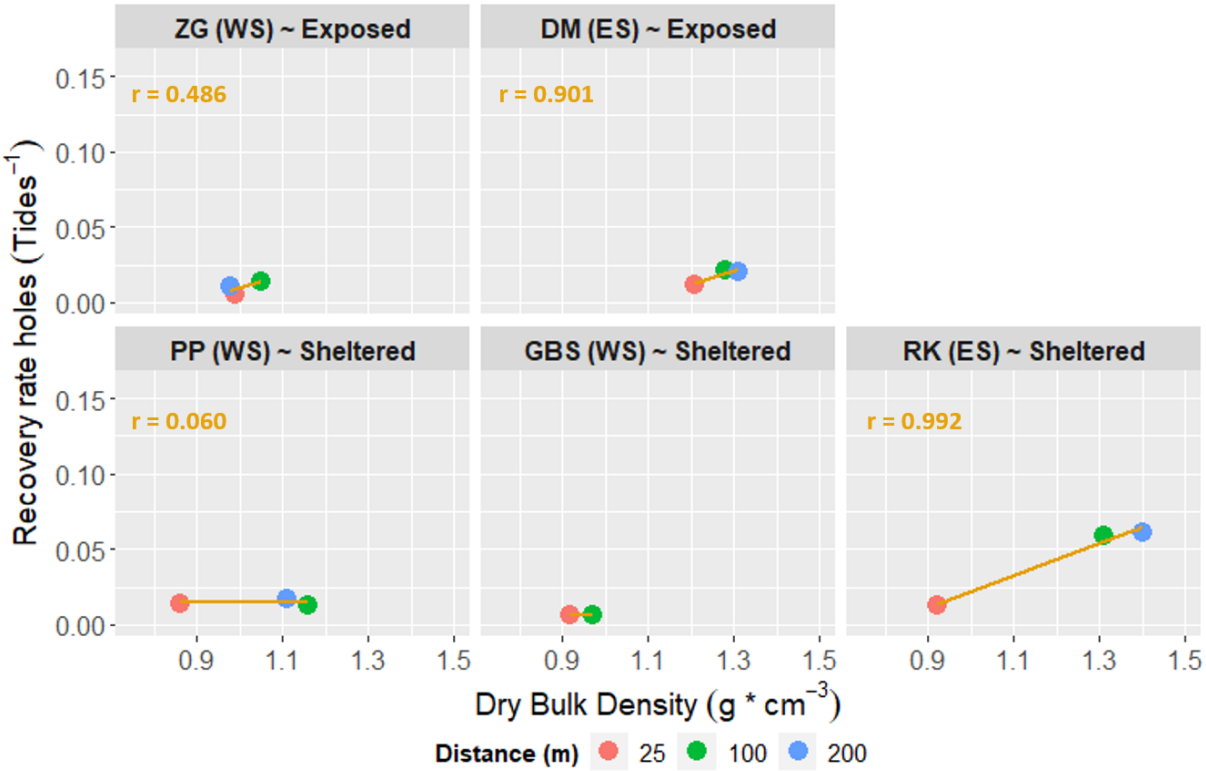

Figure A19 - Average median DBD versus the recovery time of the piles per tidal flat. The correlation coefficient in shown for each tidal flat, all the correlations are not significant (P>0.05).

Appendix S - Exposure Index versus the Recovery Rates in the Eastern- and Western Scheldt

i. Exposure Index versus the recovery rates for all fieldwork locations

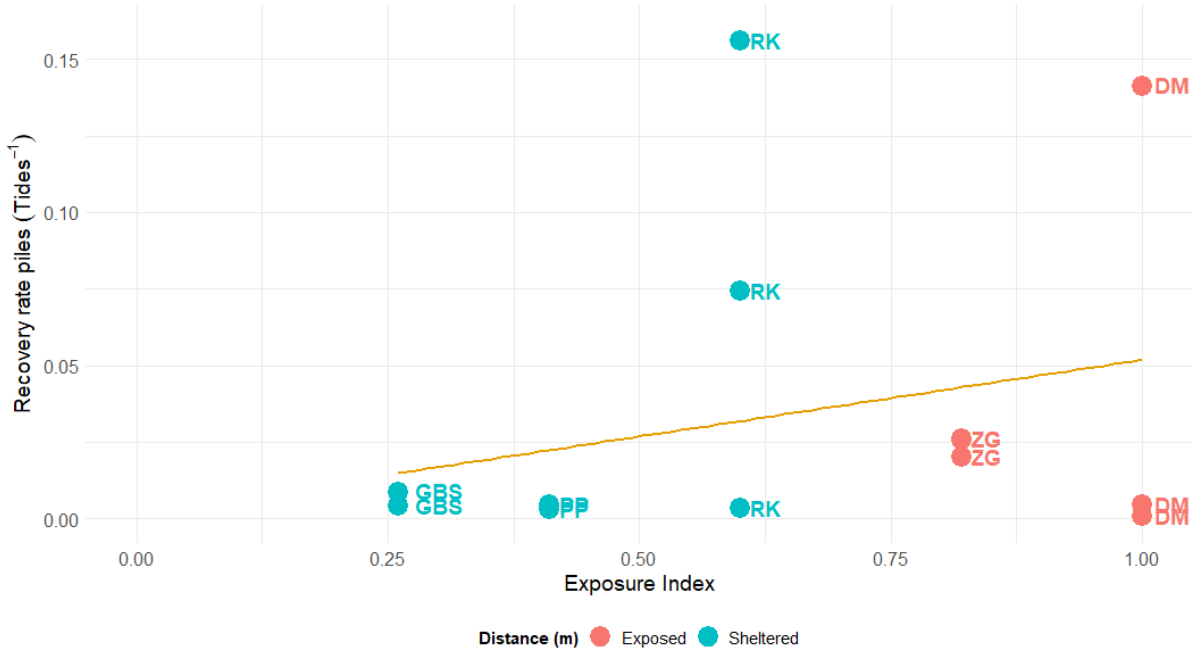

Figure A20 – Exposure Index versus the recovery rates of the piles for all fieldwork locations with their correlation coefficient (r=0.257, P>0.05)

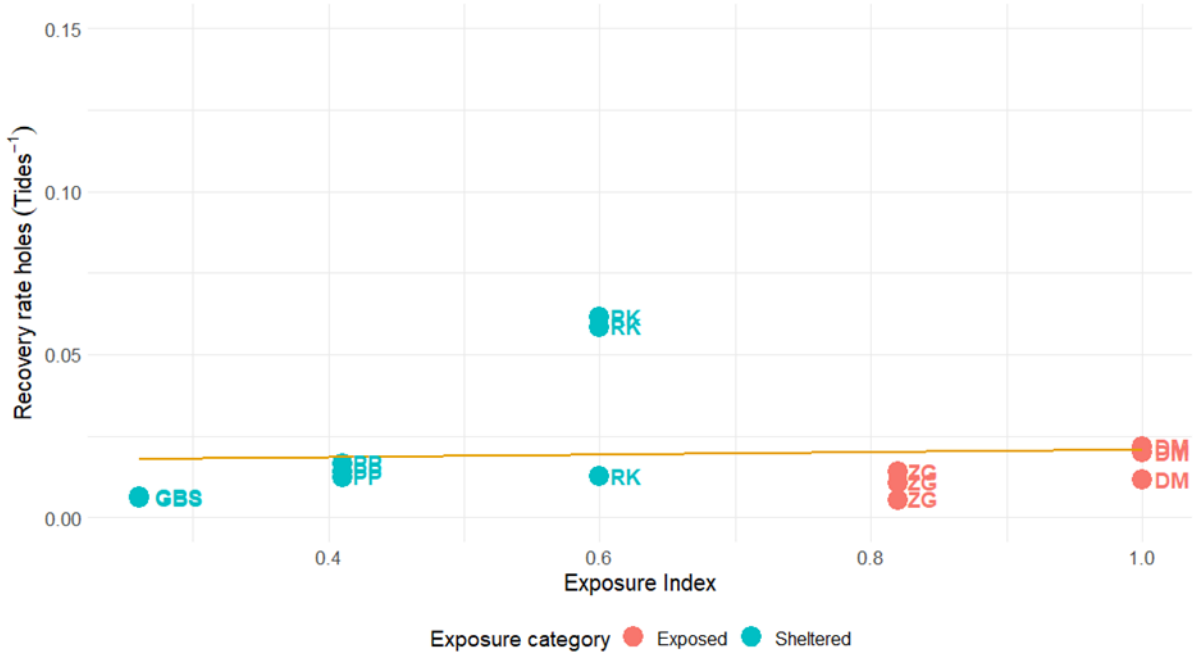

Figure A21 - Exposure Index versus the recovery rates of the piles for all fieldwork locations with their correlation coefficient (r=-0.059, P>0.05)

ii. Exposure Index versus the recovery rates in the Western Scheldt

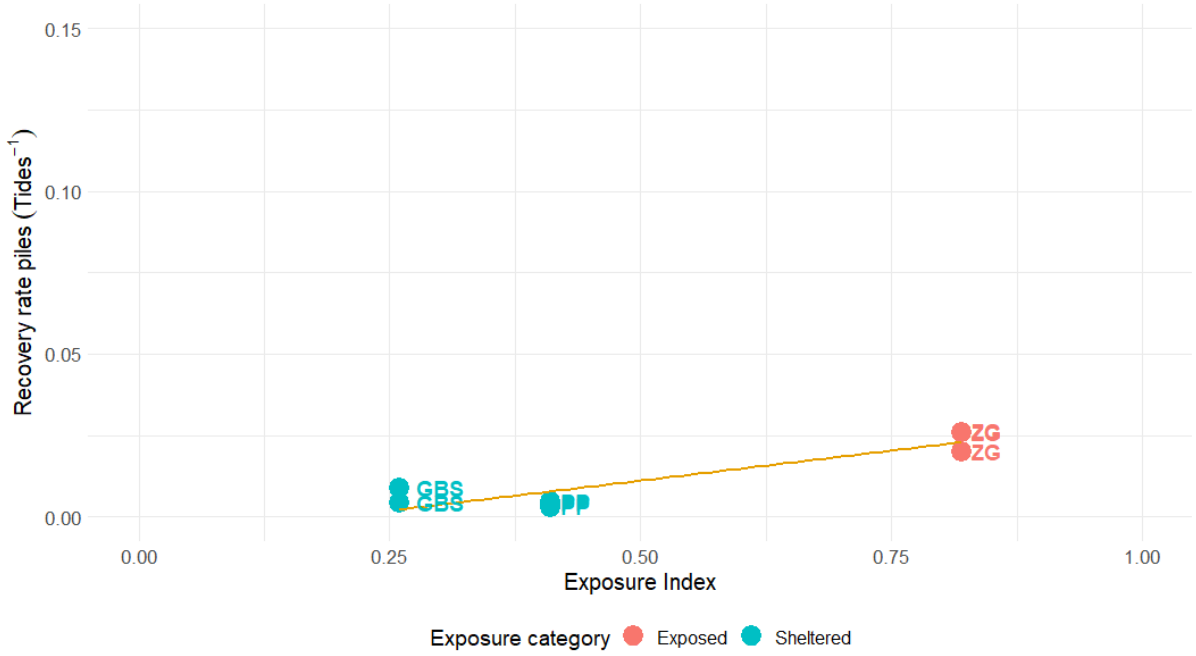

Figure A22 – Exposure Index versus the recovery rates of the piles for the fieldwork locations in the Western Scheldt with their correlation coefficient (r=0.914, P<0.05)

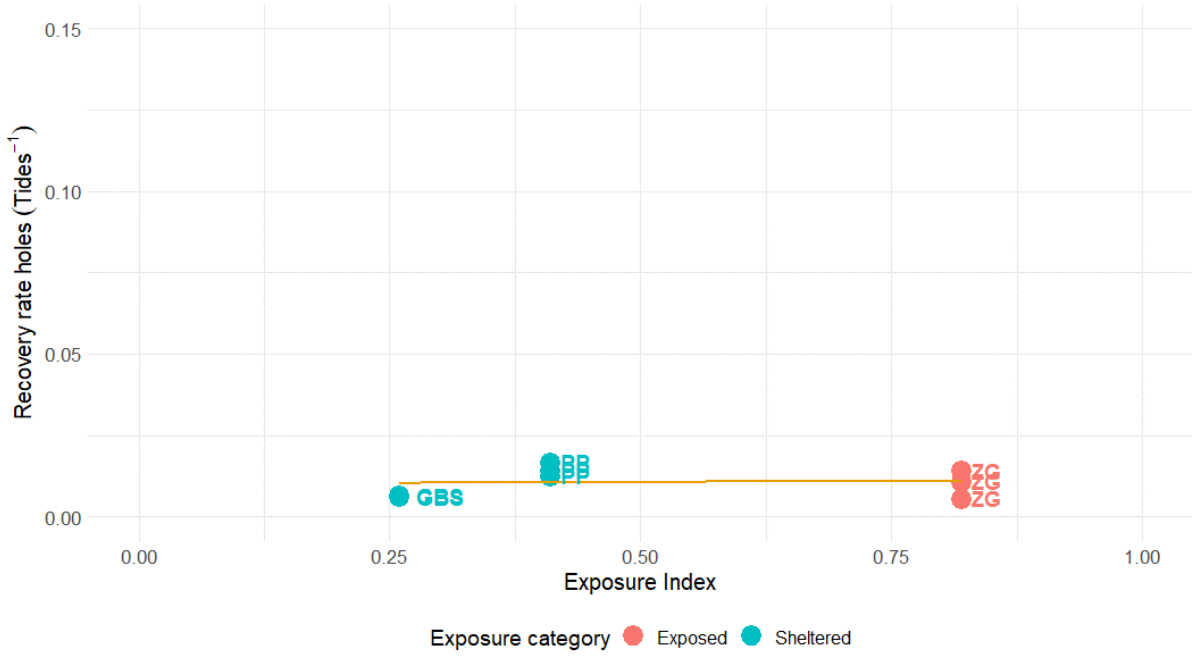

Figure A23 - Exposure Index versus the recovery rates of the holes for the fieldwork locations in the Western Scheldt with their correlation coefficient (r=0.071, P>0.05)

iii. Exposure Index versus the recovery rates in the Eastern Scheldt

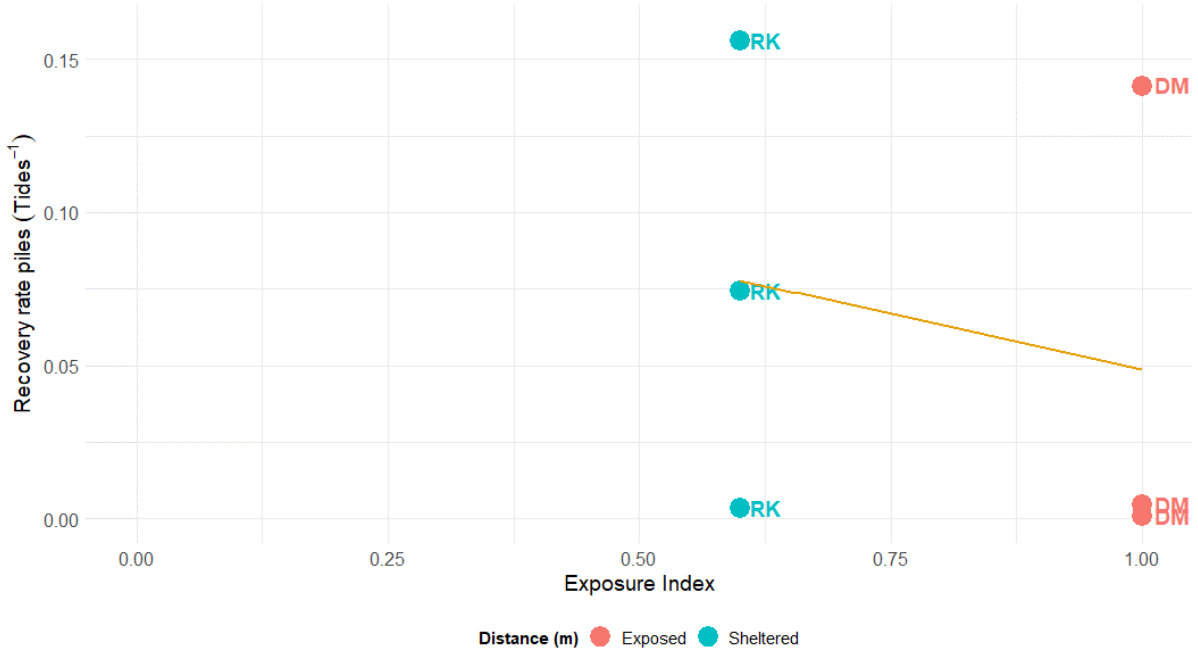

Figure A24 – Exposure Index versus the recovery rates of the piles for the fieldwork locations in the Eastern Scheldt with their correlation coefficient (r=-0.221, P>0.05)

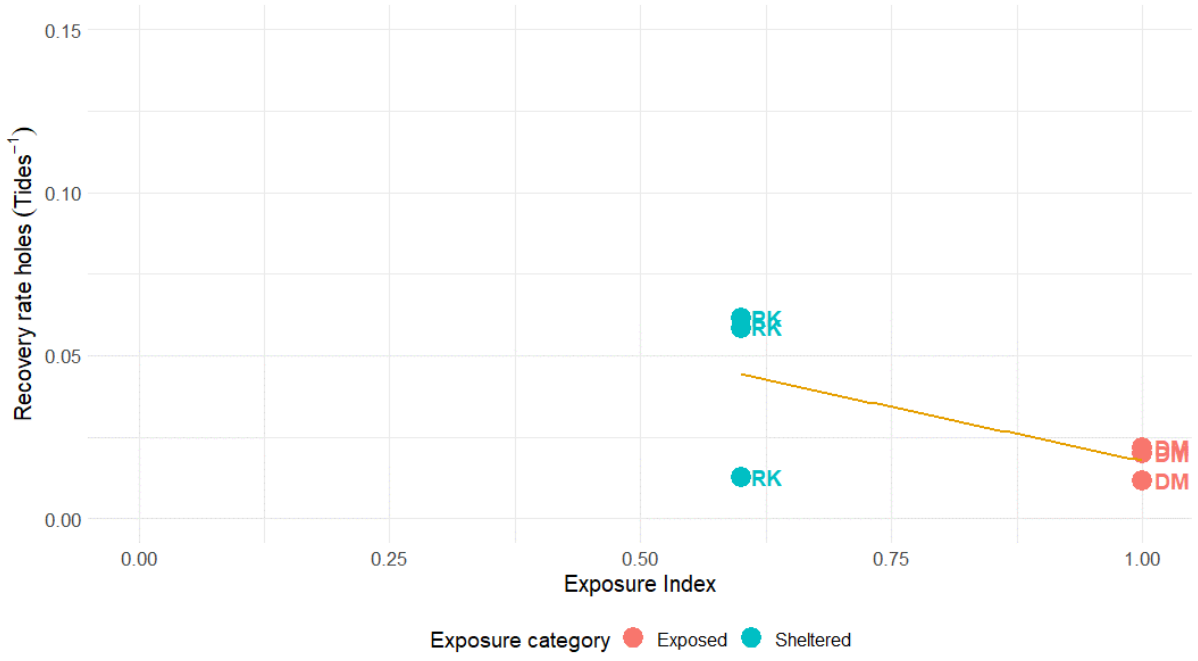

Figure A25 - Exposure Index versus the recovery rates of the holes for the fieldwork locations in the Eastern Scheldt with their correlation coefficient (r=-0.636, P>0.05)

Appendix T - Recovery Rates versus the Vegetation Change in the Eastern- and Western Scheldt

i. Recovery rates versus the long-term vegetation change for all fieldwork locations

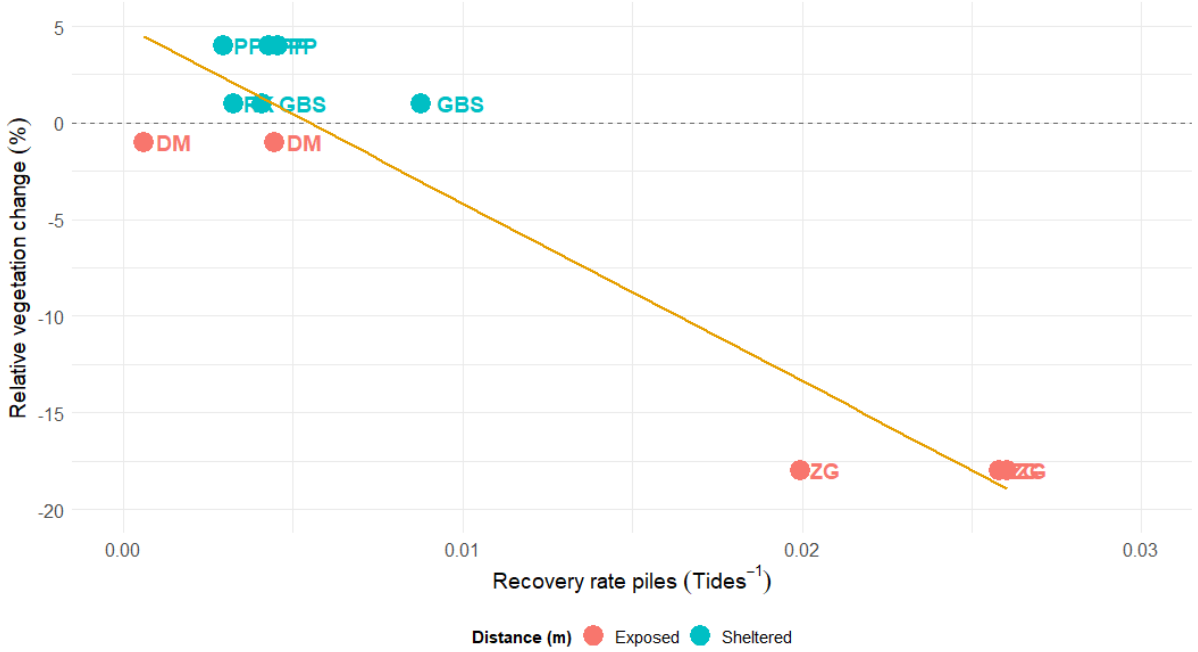

Figure A26 – Recovery rates versus the relative vegetation change (1988-2014) of the piles for all the fieldwork locations with their correlation coefficient (r=0.038, P>0.05).

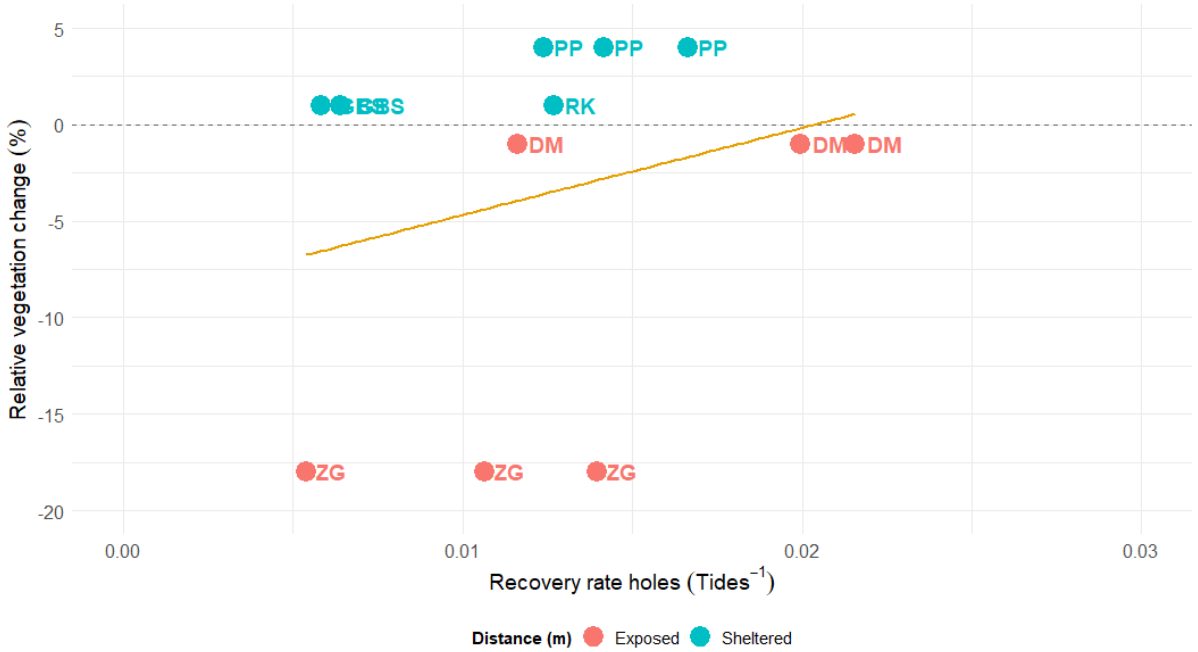

Figure A27 - Recovery rates versus the relative vegetation change (1988-2014) of the holes for all the fieldwork locations with their correlation coefficient (r=0.256, P>0.05).

ii. Recovery rates versus the long-term vegetation change for the Western Scheldt

Figure A28 – Recovery rates versus the relative vegetation change (1988-2014) of the piles in the Western Scheldt with their correlation coefficient (r=-0.974, P<0.01)

Figure A29 - Recovery rates versus the relative vegetation change (1988-2014) of the holes in the Western Scheldt with their correlation coefficient (r=0.219, P>0.05)

iii. Recovery rates versus the long-term vegetation change for the Eastern Scheldt

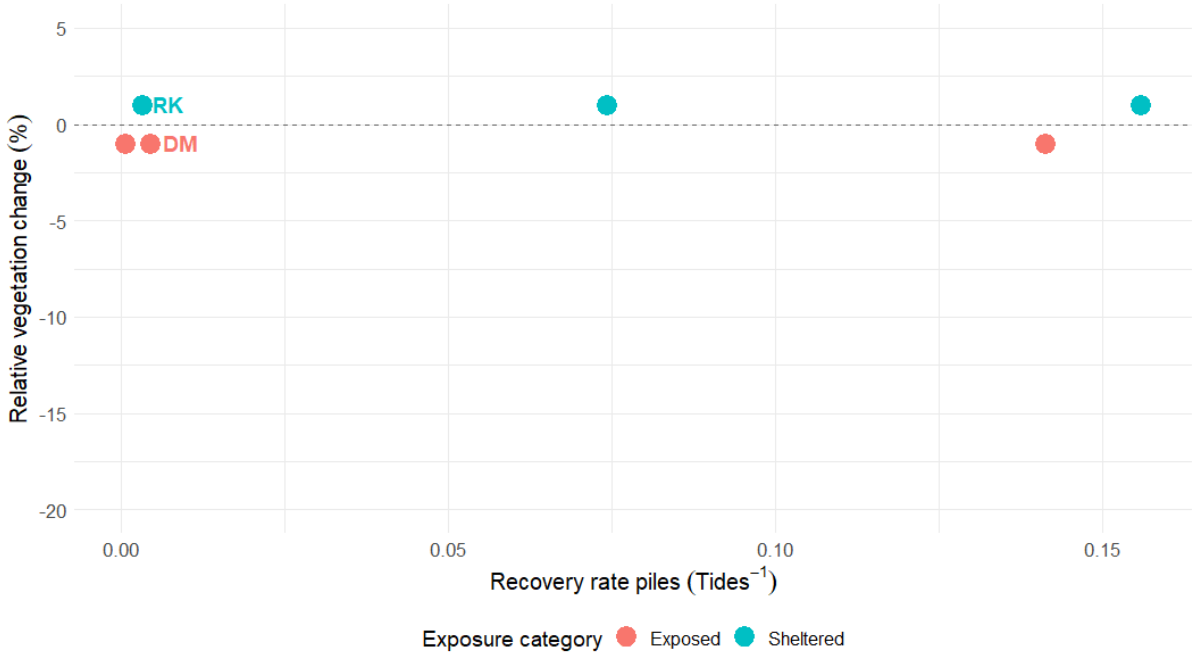

Figure A30 - Recovery rates versus the relative vegetation change (1988-2014) of the piles in the Eastern Scheldt with their correlation coefficient (r=0.221, P>0.05).

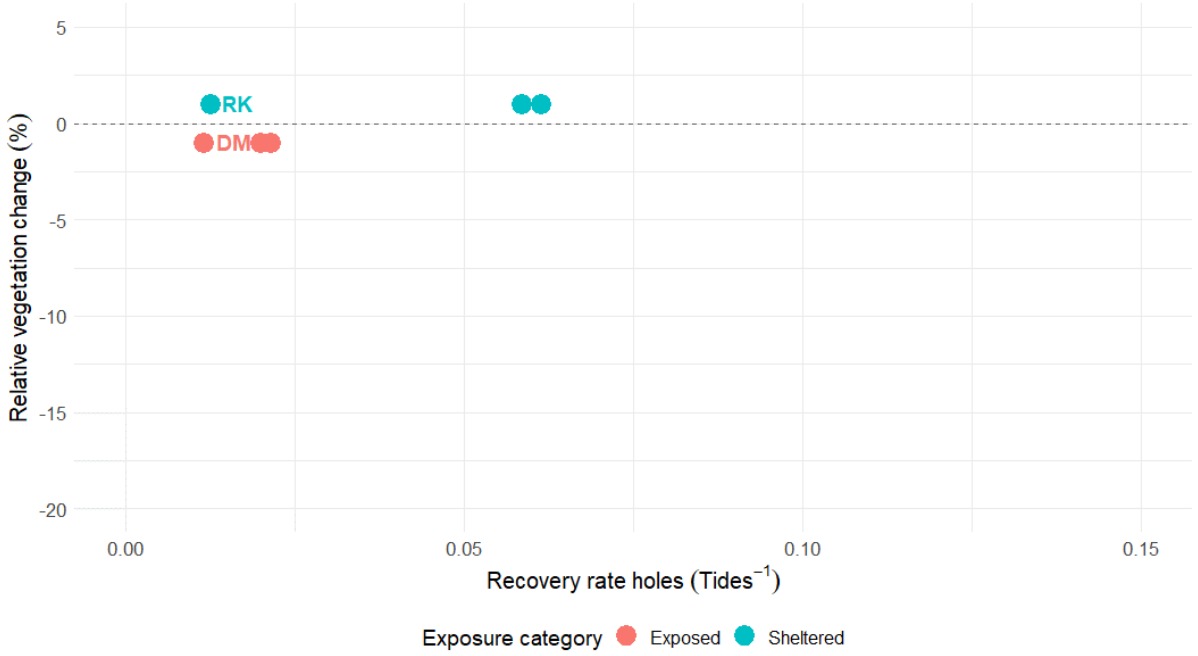

Figure A31 - Recovery rates versus the relative vegetation change (1988-2014) of the holes in the Eastern Scheldt with their correlation coefficient (r=0.636, P>0.05).